

# FRET-based visualization of cGMP dynamics in glomerular endothelial cells and podocytes

**Inaugural-Dissertation**

zur Erlangung des Doktorgrades

der Mathematisch-Naturwissenschaftlichen Fakultät

der Universität zu Köln

vorgelegt von

Nelli Rutkowski

geboren am 20.06.1990

in Obuchowka (Обуховка), Kasachstan

Köln, 2024

Berichterstatter (Gutachter):

Prof. Dr. Thomas Benzing

Prof. Dr. Peter Kloppenburg

Tag der mündlichen Prüfung: 28.05.2024

# Table of contents

LIST OF FIGURES	VI
LIST OF TABLES	VII
LIST OF ABBREVIATIONS	VIII
ABSTRACT	1
1 INTRODUCTION	2
1.1 Glomerular filtration barrier	2
1.2 cGMP signaling in the kidney	4
1.2.1 cGMP signaling in the glomerulus (endothelial cell/podocytes)	6
1.3 Pharmacological manipulation of cGMP signaling	8
1.4 Fluorescence resonance energy transfer (FRET) microscopy	9
1.4.1 FRET-based cGMP Imaging	9
2 AIM OF THE THESIS	11
3 MATERIAL AND METHODS	12
3.1 Material	12
3.1.1 Technical equipment	13
3.1.2 Software	14
3.1.3 Chemical - Reagents	15
3.1.4 Solutions - Buffer - Gels - Cell culture media	17
3.1.5 Testkits	21
3.1.6 Genotyping primer	21
3.1.7 Restriction enzyme and buffer	22
3.1.8 Online tools/Primer for Sanger Sequencing	22
3.1.9 Antibodies	22
3.2 Methods	23
3.2.1 <i>In vitro</i> characterization of cGi500	23
3.2.2 Mouse lines	25
3.3 Analysis pipeline	31
3.3.1 Selection	31
3.3.2 Line scan analysis – Intensity profile plot	32
3.3.3 CFP/YFP Ratio images	33
3.3.4 Movement correction (Galene)	33
3.3.5 Image segmentation	33

3.3.6	Calculation of baseline-normalized CFP/YFP ratio ( $\Delta R/R_0$ )	33
3.4	Statistics	34
4	RESULTS	35
4.1	Functional cGMP biosensor (cGi500) expression in HEK 293T cells	35
4.2	Targeting the NO/sGC/cGMP and NP/pGC/cGMP axis	38
4.3	Investigation of cellular biokinetics of cGMP from synthesis to export	40
4.4	Intravital imaging of cGi500-expressing glomeruli failed to demonstrate cGMP responses	41
5	MANUSCRIPT	43
	Abstract	45
5.1	Introduction	46
5.2	Methods	47
5.2.1	<i>In vitro</i> characterization of cGi500	47
5.2.2	Mouse lines	47
5.2.3	Poly-L-lysine coating	48
5.2.4	Acute kidney slices (AKS)	48
5.2.5	Custom-built perfusion system	48
5.2.6	Real-time imaging of AKS	49
5.2.7	FRET imaging data analysis	49
5.2.8	Immunostaining in optically cleared kidney slices	50
5.2.9	Statistics analyses	50
5.3	Results	51
5.3.1	Differential regulation of cGMP pathways in GECs and podocytes	51
5.3.2	cGMP levels are controlled by a higher PDE activity in GECs compared to podocytes	53
5.3.3	Predominant PDE2a activity in GECs and PDE3 & PDE5 activity in podocytes	55
5.3.4	PDE2a inhibition prevents cGMP degradation in GECs, whereas PDE3 & PDE5 inhibition augment the ANP/pGC/cGMP pathway in podocytes	56
5.4	Discussion	58
	References	62
6	DISCUSSION	68
6.1	cGMP signaling in podocytes	68
6.1.1	Evidence for pGC-mediated cGMP synthesis in podocytes	68
6.1.2	Evidence for sGC-mediated cGMP synthesis in podocytes	70

6.1.3	Suppressed global cGMP levels after simultaneous activation of sGC & pGC-pathways in podocytes	72
6.2	Phosphodiesterase (PDE) activity in podocytes	73
6.2.1	PDE3 and PDE5 predominate in podocytes	74
6.3	Inhibition of cGMP extrusion increases intracellular cGMP levels in podocytes	75
6.4	Calcium (Ca <sup>2+</sup> )-dependent mechanisms trigger cGMP release in podocytes	76
6.5	cGMP signaling in glomerular endothelial cells (GECs)	77
6.5.1	Evidence for sGC-/pGC-mediated cGMP synthesis	77
6.5.2	GECs exhibit high basal PDE activity, with PDE2a being the predominant isoform	79
6.6	Evaluating cGi500 biosensor performance for cGMP imaging: Strengths and Limitations	80
6.6.1	Comparison of cGi500 with other cGMP biosensors	80
6.6.2	Signal intensity	81
6.6.3	Isolated glomeruli vers. AKS	82
7	CONCLUSION AND PERSPECTIVES	83
	PUBLICATIONS	X
	ACKNOWLEDGEMENTS	XI
	ERKLÄRUNG	XII
	BIBLIOGRAPHY	88
	APPENDIX	118

## List of figures

Figure 1: Schematic illustration of the filter unit of the kidney, the glomerulus	2
Figure 2: Trilaminar structure of the glomerular filtration barrier	3
Figure 3: Guanylyl cyclase/cGMP signaling cascade	4
Figure 4: Working principle of the FRET-based biosensor cGi500	10
Figure 5: Custom-built imaging chamber and perfusion system for real-time imaging of isolated glomeruli	29
Figure 6: Surgery procedure for intravital imaging	31
Figure 7: Identification of damaged cells in glomeruli close to the cutting surface	32
Figure 8: cGi500 biosensor expression in HEK 293T cells	36
Figure 9: IBMX-induced cGMP accumulation in cGi500-transfected HEK 293T cell	37
Figure 10: NP/pGC and NO/sGC induced cGMP synthesis in isolated glomeruli	39
Figure 11: Elevation of intracellular cGMP following various stimuli in isolated glomeruli	41
Figure 12: Imaging of cGi500-expressing podocytes in vivo did not show convincing cGMP responses	42

### > MANUSCRIPT

Figure 1: cGMP response upon stimulation of the ANP/pGC/cGMP and NO/sGC/cGMP pathway in GECs and podocytes	52
Figure 2: Addition of the PDE inhibitor IBMX reveals higher PDE activity in GECs compared to podocytes	54
Figure 3: PDE inhibition reveals predominant PDE2a activity in GECs and PDE3 & PDE5 activity in podocytes	55
Figure 4: PDE2a inhibition prevents cGMP degradation in GECs, whereas PDE3 & PDE5 inhibition augment the ANP/pGC/cGMP pathway in podocytes	57

### > APPENDIX

Supplemental Figure 1: <i>In vitro</i> characterization of cGi500	118
Supplemental Figure 2: Visualization of the cutting process-related damage to glomeruli	119
Supplemental Figure 3: Evans Blue interferes at high concentrations with the FRET-based biosensor cGi500	120

Supplemental Figure 4: Calculated FRET (CFP/YFP) ratio from CFP and YFP fluorescence traces demonstrates cGMP generation after activation of the ANP/pGC or/and NO/sGC pathway in GECs	121
Supplemental Figure 5: Calculated FRET (CFP/YFP) ratio from CFP and YFP fluorescence traces demonstrates cGMP generation after activation of the ANP/pGC or/and NO/sGC pathway in podocytes	122
Supplemental Figure 6: Cell-specific expression of the cGMP biosensor in optically cleared AKS	124
Supplemental Figure 7: High doses of ANP and SNAP are required to elicit measurable cGi500-mediated cGMP signals	124
Supplemental Figure 8: DEA NONOate triggers cGMP synthesis in Tie2:Cre/cGi500 mice	125
Supplemental Figure 9: GECs of Cdh5:Cre/cGi500 mice respond similar to Tie2:Cre/cGi500 mice	126
Supplemental Figure 10: Long-term measurement of the cGMP/FRET response in podocytes after ANP administration	127
Supplemental Figure 11: Fluorescence spectra of cGi500	128

## List of tables

Table 1: List of materials	12
Table 2: List of technical equipment	13
Table 3: List of software	14
Table 4: List of chemicals and reagents	15
Table 5: List of solutions	17
Table 6: List of testkits	21
Table 7: List of genotyping primer	21
Table 8: List of restriction enzymes and buffer	22
Table 9: List of primer for Sanger sequencing	22
Table 10: PCR and cycling conditions	27

## List of abbreviations

ACE	Angiotensin-converting enzyme
AKS	Acute kidney slices
ANGII	Angiotensin II
ANP	Atrial natriuretic peptide
ARBs	Angiotensin II receptor blockers
ARNI	Angiotensin receptor neprilysin inhibitor
ASN	American Society of Nephrology
AT1	Angiotensin II type-1 receptor
ATP	Adenosine triphosphate
BCA	Bicinchoninic acid
BNP	Brain natriuretic peptide
bp	Base pair
BP	Blood pressure
CaCl <sub>2</sub> x 2H <sub>2</sub> O	Calcium chloride dihydrate
CFP	Cyan fluorescent protein
cGMP	Guanosine 3',5'-cyclic monophosphate
CKD	Chronic kidney disease
CNG	cGMP-gated ion channel
CNP	C-type natriuretic peptide
D(+)-Glucose x H <sub>2</sub> O	D(+)-Glucose monohydrate
DMEM	Dulbecco's Modified Eagle Medium
DMSO	Dimethyl sulfoxide
DOCA	Deoxycorticosterone acetate
DTT	Dithiothreitol
EDTA	Ethylenediamine-tetraacetic acid
ELISA	Enzyme-linked immunoassay
eNOS	Endothelial nitric oxide synthase
F:	forward
FBS	Fetal Bovine Serum
FPs	Foot processes
FRET	Förster Resonance Energy Transfer
GBM	Glomerular basement barrier
GC	Guanylyl cyclase
GC-A	Natriuretic peptide receptor A
GEC	Glomerular endothelial cells
GFB	Glomerular filtration barrier
GFR	Glomerular filtration rate
GTP	Guanosine triphosphate
HBSS	Hank's Balanced Salt Solution
HCl	Hydrogen chloride
HEK 293T	Human embryonic kidney cells
HF	Heart failure
hm	homozygous
ht	heterozygous
IBMX	3-Isobutyl-1-methylxanthine
IFIB	Interfaculty Institute of Biochemistry
iNOS	Inducible nitric oxide synthase
IR	Ischemia reperfusion
IVC	Individually ventilated cage
IVI	Intravital imaging



ivRF	<i>in vivo</i> Research Facility
KCl	Potassium chloride
KH <sub>2</sub> PO <sub>4</sub>	Potassium dihydrogen phosphate
KHB	Krebs-Henseleit buffer
KO	Knock-out
LANUV	Landesamt für Natur, Umwelt und Verbraucherschutz Nordrhein-Westfalen
LMA	Low Melt Agarose
MgCl <sub>2</sub> x 6H <sub>2</sub> O	Magnesium chloride hexahydrate
MgSO <sub>4</sub> x 7H <sub>2</sub> O	Magnesium sulphate heptahydrate
Na <sub>2</sub> EDTA x 2H <sub>2</sub> O	EDTA, Disodium Salt dihydrate
Na <sub>2</sub> HPO <sub>4</sub> x 7H <sub>2</sub> O	di-Sodium hydrogen phosphate heptahydrate
NaCl	Sodium chloride
NaHCO <sub>3</sub>	Sodium hydrogen carbonate
NaOH	Sodium hydroxide
NEP	Nepilysin
nNOS	Neuronal nitric oxide synthase
NO	Nitric oxide
NOS	Nitric oxide synthase
NP	Natriuretic peptide
NS	Nephrotic syndrome
PBS	Phosphate buffered saline
PCR	Polymerase Chain Reaction
PCR	Polymerase chain reaction
PDE	Phosphodiesterase
PFA	Paraformaldehyde
pGC	Particulate guanylyl cyclase
PH	Pulmonary hypertension
PIC	Protease Inhibitor Cocktail
PKC	Protein kinase C
PKG	Protein kinase G
PPAR-γ	Peroxisome proliferator-activated receptor γ
R:	reverse
RAAS	Renin-angiotensin-aldosterone-system
RBF	Renal blood flow
RIA	Radioimmunoassay
ROI	Region of Interest
ROS	Reactive oxygen species
rSAP	Shrimp Alkaline Phosphatase
SDS	Sodium dodecyl sulfate
sGC	Soluble guanylyl cyclase
SNAP	S-nitroso-N-acetylpenicillamine
TEA/HCl	Triethanolamine hydrochloride
tg	transgenic
Tris-HCl	Trizma® hydrochloride
TRPC	Transient receptor potential channel
v/v	volume per volume
VEGF	Vascular endothelial growth factor
VEGFR1/2	VEGF receptors 1 and 2
w/o	without
w/v	weight per volume
WR	Working reagent
wt	wildtype
YFP	Yellow fluorescent protein

## Abstract

Podocytes play a critical role in maintaining the integrity of the glomerular filtration barrier, a trilaminar structure that prevents the loss of macromolecules into the urine. These cells extend prominent cellular protrusions, termed foot processes, which contain an actin-based contractile system as a distinctive cellular structure. Podocytes can adapt to renal hemodynamic changes by modifying the foot process actin cytoskeleton, while they are exposed to significant physical forces resulting from pressure and fluid flow across the filtration slit. However, due to their limited capacity for self-renewal, podocyte loss is a hallmark in the progression of glomerular kidney diseases. Vasoactive factors, including angiotensin II (ANGII), are synthesized by glomerular cells upon stimulation and influence glomerular filtration. Among these factors, the role of the second messenger cyclic guanosine 5' monophosphate (cGMP) in podocytes and glomerular endothelial cells (GECs) remains elusive. Additionally, the presumed protective role of restored cGMP levels in various cardiovascular and renal diseases has sparked interest in exploring novel therapeutic strategies. This work aimed to evidence cGMP signaling in podocytes and GECs, and to elucidate cell-specific differences in cGMP dynamics. Using a stepwise approach, we analyzed isolated glomeruli and acute kidney slices from transgenic mice expressing the FRET-based ratiometric cGMP sensor (cGi500) either in podocytes or in endothelial cells. We stimulated both cGMP-synthesizing guanylyl cyclase systems (soluble (sGC) or particulate/membrane-bound (pGC)) independently or simultaneously. Both cell types responded with an increase in intracellular cGMP, while showing differences in both the intensity and duration of the response. Podocytes of cGi500 biosensor mice responded with a prolonged pGC-mediated cGMP signaling, emphasizing a predominant role for this pathway. GECs of cGi500 biosensor mice answered with a transient cGMP response after stimulation. Co-stimulation in podocytes did not result in the expected additive effect on cGMP levels, as observed in GECs. Moreover, increased cGMP levels were triggered by stimuli inhibiting cGMP degradation, cGMP export, or indirectly through calcium influx-related mechanisms in podocytes. Cell-specific differences in cGMP degradation were evident, with podocytes exhibiting comparatively lower baseline activity of the tested phosphodiesterase (PDE) isoforms. Notably, the most active isoforms, PDE3 and PDE5, had a preference towards the pGC/cGMP signaling pathway. On the contrary, in GECs, the basal activity of PDE2a was the highest of all isoforms tested, and had an equivalent impact on both cGMP pathways.

In summary, our data provided unprecedented insights into cell-specific dynamics of cGMP signaling in glomerular cells. These findings contribute to a deeper understanding of cGMP signaling in renal physiology and reveal potential targets for therapeutic interventions.

# 1 Introduction

## 1.1 Glomerular filtration barrier

One of the main tasks of the kidney is to filter fluids and solutes according to their molecular size and charge, aiming to preserve essential plasma proteins (e.g. albumin) within the bloodstream. The nephron, which is a fundamental structural unit of the kidney, includes the renal corpuscle connected to the tubular system. This corpuscle consists of a glomerulus surrounded by the Bowman's capsule, forming the filtration unit of the nephrons. The glomerulus plays a crucial role in blood filtration and the generation of primary urine.<sup>1</sup> Comprised of a complex network of capillaries, the glomerulus is positioned between two resistance vessels: the blood arrives via the afferent arteriole and exits through the efferent arteriole. These pre-and postglomerular arterioles contribute to renal blood flow (RBF) autoregulation by altering their diameter through vasodilation or vasoconstriction (**Figure 1**).<sup>2,3</sup>

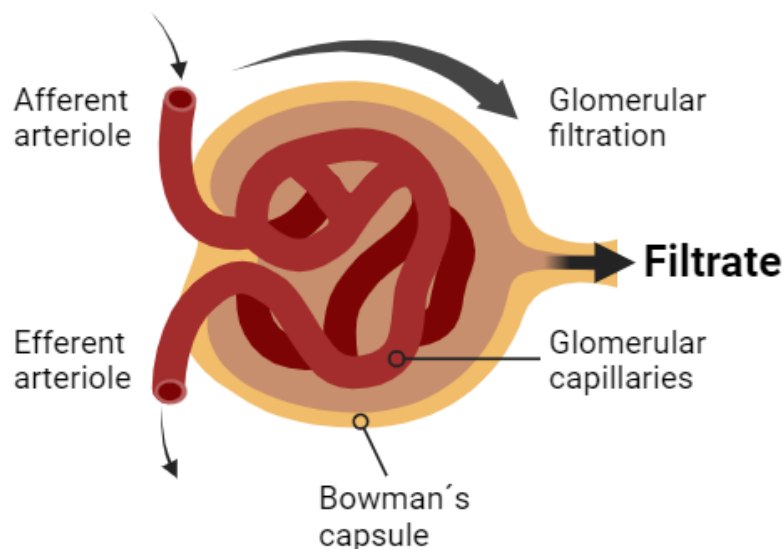


**Figure 1: Schematic illustration of the filter unit of the kidney, the glomerulus**

Blood entering through the afferent arteriole undergoes filtration across the glomerular capillary walls, producing the filtrate (primary urine) in the Bowman's capsule. Subsequently, this filtrate enters the tubule system at the urinary pole. The blood that has undergone filtration exits the glomerulus through the efferent arteriole. *Created with BioRender.com.*

The trilaminar structure of the glomerular capillary wall creates the glomerular filtration barrier (GFB), which incorporates the glycocalyx-covered fenestrated endothelium (proximal component layer), the glomerular basement membrane (GBM) and the visceral epithelial cells, known as podocytes (distal layer) (**Figure 2**).<sup>4</sup> Podocytes are terminally differentiated cells and possess a complex cellular structure consisting of a cell body and major processes that give rise to interdigitating actin-based foot processes (FPs) enwrapping the glomerular capillaries.<sup>5</sup> Adjacent FP are connected by cell-cell junctions called slit diaphragms, bridging the filtration slit between neighboring podocyte FPs.<sup>6,7</sup> An emerging field of research focuses on cell-cell communication through soluble mediators, in particular the crosstalk between endothelium and podocytes.<sup>8,9</sup> Prominent example is the expression of vascular endothelial growth factor (VEGF) in podocytes, functioning in an autocrine and paracrine manner to regulate the structure and function of GECs through ligand-receptor binding to VEGF receptors 1 (VEGFR1) and 2 (VEGFR2).<sup>10-13</sup>

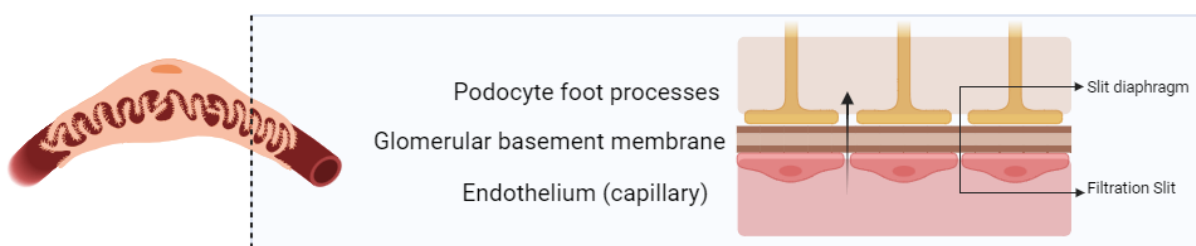


**Figure 2: Trilaminar structure of the glomerular filtration barrier**

Visual representation of a glomerular capillary surrounded by two podocytes and a sectional view of the glomerular filtration barrier (GFB), showcasing the fenestrated endothelium connected to the basement membrane and the foot processes of podocytes. Arrow indicates the filtration direction. *Created with BioRender.com.*

Elevated protein excretion (proteinuria) in the urine reflects impaired permselectivity/ increased permeability for proteins, indicating a possible dysfunction in one or more layers of the glomerular filtration barrier. Changes in the density or diameter of GECs fenestrations, characterized as transcellular holes through the peripheral cytoplasm, and glycocalyx disruptions can disturb the proximal filtration layer.<sup>14-16</sup> Changes in the slit diaphragm, cell adhesion molecules, and disturbances in actin organization, referred to as foot process effacement, can compromise structural integrity of the distal filtration layer. This can result in detachment from the GBM and consequently to podocyte cell loss.<sup>17-19</sup>

## 1.2 cGMP signaling in the kidney

In 1963, researchers first discovered the presence of cGMP in the urine of rats,<sup>20</sup> and since then, its role in controlling various cell functions in health and disease has been studied extensively.<sup>21</sup> The cGMP-dependent signal transduction induces specific biological responses that regulate renal physiological function (e.g. natriuresis, diuresis, glomerular and tubular function).<sup>22</sup> External stimuli (e.g. shear stress, release of specific neurotransmitters, vasoactive substances, hormones) initiate internal signaling cascades that culminate in the generation of the cyclic nucleotide cGMP. This leads to the activation of downstream effector molecules such as cGMP-gated ion channels (CNG), cGMP-regulated phosphodiesterase (PDE), and cGMP-dependent protein kinase G (PKG). The regulated widening of blood vessels, known as vasodilation, is an essential physiological process guided by intricate signaling cascades and can be cited as an example of cGMP-mediated signal transduction. Endothelial cells, lining the inner vascular walls, respond to stimuli by releasing nitric oxide (NO). NO diffuses into smooth muscle cells, activates the soluble guanylate cyclase and increases cGMP levels. Elevated intracellular cGMP leads to the activation of PKG, which phosphorylates various proteins, opens potassium channels and closes calcium channels. The subsequent dephosphorylation of myosin, a contractile protein, facilitates smooth muscle relaxation.<sup>23,24</sup> GTP-specific succinyl-CoA synthetase, a component of the citric acid cycle, generates guanosine triphosphate (GTP), which is enzymatically converted into cGMP by guanylyl cyclases (GC) (**Figure 3**).<sup>25,26</sup> These enzymes are located either in the cytosol (sGC) or exist as membrane-bound intracellular catalytic domains (pGC) associated with an extracellular peptide receptor domain.<sup>26–28</sup>

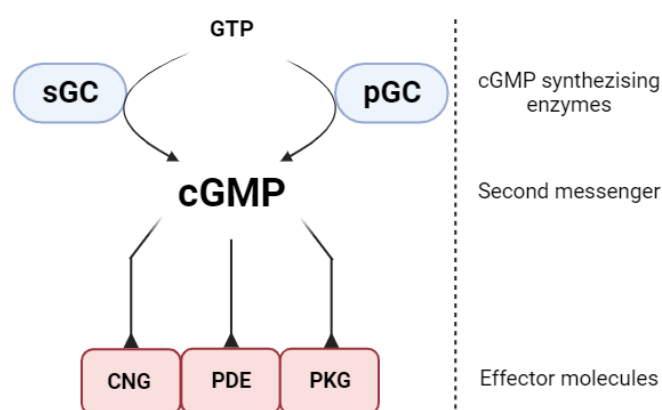


**Figure 3: Guanylyl cyclase/cGMP signaling cascade**

The second messenger cGMP is synthesized by two different guanylyl cyclase systems (sGC and pGC) from GTP. The effector molecules (cGMP-gated ion channels (CNG), cGMP-regulated phosphodiesterase (PDE), and cGMP-dependent protein kinase G (PKG)) transduce the signal and mediate physiological responses. *Created with BioRender.com.*

In the kidney, sGC is abundantly expressed as  $\alpha 1\beta 1$  heterodimer,<sup>29,30</sup> and is activated by NO binding to the ferrous heme of sGC $\beta$ .<sup>31–34</sup> The main source of endogenous NO is generated as a by-product during the enzymatic conversion of L-arginine to L-citrulline by nitric oxide synthase (NOS) enzymes. The nitrate–nitrite–NO pathway offers an alternate route where endogenous or dietary inorganic nitrate and nitrite undergo serial reduction to produce NO, thereby complementing the NOS system.<sup>35–38</sup> The termination of the NO signaling pathway can occur through various mechanisms, including sGC desensitization via heme oxidation, heme loss, heme nitrosylation by a second NO molecule, S-nitrosation of cysteine residues, or heterodimer dissociation.<sup>39,40</sup> Moreover, the accessibility of NO to sGC can be compromised by potent NO scavenger, thereby influencing the extent of its functional impact. Included among these scavengers are partially reduced molecular oxygen products ( $O_2$ ), known as reactive oxygen species (ROS), or hemoglobin present in erythrocytes.<sup>40,41</sup> The NO-dependent cGMP signaling cascade impacts various physiological functions of the kidney, including the increase of renal blood flow or the stimulation of renin secretion.<sup>42–44</sup> The primary source of renin production and secretion occurs in juxtaglomerular epithelioid cells situated within the walls of renal afferent arterioles.<sup>45</sup> Renin serves as a crucial regulator of the renin-angiotensin-aldosterone-system (RAAS), as its proteolytic enzyme activity results in the cleavage of angiotensinogen into angiotensin I, which is subsequently processed to form angiotensin II (ANGII).<sup>46</sup> The metabolism of angiotensin peptides takes place in mesangial cells, podocytes, and endothelial cells, whereas ANGI (acting through ANGI type-1 (AT1) receptor) is the main angiotensin peptide that regulates glomerular hemodynamics.<sup>47</sup> ANGI-induced formation of ROS participates in pro- and antioxidant pathways in the kidney.<sup>48</sup>

Different classes of mammalian pGC (GC-A to GC-G) have been identified.<sup>28,49</sup> The first three react to specific peptide ligands (GC-A: atrial natriuretic peptide (ANP) and brain natriuretic peptide (BNP); GC-B: C-type natriuretic peptide (CNP); GC-C: the heat stable enterotoxins of *Escherichia coli* and guanylin) and are expressed in the kidney.<sup>50–52</sup> The remaining receptors (GC-D found in the olfactory epithelium; GC-E and GC-F in the retina; GC-G in the lung, intestine, and skeletal muscle) are referred to as 'orphan' receptors due to the absence of identified activating ligands.<sup>53</sup> ANP and BNP are predominantly secreted by cardiomyocytes (ANP: atrium and BNP: ventricle) and their binding to GC-A mediates e.g. inhibition of renin secretion, an increase in the glomerular filtration rate (GFR) by dilating the afferent arterioles and constricting the efferent arterioles.<sup>54–56</sup> The ligand-receptor binding of GC-B lacks the natriuretic and diuretic effects seen with ANP/BNP binding to the GC-A receptor, and its specific physiological role in the kidney is not yet fully understood.<sup>57,58</sup> CNP has a strong binding affinity to GC-B, and accumulating data indicate that urinary CNP may play a role in the early detection of renal dysfunction.<sup>59</sup> Urinary CNP excretion was detected in individuals with nephrotic syndrome (NS),<sup>60</sup> and CNP mitigated ischemia–reperfusion (IR)-induced acute

kidney injury by inhibiting apoptotic and oxidative stress pathways.<sup>61</sup> Clearance of natriuretic peptides occurs either by receptor-mediated internalization or by degradation via NPR-C (clearance receptor), by proteolysis via neprilysin (NEP) or insulysin (insulin degrading enzyme), or by excretion.<sup>59,62</sup>

### 1.2.1 cGMP signaling in the glomerulus (endothelial cell/podocytes)

There is a scarcity of information regarding cGMP signaling within glomerular cell layers, which reflects a substantial lack of research into this signaling cascade and its impact on the filtration unit of the kidney. The existence of both cGMP synthesizing GC systems in GECs is unknown and available literature on podocytes contains conflicting data. Recent findings demonstrated strong mRNA expression of GC-A and NPR-C in podocytes, while the expression level of GC-B was low.<sup>52,63–68</sup> In GECs, on the other hand, expression of GC-A and GC-B was also observed, although to a lesser extent.<sup>52</sup> Others presented additional proof of mRNA expression of GC-B and CNP in immortalized podocytes.<sup>69</sup> Furthermore, a strong detection of ANP mRNA and NEP was found in podocytes.<sup>70–72</sup> NEP is a neutral endopeptidase and capable of degrading all three natriuretic peptides. The expression pattern of binding and degradation enzymes highlights a significant impact of natriuretic peptides on podocytes, specifically emphasizing the paracrine influence of circulating ANP. The systemic antihypertensive effect of circulating ANP was demonstrated by the appearance of salt-sensitive hypertension caused by genetic deletion of the proANP gene in mice (ANP-KO).<sup>73</sup> While salt-resistant hypertension was present in global GC-A-KO mice and endothelial cell-specific GC-A-KO mice,<sup>74,75</sup> podocyte cell-specific GC-A-KO mice showed no basal phenotype related to blood pressure (BP), GFR, or natriuresis.<sup>63</sup> However, following deoxycorticosterone acetate (DOCA) salt treatment, the mice displayed albuminuria, decreased GFR, along with heightened expression of the canonical transient receptor potential 6 channel (TRPC6) and an increase in ATP-triggered calcium influx within podocytes. The TRPC6 is a glomerular slit diaphragm-associated channel and essential for maintaining regular podocyte function and structure.<sup>76</sup> It has also been functionally linked to the podocyte actin cytoskeleton.<sup>77</sup> Genetic and developed abnormalities affecting this channel are linked to proteinuric kidney diseases,<sup>77</sup> whereas excessive intracellular calcium is linked to various types of cell death in renal cells.<sup>78</sup> Augmented TRPC6-mediated  $\text{Ca}^{2+}$  influx causes podocyte injury and damage, while the utilization of cGMP-elevating substances was shown to counteract this effect, demonstrating the protective nature of the cGMP signaling pathway.<sup>79–81</sup>

The discovery of a contractile architecture in the foot processes sensitive to vasoactive substances suggests a regulatory influence on glomerular filtration by modulating the permeability.<sup>82–85</sup> Furthermore, a link between natriuretic peptide related signaling and

mechanical stress was demonstrated *in vitro*, highlighting the influence of cGMP on the mechanobiology of podocytes.<sup>69</sup> The natriuretic peptide (NP) system is designated as an antagonist to RAAS. ANGII functions as a natural suppressor of (GC-A)-mediated cGMP synthesis through an ANGII type-1 (AT1) receptor/protein kinase C (PKC) dependent mechanism.<sup>86</sup> Nonetheless, ANGII has also been known as a stimulant for NO production in podocytes.<sup>87,88</sup> Evidence showed that the ANGII-induced podocyte phenotype shifts from being dynamically stable to adaptively migratory with a persistent activation of the RAAS.<sup>85</sup> Maintaining a balance between the RAAS and cGMP-producing systems appears pivotal for enabling podocytes to adapt to the continuous fluctuations in cardiorenal hemodynamics, emphasizing the fundamental importance of understanding these mechanisms in living animals.

The majority of available data on ANP-induced cGMP synthesis in podocytes is based on cell culture studies and indicates a consensus regarding the existence of a NP/pGC/cGMP signaling pathway in this cell type, while the presence of an active NO/sGC/cGMP signaling pathway has been questioned.<sup>29,68,72</sup> Members of the NOS family - neuronal NOS (nNOS), inducible NOS (iNOS), and endothelial NOS (eNOS) - are essential for initiating the activation of the NO/sGC/cGMP signaling pathway by producing NO. mRNA for eNOS and iNOS was detected in both human glomerular endothelial cells and podocytes.<sup>80</sup> Although there was minimal protein expression of eNOS in podocytes, it was abundant in glomerular endothelial cells. Moreover, the presence of sGC was confirmed in both cell types using human renal tissue,<sup>90</sup> and the subunits were identified in cultured human cell lines (podocytes: sGC $\alpha$ 1, sGC $\alpha$ 2, sGC $\beta$ 1 and sGC $\beta$ 2; glomerular endothelial cells: sGC $\alpha$ 2 and sGC $\beta$ 2).<sup>80</sup> Despite deviations in species-dependent sGC detection (especially in murine samples), a NO-induced increase in intracellular cGMP was observed in immortalized podocyte cell lines,<sup>68,72,80</sup> podocytes of isolated glomeruli<sup>88,91</sup> as well as in glomeruli of kidney slices.<sup>92</sup> In eNOS-KO mice, the deficiency of the NO-producing enzyme alone led to the occurrence of mild glomerular disease, characterized by podocyte injury and low-grade albuminuria.<sup>93</sup> In young and aged eNOS-KO mice, the podocyte number was significantly diminished in comparison with wild type mice.<sup>94</sup> Furthermore, Hart et al. showed that NO deficiency leads to TRPC6 overexpression upon adriamycin-induced nephropathy in eNOS-KO mice and postulated the presence of a paracrine (e)NOS/NO/sGC signaling between glomerular endothelial cells and podocytes.<sup>80</sup> The impact of autocrine/paracrine nitric oxide (NO) production on podocytes remains largely unexplored.



### 1.3 Pharmacological manipulation of cGMP signaling

Multiple medications addressing cGMP deficiency in disease states have been approved and established as treatment options, primarily for pulmonary and cardiovascular diseases.<sup>95–97</sup> Accumulating evidence emphasizes renoprotective properties linked to reestablished cGMP levels in kidney disease, positioning the cGMP signaling pathway as a potential therapeutic target and underlining the need for basic research on cell-specific differences in renal cell types.<sup>22,98–100</sup> The novel medications seek to counteract the pathologically decreased cGMP synthesis through various mechanisms: activating sGC NO-independently with/without heme, inducing specific subtypes of guanylyl cyclases with native and designer natriuretic peptides, inhibiting degradation by specific PDE isoform inhibitors, blocking NPR-C or NEP activity and targeting the NO pathway by supplementation diets.<sup>101–108</sup> PDE5, 6 and PDE9 are cGMP-specific PDEs and are essential for the hydrolysis of sGC- and pGC-synthesized cGMP pools. The other identified PDE isoforms are either cAMP-specific PDEs (PDE4, 7, and 8) or exhibit dual-specificity (PDE1, 2, 3, 10, and 11).<sup>109</sup> Sildenafil, a well-studied PDE inhibitor, effectively blocks PDE5 activity, exhibits vasorelaxant properties and is used in clinical practice to treat erectile dysfunction and pulmonary hypertension (PH).<sup>110–113</sup> Multiple studies have linked PDE5 inhibition with favorable renal effects.<sup>114–117</sup> In addition, there is increasing evidence that podocytes respond to PDE5 inhibition, emphasizing the significance of interactions among cGMP, PKG-I, Peroxisome proliferator-activated receptor  $\gamma$  (PPAR- $\gamma$ ), and TRPC6 signaling pathways in glomerular diseases.<sup>79–81,118</sup> Another promising approach is the inhibition of PDE9a, which is highly expressed in the kidney,<sup>119</sup> and augments ANP-mediated cGMP synthesis, while showing no response to NO/cGMP activation.<sup>120,121</sup> In diseases where NO-dependent cGMP synthesis is suppressed, PDE9a inhibition could potentially be utilized as a therapeutic strategy. The cGMP-synthesizing guanylyl cyclase system and RAAS function as opponents, are tightly regulated and prone to imbalance in disease states. ANGII has vasoconstrictive properties and was shown to upregulate PDE5, which enhanced hydrolysis of NP-mediated cGMP synthesis.<sup>122</sup> Inhibiting the conversion of angiotensin I to ANGII by angiotensin-converting enzyme (ACE) or receiving angiotensin II receptor blockers (ARBs) protects the kidneys of patients with chronic kidney disease (CKD).<sup>123,124</sup> Furthermore, combination therapy with the angiotensin receptor neprilysin inhibitor (ARNI) reduced hospitalization for heart failure (HF) patients and all-cause mortality in a landmark clinical trial (PARADIGM-HF).<sup>125</sup> Overall, targeted treatment of deficiency and/or impairment of the cGMP system in kidney disease is once again the focus of research, while novel medications are being developed.

## 1.4 Fluorescence resonance energy transfer (FRET) microscopy

Fluorescence resonance energy transfer (FRET) is a distance-dependent physical phenomenon where energy is transferred nonradiatively from an excited donor fluorophore to the acceptor fluorophore through intermolecular long-range dipole–dipole coupling. FRET serves as a precise measurement of molecular proximity within angstrom distances (10-100 Å) and is efficient when the donor and acceptor are positioned within the Förster radius. The Förster radius is the distance at which half the excitation energy of the donor is transferred to the acceptor, typically falling within the range of 3–6 nm.<sup>126</sup> Basic requirements for FRET are:<sup>127,128</sup>

- (i) the emission spectrum of the donor fluorophore and the absorbance spectrum of the acceptor molecules must overlap (spectral overlap integral)
- (ii) the donor and acceptor fluorophores must be positioned within a specific range, typically between 1 and 10 nanometers.
- (iii) the dipoles of the donor and acceptor molecules should be oriented in a favorable manner relative to each other.
- (iv) Controlling environmental factors like temperature, pH, and ionic strength is crucial as they can impact the efficiency of FRET during experiments.

### 1.4.1 FRET-based cGMP Imaging

Conventional biochemical techniques to measure cGMP levels involve radioactive cGMP tracer (Radioimmunoassay (RIA)) or non-radioactive methods (Enzyme-linked immunoassay (ELISA)) that bind to anti-cGMP antibodies.<sup>129–132</sup> An alternative approach includes indirect evidence through a traditional Western blot, which detects the phosphorylation state of downstream targets resulting from the activation of cGMP-PKG kinase activity by using phospho-specific antibodies.<sup>133</sup> All of these techniques share a common necessity: the cells/tissue need to undergo lysis to liberate the cyclic nucleotide in quantities sufficient to meet the detection limit of the assays. Moreover, it is standard practice to include non-specific PDE inhibitors like isobutylmethylxanthine (IBMX) to prevent the degradation of cGMP during preparation. As a result, the ability to effectively monitor fluctuating intracellular cGMP levels with a spatiotemporal resolution is compromised. To overcome these obstacles, genetically encoded fluorescent cGMP biosensors have been developed that enable real-time imaging of this second messenger.<sup>130,134</sup> The cGMP detection can involve either FRET-based (e.g. Red cGES-DE5)<sup>135</sup> or non-FRET-based (e.g. FlincG)<sup>136</sup> fluorescent indicators and rely on either intensimetric (e.g. Green cGull)<sup>137</sup> or ratiometric (e.g. PfPKG)<sup>138</sup> fluorescence principles. Biosensors have the capability to move freely within the cell or can be directed to specific subcellular microdomains by attaching them to particular proteins or short peptide sequences.

One of the extensively used cGMP biosensors is cGi500, classified as a monomolecular ratiometric FRET-based biosensor.<sup>139,140</sup> The probe consists of tandem cGMP-binding sites of PKG-I, positioned between cyan fluorescent protein (CFP) and yellow fluorescent protein (YFP), both of which are derivatives of green fluorescent protein (GFP)(**Figure 4**). The interaction with cGMP induces a change in conformation that modifies the distance between the donor and acceptor fluorophores, consequently decreasing the FRET efficiency. The CFP/YFP emission ratio reflects changes in intracellular cGMP concentrations. The expression of cGi500 in transgenic mice was achieved by a knock-in strategy into the Rosa26 locus along with Cre/lox-activatable expression of the sensor, driven by the cytomegalovirus early enhancer/chicken  $\beta$ -actin/ $\beta$ -globin promoter. Mating with Cre mice enables cell-specific biosensor expression, facilitating real-time FRET/cGi500 imaging in selected cell types across a presumed physiological range of 100 nM to 3  $\mu$ M.<sup>140</sup> The sensor has previously been used in the isolation of cells, tissues, organs, and *in vivo* experiments.<sup>92,140–143</sup>

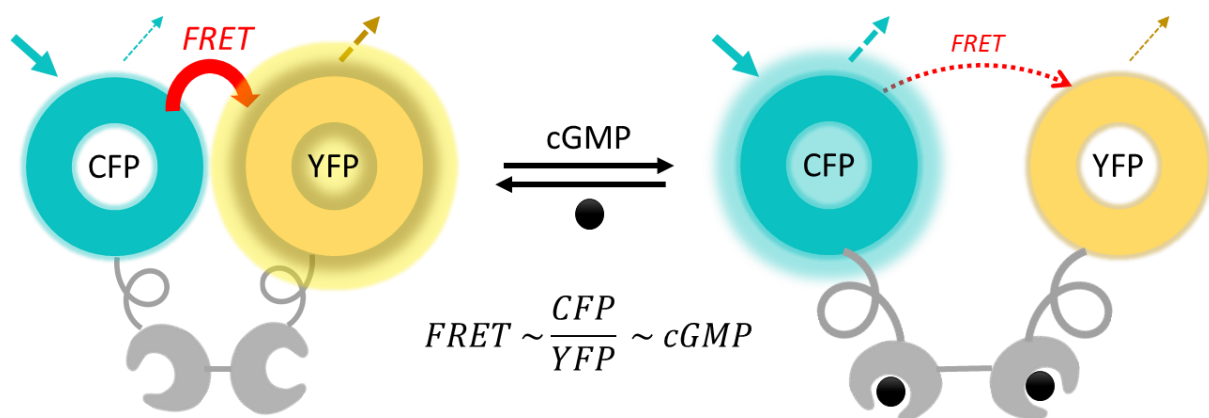


**Figure 4: Working principle of the FRET-based biosensor cGi500**

In the absence of cGMP, FRET takes place from the excited CFP to YFP, resulting in light emission from YFP. Upon the binding of cGMP, a conformational change occurs, causing a decrease in FRET efficiency. As a result, the light emission from YFP is diminished, while the emission from CFP is increased. Monitored FRET response (CFP/YFP emission ratio) reflects changes in intracellular cGMP concentration.

## **2 Aim of the thesis**

Therapeutic modulation of the cGMP pathway has only recently entered clinical practice and demonstrated that its broad spectrum of beneficial effects extends beyond its protective function in cardiovascular diseases. The lack of consistent and relevant literature on the presence of cGMP synthesizing systems in glomerular cell layers hampers our understanding of associated renal physiological functions. Most of the available data relies on methods that involve cell destruction and, as a result, cannot comprehensively capture the spatial and temporal dynamics of cGMP-related systems. The objective of this thesis was to gain a deeper insight into the spatial cGMP dynamics of podocytes and glomerular endothelial cells in their healthy state. Expression of the FRET-based cGMP biosensor in two different model organisms, HEK 293T cells and transgenic mice, allowed the visualization of cGMP dynamics in real time in intact cells while preserving the physiological environment. This approach enabled us to test agonists and antagonists of cGMP signaling in a close-to-native scenario.

## 3 Material and methods

### 3.1 Material

**Table 1: List of materials**

Material	Catalog Number	Company
μ-Dish 35 mm, high Glass Bottom	81158	Ibidi
μ-Slide 8 Well, ibiTreat	80826	Ibidi
8-Lid chain, flat	65.989.002	Sarstedt
Blades	121-6	Ted Pella
Cell lifter	3008	Corning
Cell Strainer, 100 μm	83.3945.100	Sarstedt
CELLSTAR™ 96 Well Cell Culture Plate	655180	Greiner BioOne
CELLSTAR™ tubes 15 ml	188271-N	Greiner BioOne
CELLSTAR™ tubes 50 ml	227261	Greiner BioOne
Corning® 100 mm TC-treated Culture Dish	430167	Corning
Corning® 150 mm TC-treated Culture Dish	430599	Corning
Corning® 35 mm TC-treated Culture Dish	430165	Corning
Coverslip (18 x 18 mm # 1.5)	LH22.1	Roth
Coverslip Ø 18 mm # 1.5	0117580	Marienfeld
Coverslip Ø12 mm # 1.5	11911998	Gerhard Menzel
Discardit™ 5 ml Syringe	309050	Becton Dickinson
Dynabeads M-450 Tosyl-activated	14013	Thermo Fisher
Female Luer Lock	LF31	Drifton A/S
Instant Adhesive	Best-CA 221	Best Klebstoffe
Masterflex® silicone hose	96400-13	Cole-Parmer
Micro tubes 1.5 ml	72.690.001	Sarstedt
Microfuge Tube Polypropylene (1.5 ml)	357448	Beckman Coulter
Multiply®-μStrip 0.2 ml chain	72.985.002	Sarstedt
Original Perfusor® Line	8723060	Braun SE
Parafilm™	PM-996	Bemis
Peel-A-Way® S-22	E6032-1CS	Sigma
Petri dish, 92 x 16 mm (Agar plates)	82.1473	Sarstedt
Plastipak™ 1 ml Syringe	303172	Becton Dickinson

*Continued on next page*

Polyethylene tubing (PE10)	B-PE-10-100FT	Braintree Scientific
Rotilabo®-syringe filter, 0.22 µm	P666.1	Roth
SafeSeal tube 1.5 ml, brown	72.706.001	Sarstedt
Scalpel No.21	E72042-21	Feather
Sealing foam tape, 10mm(W)x1mm(T)x16.4Ft.(L)		SourcingMap
Serological pipette 10 ml	86.1254.001	Sarstedt
Serological pipette 25 ml	86.1685.001	Sarstedt
Serological pipette 5 ml	86.1253.001	Sarstedt
Sterican® Nr.20 27G x ¾	260092	Braun
Surgical suture (5-0-USP)	H2F	Resorba
Suture material (6-0 USP)	88153	Resorba
TipOne® Pipette Tip 10 µl, refill	S1111-3700	Starlab
TipOne® Pipette Tip 1000 µl, refill	S1111-6700	Starlab
TipOne® Pipette Tip 200 µl, refill	S1111-1700	Starlab

### 3.1.1 Technical equipment

**Table 2: List of technical equipment**

Equipment	Provider
Avanti® J-26S XPI	Beckman Coulter
Bioruptor®Pico	Diagenode
Buffer Puffer™ Gel systems	OWL
Centrifuge 5424	Eppendorf
CO <sub>2</sub> Incubator BD 115	Binder
Corning® LSE™ Mini Microcentrifuge	Corning
Digital Heatblock II	VWR
DynaMag™-2 Magnet	Thermo Fisher
Electrophoresis Power Supply EPS-601	Amersham Pharmacia
EnSpire® Multimode Plate Reader	PerkinElmer
FiveEasy F20	Mettler Toledo
Gel iX 20 Imager	Intas Science Imaging
Hair Trimmer Contura (HS61)	Wella
Heating system (water) (KS 92-1)	Medres
IKA®-Schüttler MTS 4	IKA-Labortechnik
IKAMAG® RET	IKA-Labortechnik

*Continued on next page*

Isoflurane Vapor	Dräger
Kidney Holder (custom made)	Medres
Knock out box	Medres
LOG200 TC 5005-0204	Dostmann Electronic
LSM Meta 710 Axio Observer	Zeiss
Masterflex® L/S® Easy-Load® II	Cole-Parmer
Masterflex® L/S® peristaltic pump	Cole-Parmer
Microscope Stage Chamber MS4	Digitimer
Minichiller 300	Huber
Multifuge® 4 KR	Heraeus
Multitron Pro	Infors HT
NanoDrop® 1000 Spectrophotometer	Thermo Fisher
Objective heating collar OBJ-COLLAR-3342	Okolab
S1000™ Thermal Cycler	Bio-Rad
Slice anchor SHD-42/10	Multi Channel Systems
Stereo Microscope M80	Leica Microsystems
TCS SP8 gSTED 3X microscope	Leica Microsystems
TCS SP8 MP-OPO microscope	Leica Microsystems
Temperature controller H401-T-CONTROLLER	Okolab
Truelife Invio BW Double	Mercateo
Ultracentrifuge Optima MAX-XP	Beranek
Vibratome Leica VT 1200S	Leica Microsystems
Vortexer REAX2000	Heidolph
Waterbath WNB 22	Memmert

### 3.1.2 Software

**Table 3: List of software**

Software	Company
EnSpireManager	PerkinElmer
Galene 2.2.0	Sean C. Warren
Graphpad 10.1.0 (316)	GraphPad Software Inc.
ImageJ/Fiji 1.54f	Wayne Rasband
INTAS GelDoc	Intas
LAS X	Leica Microsystems

*Continued on next page*

Nanodrop100  
ZEN 2009

Thermo Fisher  
Zeiss

### 3.1.3 Chemical - Reagents

**Table 4: List of chemicals and reagents**

Chemicals/Reagents	Catalog Number/Company
0.1% (w/v) Poly-L-lysine solution	P8920/Sigma
1% (w/v) Ethidium bromide solution	2218.2/Roth
1-thioglycerol	M1753/Sigma
3-Isobutyl-1-methylxanthine (IBMX)	I5879/Sigma
6X Loading dye	R0611/Thermo Fisher
70-kDa Texas Red dextran	D1830/Invitrogen
Acetic acid	1.00056.1000/Merck
Adenosine-5'-triphosphate disodium salt hydrate (ATP)	A2383-25G/Sigma
Agarose	A9539/Sigma
Ampicillin	K029.2/Roth
Atrial natriuretic factor (1-28) trifluoroacetate (ANP)	01-4030380/Bachem
Avanafil	A12619/Hölzel
BAY 60-7550	Cay10011135/Biomol
BNP-45 (mouse) trifluoroacetate salt (BNP)	4095506.0500/BACHEM
Boric acid	B0252/Sigma
Bradykinin	J63131.MA/Alfa Aeser
Calcium chloride dihydrate (CaCl <sub>2</sub> x 2H <sub>2</sub> O)	HN04.2/Roth
Cilostamide	A13596/Hölzel
Collagenase from Clostridium histolyticum, Type IA	C9891/Sigma
cOmplete™ EDTA-free Protease Inhibitor (PIC w/o EDTA)	4693132001/Roche
D(+)-Glucose monohydrate (D(+)-Glucose x H <sub>2</sub> O)	K23604142/Merck
D(+)-Glucose	G7021/Sigma
D-Fructose	F0127/Sigma
Dimethyl sulfoxide (DMSO)	1.02952.1000/Merck
di-Sodium hydrogen phosphate heptahydrate (Na <sub>2</sub> HPO <sub>4</sub> x 7H <sub>2</sub> O)	X987.2/Roth
Dithiothreitol (DTT)	A2948.0005/Applichem
EDTA, Disodium Salt dihydrate (Na <sub>2</sub> EDTA x 2H <sub>2</sub> O)	EDTAD250/Quantum
Ethanol	9065.3/Roth

*Continued on next page*



Ethylenediamine-tetraacetic acid (EDTA)	EDS/Sigma
Evans blue	E2129/Sigma
GeneRuler 1 kb DNA ladder	SM0311/Thermo Fisher
Gibco™ 0.05% Trypsin-EDTA (1X)	25300-054/Thermo Fisher
Gibco™ DMEM - high glucose	31966-021/Thermo Fisher
Gibco™ DMEM - high glucose	D1145/Sigma
Gibco™ Fetal Bovine Serum (FBS)	10270-106/Thermo Fisher
Gibco™ GlutaMAX-I (100X)	35050-061/Thermo Fisher
Guanosine 3',5'-cyclic monophosphate (cGMP)	G7504/Sigma
HEPES	HN78.3/Roth
Hydrogen chloride (HCl)	T134/Roth
Isoflurane	103058/Piramal Healthcare
Jedi2	SML2532-5MG/Sigma
LB-Agar	X965.1/Roth
LB-Medium	X964.2/Roth
Low-melting Agarose	BS 20.47.025/Bio&Sell
Magnesium chloride hexahydrate (MgCl <sub>2</sub> x 6H <sub>2</sub> O)	2189.2/Roth
Magnesium sulphate heptahydrate (MgSO <sub>4</sub> x 7H <sub>2</sub> O)	P027.2/Roth
Nitroglycerin/glycerol trinitrate 1mg/ml	Carinopharm
Normal Saline (0.9%)	Rev.03/Fresenius Kabi
Paraformaldehyde (PFA)	P6148/Sigma
PF-04449613	PZ0349/Sigma
Phosphate buffered saline (PBS)	D5652/Sigma
Potassium chloride (KCl)	6781.1/Roth
Potassium dihydrogen phosphate (KH <sub>2</sub> PO <sub>4</sub> )	3904.1/Roth
Probenecid	Cay14981-5/Cayman
REDTaq® ReadyMix™	R2523/Sigma
Roflumilast	A10804/Hözel
S-nitroso-N-acetylpenicillamine (SNAP)	Cay82250/Biomol
Sodium chloride (NaCl)	3957.1/Roth
Sodium dodecyl sulfate (SDS)	L3771/Sigma
Sodium hydrogen carbonate (NaHCO <sub>3</sub> )	6885.2/Roth
Sodium hydroxide (NaOH)	98108.290/VWR
Sodium pyruvate solution	S8636/Sigma
Tamgesic® 1 ml	Indivior
Triethanolamine hydrochloride (TEA/HCl)	T1502/Sigma

*Continued on next page*

Tris 1 M pH8.0 RNasefree	AM9855G/Ambion
Triton® X-100	A4975/AppliChem
TriTrack DNA Loading Dye (6X)	R1161/Thermo Fisher
Trizma® base	T1503/Sigma
Trizma® hydrochloride (Tris-HCl)	T3253/Sigma
Water	W1754-1VL/Sigma

### 3.1.4 Solutions - Buffer - Gels - Cell culture media

**Table 5: List of solutions**

Solution/Buffer	Composition										
<u>LB-Agar plate with Ampicillin</u>	Dissolve 32.0 g of LB-Agar in 1.0 L ddH <sub>2</sub> O Sterilize by autoclaving Cool to 50°C in a temperature-controlled water bath Add 1 ml of 100 mg/ml Ampicillin (Sterile filtered) Homogenize for 2 min on a magnetic stirrer Pour into plates										
<u>Liquid LB-Medium</u>	Dissolve 20.0 g LB-Medium in 1.0 L ddH <sub>2</sub> O Sterilize by autoclaving Cool to RT and store at 4°C → 100 ml with Ampicillin Add 100 µl of 100 mg/ml Ampicillin (Sterile filtered)										
<u>Agarose Gel</u>	→ TAE-Buffer 25X <table> <tr> <td>Trizma Base</td> <td>121.0 g</td> </tr> <tr> <td>Acetic acid</td> <td>28.5 ml</td> </tr> <tr> <td>Na<sub>2</sub>EDTA x 2H<sub>2</sub>O</td> <td>18.6 g</td> </tr> </table> Dissolve in 1.0 L ddH <sub>2</sub> O → TAE-Buffer 1X <table> <tr> <td>TAE-Buffer 25X</td> <td>80.0 ml</td> </tr> </table> Add 3.6 L ddH <sub>2</sub> O Add 200 µl 1% (w/v) Ethidium bromide solution → 1%/ 2% (w/v) Agarose Gel <table> <tr> <td>Dissolve 4.0 g/8.0 g Agarose in 400 ml TAE-Buffer 1X</td> <td></td> </tr> </table> Boil in the microwave and store at 60°C	Trizma Base	121.0 g	Acetic acid	28.5 ml	Na <sub>2</sub> EDTA x 2H <sub>2</sub> O	18.6 g	TAE-Buffer 25X	80.0 ml	Dissolve 4.0 g/8.0 g Agarose in 400 ml TAE-Buffer 1X	
Trizma Base	121.0 g										
Acetic acid	28.5 ml										
Na <sub>2</sub> EDTA x 2H <sub>2</sub> O	18.6 g										
TAE-Buffer 25X	80.0 ml										
Dissolve 4.0 g/8.0 g Agarose in 400 ml TAE-Buffer 1X											

DMEM/10% (v/v) FBS

Add 50.0 ml FBS to 500 ml DMEM (Cat. No. 31966-021)

Phenol red free DMEM

Add 50.0 ml FBS to 500 ml DMEM (Cat. No. D1145)

GlutaMAX-I 5.0 ml

Sodium pyruvate solution 5.0 ml

Transfection Reagent

→ 0.25 M CaCl<sub>2</sub>

Dissolve 18.4 g CaCl<sub>2</sub> x 2H<sub>2</sub>O in 500 ml ddH<sub>2</sub>O

Filter sterile with 0.22 µm (bottle top filter)

→ 2X HEBS (Brian's Mix)

HEPES Acid 10.0 g

NaCl 16.0 g

KCl 0.7 g

Na<sub>2</sub>HPO<sub>4</sub> x 7H<sub>2</sub>O 0.3 g

D(+)-Glucose 2.0 g

10X PBS 10.0 ml

Dissolve in 900 ml ddH<sub>2</sub>O

Adjust pH to 7.09 (with approx. 3 ml 5N NaOH, then with 1 N NaOH exactly to pH 7.09)

Fill up to 1.0 L with ddH<sub>2</sub>O and filter sterile with 22 µm (bottle top filter)

Homogenization buffer (50.0 ml)

(50 mM) NaCl 146.1 mg

(1 mM) EDTA 18.6 mg

(50 mM) TEA/HCl 464.1 mg

Adjust pH to 7.4 with NaOH

Fill up to 50.0 ml with ddH<sub>2</sub>O and store at RT

→ ready-to-use

For 12 dishes, prepared on the day of harvest

Homogenization buffer 4.2 ml

(2 mM) 1 M DTT 8.4 µl

PIC w/o EDTA 1.7 µl

Buffer A (50.0 ml)

(50 mM)	TEA/HCl	464.1 mg
	Adjust pH to 7.4 with NaOH	
	Fill up to 50.0 ml with ddH <sub>2</sub> O and store at RT	
→ ready-to-use	Prepared on the day of measurement	
	Buffer A	3.7 ml
(2 mM)	1 M DTT	7.4 µl
(10 mM)	1 M MgCl <sub>2</sub>	36.8 µl

Base Solution 50X (50.0 ml)

	5 N NaOH	12.5 ml
	0.5 M EDTA	1.0 ml
	ddH <sub>2</sub> O	36.5 ml
→ ready-to-use (1X)	Stock solution 50X	0.5 ml
	ddH <sub>2</sub> O	24.5 ml
	pH 12 (self-adjusting)	

Neutralization Solution 50X (50.0 ml)

	Tris-HCl	15.8 g
	Fill up to 50.0 ml with ddH <sub>2</sub> O	
→ ready-to-use (1X)	Stock solution 50X	0.5 ml
	ddH <sub>2</sub> O	24.5 ml
	pH 5 (self-adjusting)	

HBSS Solution A 10X (1.0 L)

	KCl	4.0 g
	Na <sub>2</sub> HPO <sub>4</sub> x 7H <sub>2</sub> O	0.9 g
	KH <sub>2</sub> PO <sub>4</sub>	0.6 g
	NaHCO <sub>3</sub>	3.5 g
	NaCl	80.0 g
	D(+)-Glucose	10.0 g
	Add ddH <sub>2</sub> O to 1.0 L and adjust pH to 7.4	
	Filter sterile and store at 4°C	

HBSS Solution B 10X (1.0 L)

CaCl <sub>2</sub> x 2H <sub>2</sub> O	1.9 g
MgCl <sub>2</sub> x 6H <sub>2</sub> O	1.0 g
MgSO <sub>4</sub> x 7H <sub>2</sub> O	1.0 g
Fill up to 1.0 L with ddH <sub>2</sub> O and store at 4°C	

HBSS Buffer 1X (ready-to-use)

1 ml Solution A + 1 ml Solution B  
Add 8 ml ddH<sub>2</sub>O and store at 4°C

Imaging buffer (pH 7.4) (1.0 L)

140 mM NaCl	8.2 g
5 mM KCl	0.4 g
1.2 mM MgSO <sub>4</sub> x 7H <sub>2</sub> O	0.3 g
2 mM CaCl <sub>2</sub> x 2H <sub>2</sub> O	0.3 g
5 mM HEPES	1.2 g
Fill up to 1.0 L with ddH <sub>2</sub> O	
Adjust to pH 7.4 with NaOH	
→ 1 M D(+)-Glucose x H <sub>2</sub> O	Dissolve 9.9 g in 50.0 ml ddH <sub>2</sub> O, Store at 4°C
→ ready-to-use	Prepared on the day of measurement
(5 mM)	Add 1 M D(+)-Glucose x H <sub>2</sub> O 5.0 ml

10X KHB stock solution (2.0 L)

→ Solution A (1.0 L)	CaCl <sub>2</sub> x 2H <sub>2</sub> O	7.34 g
	Fill up to 1.0 L with ddH <sub>2</sub> O	
→ Solution B (1.0 L)	KCl	7.46 g
	NaCl	138 g
	MgSO <sub>4</sub> x 7H <sub>2</sub> O	5.42 g
	KH <sub>2</sub> PO <sub>4</sub>	3.26 g
	Fill up to 1.0 L with ddH <sub>2</sub> O	
	Mix Solution A+B for the final stock solution	
	Store at 4°C for about 6 months	
→ ready-to-use (1X) (1.0 L)	Prepared on the day of slicing	
	10X KHB	100 ml
	NaHCO <sub>3</sub>	2.1 g
	D(+)-Glucose x H <sub>2</sub> O	5.0 g
	HEPES	2.4 g
	Fill up to 1.0 L with ice-cold ddH <sub>2</sub> O	

Clearing solution (1.0 L)

(200 mM)	Boric acid	12.36 g
(4% w/v)	SDS	40.0 g
	Fill up to 1.0 L with ddH <sub>2</sub> O	
	Adjust to pH 8.5 with NaOH	

Saturated fructose solution (20 ml)

(80.2%, w/w)	D-Fructose	20.25 g
	Add 5 ml ddH <sub>2</sub> O	
	Heat to 60-70°C (1-4 h completely dissolved)	
(0.5%, v/v)	1-Thiglycerol	100 µl
	Fill up to 20 ml with ddH <sub>2</sub> O	

**3.1.5 Testkits****Table 6: List of testkits**

Kit	Company	Catalog Number/LOT
GeneJET Plasmid Miniprep Kit	Thermo Scientific	K0503/00667076
NucleoBond® Xtra Midi Kit	Macherey-Nagel	740410.100/2206-004
Pierce™ BCA Protein Assay Kit	Thermo Scientific	23225/4F285907

**3.1.6 Genotyping primer****Table 7: List of genotyping primer**

Primer	Orientation:Sequence (5' to 3')	Amplicon size (bp)
Beta globin	F: TGCTCACACAGGATAGAGAGGGCAGG R: GGCTGTCCAAGTGATTCAGGCCATCG	494 → wt
Cre	F: ACCCGACGGTCTTTAGGG R: GCAAACGGACAGAAGCATTT	494 + 269 → tg/wt
Cdh5.cre	F: GCTCGGCCCTGGACAGAC R: GTGAAACAGCATTGCTGTCACTT	494 + 363 → tg/wt
mTmG wt	F: CTCTGCTGCCTCCTGGCTTCT R: CGAGGCGGATCACAAGCAATA	330 → wt 330 + 250 → ht
mTmG tg	R: TCAATGGGCGGGGGTTCGTT	250 → hm

wt\* wildtype, tg\* transgenic, ht\* heterozygous, hm\* homozygous

### 3.1.7 Restriction enzyme and buffer

**Table 8: List of restriction enzymes and buffer**

Enzyme/Cut Site (5' to 3')	Company	Catalog Number/LOT
EcoRI (20.000 U/ml)/(G/AATTC)	BioLabs	R0101S/0331305
NEBuffer™ EcoRI/SspI	BioLabs	B0101S/0704
NEBuffer™ 2.1	BioLabs	B7202S/10029698

### 3.1.8 Online tools/Primer for Sanger Sequencing

Primer design for sequencing: <https://benchling.com> (Benchling, Inc., San Francisco, US)

Oligo synthesis: <https://idtdna.com> (Integrated DNA Technologies, Inc., Coralville, US)

**Table 9: List of primer for Sanger sequencing**

Primer	Orientation:Sequence (5' to 3')
CFP fsp	F:GGCTAACTAGAGAACCCACTGCTTACTGGC
cGMP-BD fsp	F:AGGAGATGTGGGGTCACTGGTGTATGT
YFP Rsp	R:CACCAGCCACCACCTTCTGATAGGC

### 3.1.9 Antibodies

#### Primary:

$\alpha$ -nephrin

→ 1:100, guinea pig, 20R-NP002, Fitzgerald Industries International, Inc., Acton, US

CD31/PECAM-1

→ 1:200, goat, AF3628, R&D Systems, Inc., Minneapolis, US

GFP-Alexa647

→ 1:100, rabbit, A-31852, Thermo Fisher Scientific Inc., Massachusetts, US

#### Secondary:

donkey anti-guinea pig Atto594

→ 1:100, coupled in house

donkey anti-goat Atto594

→ 1:100, coupled in house

## 3.2 Methods

### 3.2.1 *In vitro* characterization of cGi500

The plasmid DNA MH20\_pCMV\_cGi500 (7767 bp) encoding the single-chain cGMP biosensor cGi500 (**Supplemental Figure 1**) was kindly provided by Prof. Dr. Robert Feil from the Interfaculty Institute of Biochemistry (IFIB), University of Tübingen, Germany. To elute the filter paper-spotted plasmid (5 µg) the marked area was excised and 50 µl of Tris (pH 8.0) was added to the 1.5 ml tube. Plasmid release from the filter was provoked by incubation at RT for 1 h followed by storage at 4°C. Verification of the recombinant plasmid construction was completed by Sanger sequencing (Microsynth AG, Balgach, CH, <https://srvweb.microsynth.ch/>).

#### 3.2.1.1 Bacterial transformation with Mini- & Midi preparation

Production of a sufficient quantity of cGi500 for subsequent applications required bacterial transformation with chemically competent cells. DH10B T1 served as the bacterial strain of choice with well-proven transformation efficiency and susceptibility to chemical treatment. After thawing the cells on ice, 50 µl of bacteria were added to 5 µl of plasmid DNA and mixed gently. The mixture was incubated on ice for 30 min and then subjected to a heat shock interval of 45 seconds at 42°C in a water bath. Briefly, after 2 minutes on ice, the transformation was spread onto a 10 cm LB-Agar plate containing Ampicillin (decontaminate). The dried plate was incubated at 37°C overnight. Only cells harboring the plasmid form single colonies and were picked in the afternoon for inoculation of 3 ml liquid LB-Medium with Ampicillin for a starter culture ("mini culture"). Incubation at 37°C for approximately 12-16 h hours with shaking at 250-300 rpm maintained bacterial growth with enriched cell number and high yields of plasmid DNA. The plate was sealed with parafilm and stored with the lid down at 4°C. Plasmid harvest and purification was performed using the GeneJET Plasmid Miniprep Kit according to the manufacturer's instructions with elution in 50-100 µl elution buffer (10 mM Tris-HCl, pH 8.5). Purified plasmid DNA was quantified using the NanoDrop 1000 Spectrophotometer with subsequent storage at 4°C.

A mini digest was prepared to confirm the vector construction prior to sequencing. The restriction enzyme digest was composed of 10 µl miniprepped plasmid DNA (111.2 ng/µl) along with 1 µl enzyme EcoRI + 1.5 µl NEBuffer 2.1 (10X) and filled up to 15 µl with ddH<sub>2</sub>O. The digest mixture was incubated for 30 min at 37°C in the heating block and then centrifuged for a few seconds. Virtually digested and experimentally confirmed by a 1% (w/v) agarose gel, DNA Ladder GeneRuler 1 kb, 2 µl Loading dye and electrophoresis (80 V, 400 mA, 45 min), the result consists of two DNA fragments with a length of 5433 bp and 2334 bp.



Following confirmatory Sanger sequencing with the designed primer named CFP fsp, cGMP-BD fsp, YFP Rsp, the residue of the mini culture was used to increase the yield of isolated plasmid DNA. For this purpose, 4 g LB-Medium was dissolved in 200 ml ddH<sub>2</sub>O, 200 µl of 100 mg/ml Ampicillin was added and the solution was inoculated in the afternoon. The Midi preparation was incubated in a sterile 500 ml Erlenmeyer flask overnight at 37°C with 90-120 rpm in a shaking incubator. The application of the NucleoBond™ Xtra Midi Kit according to the manufacturer's instructions completed the purification of the plasmid. Purified plasmid DNA was quantified using the NanoDrop 1000 Spectrophotometer with subsequent storage at 4°C. Eluates were diluted if the value exceeded the upper measurement range of 3000 ng/ul.

### **3.2.1.2 HEK 293T cell transient transfection and harvest**

HEK 293T cells cultured in Dulbecco's Modified Eagle Medium (DMEM) (Cat. No. 31966-021) with 10% fetal bovine serum (FBS) were splitted 1:6 in 12 x 10-cm dishes the day before transfection. On the day of transfection, 500 µl of CaCl<sub>2</sub> was added to a 1.5 ml tube for each experimental point together with 5 µg cGi500 DNA (Midi prep). While vortexing, 500 µl of 2X HEBS was added dropwise into the diluted DNA with additional 5 sec of vortexing. For each dish, 980 µl of DNA solution was added dropwise onto the cells, then the plate was moved from top to bottom and from right to left to distribute the DNA solution evenly. The cells were incubated at 37°C in a CO<sub>2</sub> incubator starting from 10 am with replacing the present medium after 7 h by 8 ml of phenol red free DMEM (Cat. No. D1145) supplemented with 10% FBS, 1% GlutaMAX-I and 1% Sodium pyruvate solution.

Two days after transfection: Dishes showing a cell confluency of 80-95% and a transfection rate of 90-95% were further processed according to the protocol published by Russwurm et al.<sup>139</sup> Transfected cells from a 10-cm dish (1x10<sup>7</sup> cells) were harvested and lysed. All preparation steps were performed on ice. After the dishes were washed twice with ice-cold 5 ml of sterile PBS, 300 µl of freshly prepared homogenization buffer (pH 7.4, ice-cold) was added. Following cell scraping, the lysate (approximately 600 µl) was transferred to sterile 1.5 ml tubes and subsequently sonicated (5 sec ON, 30 sec OFF, 1 cycle) and ultracentrifuged (100,000 g for 30 min at 4°C). The supernatant was transferred to brown 1.5 ml tubes and stored at - 20°C.

### **3.2.1.3 Bicinchoninic acid (BCA) assay**

The quantitative protein determination was performed with the Pierce™ BCA Protein Assay Kit. Components of the homogenization buffer (50 mM TEA/HCl, 2 mM DTT) are listed as interfering factors in the compatibility table for the protein assay and influence the determined protein concentration due to their metal chelating properties. Consequently, the ratio of BCA

reagent A to B was adjusted from 50:1 to 50:5 in the preparation of the BCA working reagent (WR). According to the manufacturer's instructions, the microplate procedure involved the addition of 200  $\mu$ l of WR (50:5/A:B) to 10  $\mu$ l of sample replicate (cGi500 cytosolic fractions) in a 96-well F-bottom plate, followed by 30 sec on a plate shaker and 30 min of incubation at 37°C. For another 15 min the plate was kept at RT followed by absorbance measurement at 562 nm on the EnSpire Multimode Plate Reader.

#### **3.2.1.4 Live-cell imaging of cGi500-transfected HEK 293T cells**

HEK 293T cells cultured in DMEM/10% (v/v) FBS were splitted 1:6 in 10-cm dishes the day before the cells were washed with 1X PBS and trypsinized with 1 ml for 5 min at 37°C. Trypsin inactivation was achieved by adding 9 ml of pre-warmed supplemented phenol red free DMEM. The cell suspension was diluted (1 ml + 4 ml supplemented phenol red free DMEM) and sub-cultivated in  $\mu$ -Slide 8 Well (ibiTreat) chambers. The next day, the cells were transfected as described in chapter 3.2.1.2 using 150 ng cGi500 DNA with media exchange after 6 h. One day later, the experiment was performed by exchanging the medium with freshly prepared imaging buffer (RT) and incubating the cells for 20 min. Administration of isobutylmethylxanthine (IBMX, stock: 10 mM dissolved in DMSO), a cGMP-enhancing compound, was performed by pipetting 50  $\mu$ l of a 600  $\mu$ M predilution directly into the imaging-buffer filled IbiWell (250  $\mu$ l). Time-lapse images were captured every 2 sec with a confocal microscope (LSM Meta 710, Inverse, Axio Observer, Carl Zeiss AG) equipped with a Plan-Apochromat 20x/0.8 M27 objective (Zeiss) in conjunction with ZEN 2009 (Zeiss). Donor fluorophore (CFP) excitation was performed at 405 nm together with a dichroic beam splitter (MBS-405) and simultaneous detection of CFP and YFP emission at  $480 \pm 25$  nm and  $535 \pm 20$  nm. Intensity changes in the 512 x 512 x 16-bit emission images (mean fluorescence intensity) were offline analyzed to calculate the baseline-normalized CFP/YFP emission ratio ( $\Delta R/R_0$ ) reflecting cGMP concentration changes.

#### **3.2.2 Mouse lines**

Animals were housed according to standardized specific pathogen-free conditions in CECAD's *in vivo* research facility (ivRF). Kept in individually ventilated cage systems (IVC cages type II long) with centrally monitored light periodicity (light/dark cycle 12h/12h,  $55 \pm 10\%$  humidity,  $22 \pm 2^\circ\text{C}$  room temperature), they had access to standard rodent chow and tap water *ad libitum*. The experimental procedures were evaluated and approved by the State Agency for Nature, Environment and Consumer Protection North Rhine-Westphalia (Landesamt für Natur, Umwelt und Verbraucherschutz Nordrhein-Westfalen (LANUV NRW) VSG 81-02.04.2018.A351 and 4.18.023).

The 'floxed' cGi500 sensor line Gt(ROSA)26Sor<sup>tm1(CAG-ECFP/EYFP\*)</sup>Feil (mixed background 129 SV, C57BL/6N, C57BL6/NRj >70%) was provided by Prof. Dr. Robert Feil from the Interfaculty Institute of Biochemistry (IFIB), University of Tübingen, Germany and generation was described previously.<sup>140</sup> Cell-specific Cre-driver mouse lines were leveraged for crossbreeding to achieve cytosolic cGi500 biosensor expression in podocytes (Pod:Cre line<sup>144</sup> resulting in Pod:Cre/cGi500) or endothelial cells (Tie2:Cre line<sup>145</sup> or Cdh5:Cre line<sup>146</sup> resulting in Tie2:Cre/cGi500 or Cdh5:Cre/cGi500). Experiments were performed with Pod:Cre/cGi500 mice carrying two cGi500 alleles, whereas Tie2:Cre/cGi500 or Cdh5:Cre/cGi500 mice carried one cGi500 allele. Reported nonspecific recombination in the F2 generation of Tie2:Cre mice restricted its use to the F1 generation.<sup>147,148</sup> To exclude gender-specific variations, mice of both sexes were used at 8-27 weeks of age.

### **3.2.2.1 Genotyping**

#### **3.2.2.1.1 HotSHOT DNA preparation**

The ear puncture of the laboratory mice *Mus musculus* served as identification and tissue sampling for the preparation of genomic DNA using HotSHOT.<sup>149</sup> The biopsy material stored at -20°C was mixed with 75 µl base solution (alkaline lysis reagent) and incubated at 95°C for 30 min. Cooled to 4°C-10°C, the same amount of neutralization solution was added with final vortexing.

#### **3.2.2.1.2 Setup of polymerase chain reaction (PCR)**

To prepare the PCR reaction, the REDTaq® ReadyMix™ PCR reaction mix was used according to the manufacturer's instructions with the addition of the specific primers listed in section 3.1.6. Gel electrophoresis at 120 V, 400 mA for 45 min in combination with a 2% (w/v) agarose gel was used to separate PCR products (12 µl/sample) according to their fragment length in base pairs.

**Table 10: PCR and cycling conditions**

Reaction composition	Cycling conditions
<p><b>ROSA26</b></p> <p>5 µl ddH<sub>2</sub>O</p> <p>1 µl mTmG wt_F (10 µM)</p> <p>1 µl mTmG wt_R (10 µM)</p> <p>1 µl mTmG tg_R (10 µM)</p> <p>10 µl REDTaq®</p> <p>2 µl DNA</p>	<p><b>ROSA26</b></p> <p>94°C 3 min</p> <p>94°C 30 sec</p> <p>61°C 60 sec</p> <p>72°C 60 sec</p> <p>goto step 2,</p> <p>repeat 35 times</p> <p>72°C 120 sec</p> <p>10°C for ever</p>
<p><b>CRE</b></p> <p>5 µl ddH<sub>2</sub>O</p> <p>1 µl Beta globin_F (10 µM)</p> <p>1 µl Beta globin_R (10 µM)</p> <p>1 µl Cre_F (10 µM)</p> <p>1 µl Cre_R (10 µM)</p> <p>10 µl REDTaq®</p> <p>2 µl DNA</p>	<p><b>CRE</b></p> <p>94°C 3 min</p> <p>94°C 45 sec</p> <p>59°C 60 sec</p> <p>72°C 45 sec</p> <p>goto step 2,</p> <p>repeat 30 times</p> <p>72°C 10 min</p> <p>10°C for ever</p>
<p><b>Cdh5</b></p> <p>5 µl ddH<sub>2</sub>O</p> <p>1 µl Beta globin_F (10 µM)</p> <p>1 µl Beta globin_R (10 µM)</p> <p>1 µl Cdh5.cre_F (10 µM)</p> <p>1 µl Cdh5.cre_R (10 µM)</p> <p>10 µl REDTaq®</p> <p>2 µl DNA</p>	<p><b>Cdh5</b></p> <p>94°C 3 min</p> <p>94°C 30 sec</p> <p>58°C 30 sec</p> <p>72°C 45 sec</p> <p>goto step 2,</p> <p>repeat 35 times</p> <p>72°C 5 min</p> <p>15°C for ever</p>

### 3.2.2.2 Isolation of mouse glomeruli

Isolation of mouse glomeruli was prepared according to the protocol of Takemoto et al.<sup>150</sup> Modifications started with euthanizing the animals directly by cervical dislocation without prior anesthesia. The kidneys were removed from the abdomen with all connected vessels including the aorta and stored intermediately in ice-cold HBSS (Hank's Balanced Salt Solution) buffer. After removal of muscle tissue and fat, the aorta was longitudinally incised to allow insertion of a 27G needle into the renal artery. This enabled perfusion with Dynabeads M-450 tosyl-activated, bead size  $\phi$  4.5 µm (20 µl/ml HBSS) followed by removal of the kidney capsule. Cutting the kidney into small pieces preceded digestion with Collagenase IA (1 mg/ml) at 37°C for 20 min with gentle shaking. After digestion, the tissue-solution mixture was homogenized using a 1000 µl pipette tip (tip cut off) and transferred to a 100 µm filter (sitting on top of a 50 ml Falcon on ice). The tissue was gently pushed through the filter with the cone of a 5-ml syringe, interspersed with several washes with 3-5 ml of ice-cold HBSS buffer. This procedure was repeated with a second 100-µm filter before the flow-through was loaded into several 1.5-ml tubes placed in the DynaMag™-2 Magnet. The magnetic beads in the capillary loops of the glomeruli cause adhesion to the magnet so that the remaining eluate can be removed. After

removal of the magnet, the isolated glomeruli are pooled in 1 ml HBSS buffer in a 1.5 ml tube and stored on ice under exclusion of light for further use. In order to keep the quality of the isolation constant and to identify possible sources of error, the time of sacrifice, the end of isolation as well as the quality of perfusion were noted.

#### **3.2.2.2.1 Poly-L-lysine coating**

Immobilization of isolated glomeruli for real-time imaging was performed by coating coverslips ( $\emptyset$  18 mm, #1.5) with a 0.1% (w/v) poly-L-lysine solution (dropwise applied) for 15 min in a large petri dish. After incubation, the coverslips were washed three times with ddH<sub>2</sub>O, placed on a tissue paper to dry, and sterilized under UV light (15 min). After transferring to the large petri dish and sealing with the lid, the coated coverslips were stored at RT.

#### **3.2.2.2.2 Custom-built imaging chamber and perfusion system**

Real-time imaging requirements were met by fabricating an imaging chamber that allows insertion of coverslips ( $\emptyset$  18 mm, #1.5) with an interfaced perfusion system. The construction of the imaging chamber and the microscope stage insert (**Figure 5**) was realized in cooperation with the Zentrale Wissenschaftliche Werkstatt of the Medical Faculty, University of Cologne. The complete superfusion system is shown in **Figure 5D**, demonstrating where the side ports of the microscope stage insert will be connected:

- (1) Original Perfusor® Line, Type: IV Standard-PE
- (2) Masterflex®, Peroxide-Cured Silicone Tubing; L/S 13
- (3) Masterflex® L/S® peristaltic pump (Cat. No. 07555-15) with Masterflex® L/S® Easy-Load® II
- (4) The tubing end of the Original Perfusor® Line inserted in 1 ml Stripette®

The setup allowed image acquisition while the submerged glomeruli were continuously rinsed with buffer or stimulants/inhibitors. Restriction of flow to one spot in the center of the coverslip resulted in consistent exposure of chemicals. Therefore, immobilization of the glomeruli on the poly-L-lysine coated coverslips was a critical necessity.



**Figure 5: Custom-built imaging chamber and perfusion system for real-time imaging of isolated glomeruli**

(A) Closed imaging chamber. (B) Upper ring (left) and lower ring with coverslip cavity (right). (C) Microscope stage insert (pink) with yellow inlet and outlet needle functioning as side ports for fluid exchange. (D) Assembled superfusion system.

### 3.2.2.2.3 Real-time imaging of isolated glomeruli

Prior to FRET measurements, the tubing of the assembled superfusion system was flushed with 70% EtOH and freshly prepared imaging buffer (RT). Isolated glomeruli (10  $\mu$ l) from Pod:Cre/cGi500 mice were positioned centrally onto the submerged coated coverslip, allowing them to stick onto the surface for about 5 min. To obtain a stable baseline, the cGi500-expressing glomeruli were superfused for 5 min with imaging buffer (flow rate: 1 ml/min). Images were captured every 2 sec, recording 40 frames for baseline, followed by drug exposure (frame 40 to 305) and wash-out with imaging buffer (RT) until 570 frames were acquired. FRET/cGi500 imaging was performed with a confocal microscope (LSM Meta 710, Inverse, Axio Observer, Carl Zeiss AG) equipped with a Plan-Apochromat 20x/0.8 M27 objective (Zeiss) in conjunction with ZEN 2009 (Zeiss). Donor fluorophore (CFP) excitation was performed at 405 nm together with a dichroic beam splitter (MBS-405) and simultaneous

detection of CFP and YFP emission at  $480 \pm 25$  nm and  $535 \pm 20$  nm. Intensity changes in the 512 x 512 x 16-bit emission images (mean fluorescence intensity) were offline analyzed to calculate the baseline-normalized CFP/YFP emission ratio ( $\Delta R/R_0$ ) reflecting cGMP concentration changes.

Real-time imaging of acute kidney slices is described in detail in **chapter 5.2.6**.

### **3.2.2.3 Intravital imaging (IVI)**

Pod:Cre/cGi500 mice (3-4 weeks old) were prepared for intravital imaging according to the procedure published by Binz-Lotter et al.<sup>151</sup> Anesthetized/analgesized with isoflurane/buprenorphine (0.05 mg/kg), the mouse was fixed on the temperature-controlled surgery stage and underwent catheterization (Polyethylene tubing (PE10), Braintree Scientific, Cat. No. B-PE-10-100FT) of the right carotid artery through a longitudinal incision (**Figure 6**). The mouse was repositioned, shaved at the incision site to exteriorize the kidney and subsequently immobilized in a custom-build kidney holder (Medres, medical research company GmbH) for imaging. Intravital imaging was performed using an upright multiphoton microscope (TCS SP8 MP-OPO, DM 6000 CFS, Leica Microsystems) with an IR Apo L25x/0.95 W objective (Leica) in conjunction with LAS X (Leica software). Biosensor excitation was performed at 860 nm together with a YFP/DsRed (BP 535/30) filter and simultaneous detection of CFP and YFP emission at 467-499 nm and 500-550 nm (HyD-RLD detector) with following settings: 1000 Hz, Bidirectional ON, Line Average 2. Blood circulation was labeled with 70 kDa Texas Red dextran dissolved in 0.9% NaCl.

Intensity changes in the 512 x 512 x 16-bit emission images (mean fluorescence intensity) were offline analyzed to calculate the baseline-normalized CFP/YFP emission ratio ( $\Delta R/R_0$ ) reflecting cGMP concentration changes.

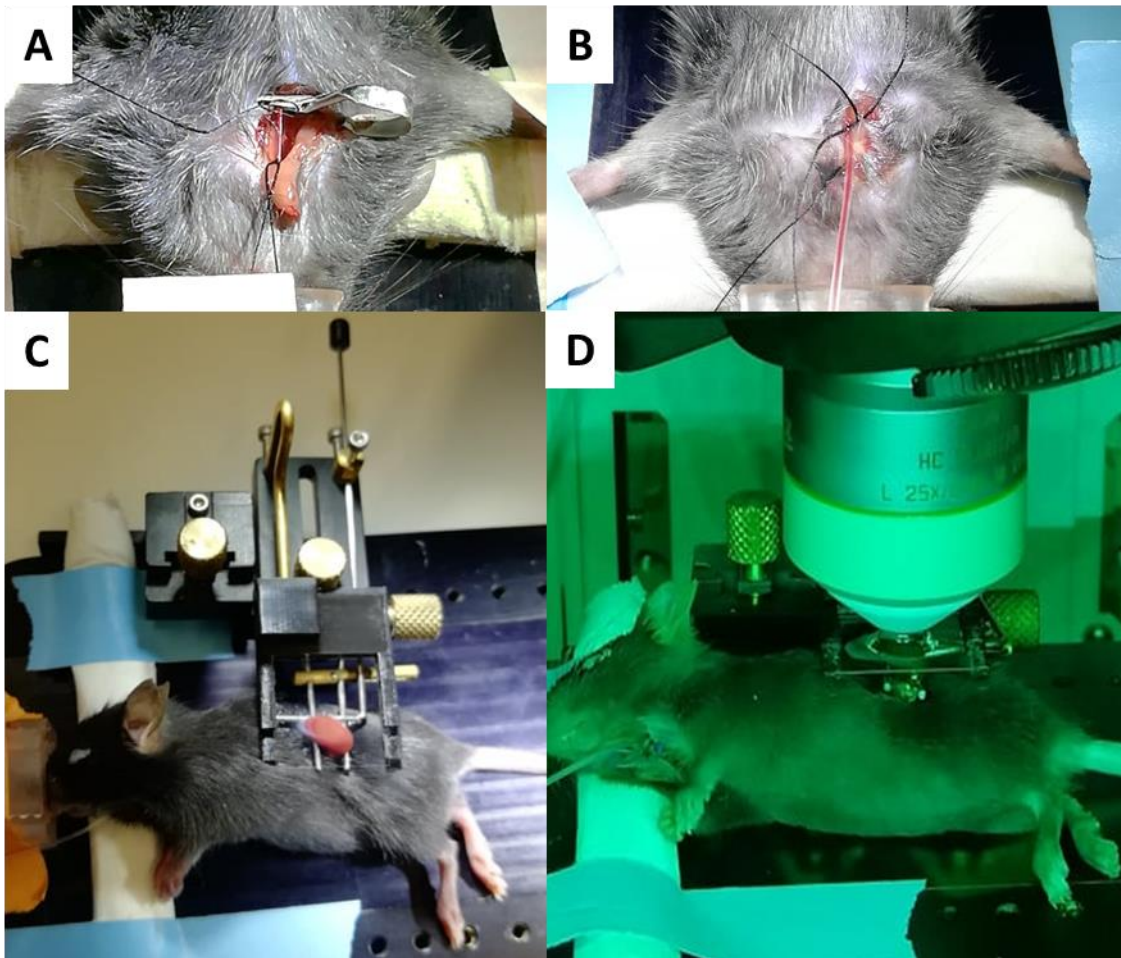


**Figure 6: Surgery procedure for intravital imaging**

(A) Isolation of the right carotid artery with caudal occlusion (clamp) and cranial blockage by a knot. (B) Successful catheterization was evidenced by the inflow of blood into the PE hose filled with saline solution. The catheter was secured by an additional knot around the artery. (C) Immobilized kidney clamped in the custom-build holder with positioned coverslip. (D) Mouse placed under the upright microscope awaiting injection of the test substance through the inserted catheter.

### 3.3 Analysis pipeline

Data analysis was conducted using ImageJ/Fiji (NIH) and Excel (Microsoft Corporation).

#### 3.3.1 Selection

**HEK 293T cells:** Analyzed cells of the FRET/cGi500/HEK 293T imaging data were selected based on cell morphology, sensor localization (homogeneously distributed, no bright spots) and fluorescence brightness (avoidance of dim and very bright cells).

**Isolated glomeruli:** Due to the separation process, isolated glomeruli are subjected to mechanical forces that lead to cell detachment. Only glomeruli with preserved integrity and



minor structural changes were analyzed. The possibility of damaged cells within this cell cluster cannot be excluded.

**Acute kidney slices (AKS):** Glomeruli damaged by the cutting process of AKS display noticeable morphological changes, which are evident in the form of swollen and rounded cellular structures (**Figure 7**). ROIs (whole glomeruli) exhibiting increased intensity in the Evans Blue detection channel were excluded from the analysis due to the azo dye's ability to permeate through ruptured membranes, resulting in cellular staining.

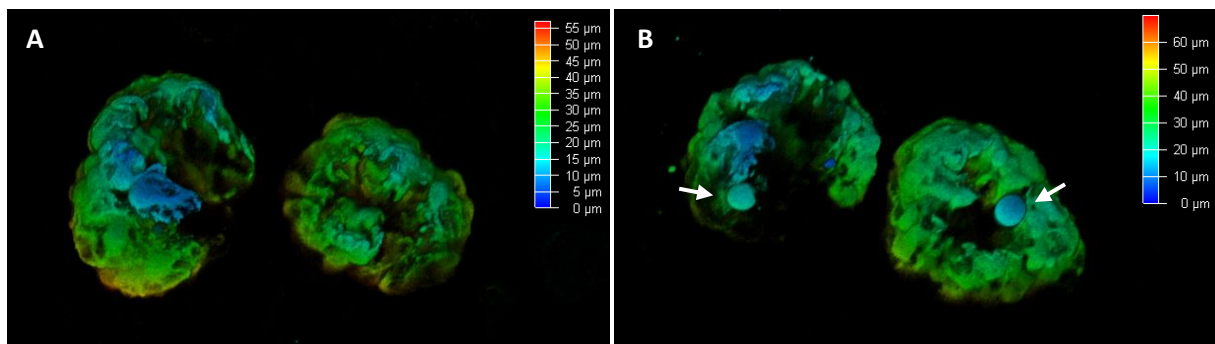


**Figure 7: Identification of damaged cells in glomeruli close to the cutting surface**

Representative images of glomeruli identified as undamaged (**A**) or damaged (**B**, white arrows) by their morphology using Z-stack depth coding.

**IVI:** Intravital imaging was performed on superficial glomeruli due to the limitations associated with multiphoton microscopy in terms of tissue penetration depth caused by high cellular heterogeneity of the kidney.

### 3.3.2 Line scan analysis – Intensity profile plot

Evidence of pixel-precise alignment of the acquired CFP and YFP images is particularly important for ratiometric time-lapse FRET analysis and indicates colocalization of the two fluorophores, functional basis of the intramolecular FRET biosensor.

- ImageJ commands

Load raw data>Select line width tool \*Straight\*>Select line width>Add line to ROI Manager

Image>Color>Split Channels

Analyze>Plot Profile for CFP and YFP channel>Data>Save data (Excel)>Normalize to highest value

### 3.3.3 CFP/YFP Ratio images

The changing FRET ratio (CFP/YFP) served as an index of the cGMP increase in HEK 293T cells after IBMX administration and was visualized according to the protocol published by Kardash et al. with minor modifications.<sup>152</sup>

- ImageJ commands

Load raw data>ROI selection for Crop>Crop both channels: Image>Crop>Image>Color>Split Channels

32-Bit conversion (necessary for thresholding): For both channels: Image>Type>32 bit

Threshold (Only for YFP image): Image>Adjust>Threshold>Select Default, B&W, Dark Background>Press Apply>Set to NaN

Ratio CFP/YFP: Plugins>Ratio Plus>CFP image for image 1, YFP image for image 2

Pseudo-color (Lookup Tables): Click on the new Ratio image: Image>Lookup table>Green Fire Blue>Analyze>Tools>Calibration bar

Scale bar: Analyze>Tools>Scale bar

### 3.3.4 Movement correction (Galene)

Raw imaging data from real-time measurements of AKS and IVI were processed with the open-source package Galene.<sup>153</sup> Sample motion was corrected with realignment mode: Warp, points: 10.

### 3.3.5 Image segmentation

The image segmentation approach published by Thunemann et al. was applied to IVI data to visualize FRET changes evoked by the binding of cGMP to cGi500 *in vivo*.<sup>142</sup>

### 3.3.6 Calculation of baseline-normalized CFP/YFP ratio ( $\Delta R/R_0$ )

For FRET/cGi500 imaging data selected ROIs (region of interest) defined a whole cell (HEK 293T) or a single glomerulus (isolated glomeruli, AKS, IVI). The  $CFP_{ROI(t)}$  and  $YFP_{ROI(t)}$  emission intensities from the time-laps recordings were extracted and saved (Excel) followed by baseline normalization (HEK 293T, AKS, IVI: 0-20 frames, Isolated glomeruli: 0-40 frames) leading to  $\Delta F/F_0$  values (formula not shown). Prior to baseline normalization, division of  $CFP_{ROI(t)}$  by  $YFP_{ROI(t)}$  resulted in CFP/YFP emission intensity ratios reflecting cGMP concentration changes as  $\Delta R/R_0$  (**Formula 1-3**).

CFP/YFP emission intensity ratio  $R(t) = \frac{CFP_{ROI(t)}}{YFP_{ROI(t)}} \quad (1)$

Baseline normalization  $R_0 = \frac{1}{n} \sum_{t_0}^{t_1} R(t) \quad (2)$

%Single change relative to baseline  $\frac{\Delta R}{R_0} = \frac{R(t) - R_0}{R_0} \times 100\% \quad (3)$

(t) Time dependency

(n) Obtained baseline frames: 20 or 40

(t<sub>0</sub> to t<sub>1</sub>) Ratio values during the baseline period (20 or 40 frames)

### 3.4 Statistics

Statistics were performed using GraphPad Prism 10.1.0 (Graphpad Software, Inc.) utilizing a paired, two-tailed Student's t-test or One-way ANOVA (Tukey's post hoc test or Dunnett T3, Šídák's multiple comparisons test) to assess differences between groups. Differences between groups were considered statistically significant if  $p < 0.05$  (P value style "GP"). Results are reported as mean  $\pm$  standard error of the mean (SEM). Figure legends indicate the number of animals used.

## 4 Results

### 4.1 Functional cGMP biosensor (cGi500) expression in HEK 293T cells

For the systematic characterization of the FRET-based ratiometric biosensor, HEK 293T cells were used as a cellular tool. Based on horizontal gene transfer, the plasmid MH20\_pCMV\_cGi500 (7767 bp) encoding the single-chain cGMP biosensor cGi500 was successfully transfected into the host cells, leading to recombinant protein expression. Sanger sequencing and restriction enzyme digestion verified the recombinant plasmid sequence and matched the expected results of the virtual EcoRI digest, resulting in 2334 bp and 5433 bp long fragments (**Figure 8A**). Transfected adherent HEK 293T cells exhibited homogenous expression of the cGMP biosensor, primarily within the cytosolic region. Following donor fluorophore (CFP) excitation of the FRET construct at 405 nm, the cGMP equilibrium was visualized by simultaneous emission detection of CFP and YFP at  $480 \pm 25$  nm and  $535 \pm 20$  nm (**Figure 8B**). For the subsequent functional validation of the sensor, pixel-precise alignment of the emission FRET images was a fundamental component, as deviations can lead to a weaker FRET response based on the calculated %signal change from CFP/YFP emission ratios. The line scan analysis involved averaging pixels along a designated line (width: 15 pixels), which extended diagonally across the cell periphery through the soma. The intensity profiles of CFP and YFP were normalized to the highest value and were superimposed, confirming the absence of misalignment (**Figure 8C**).

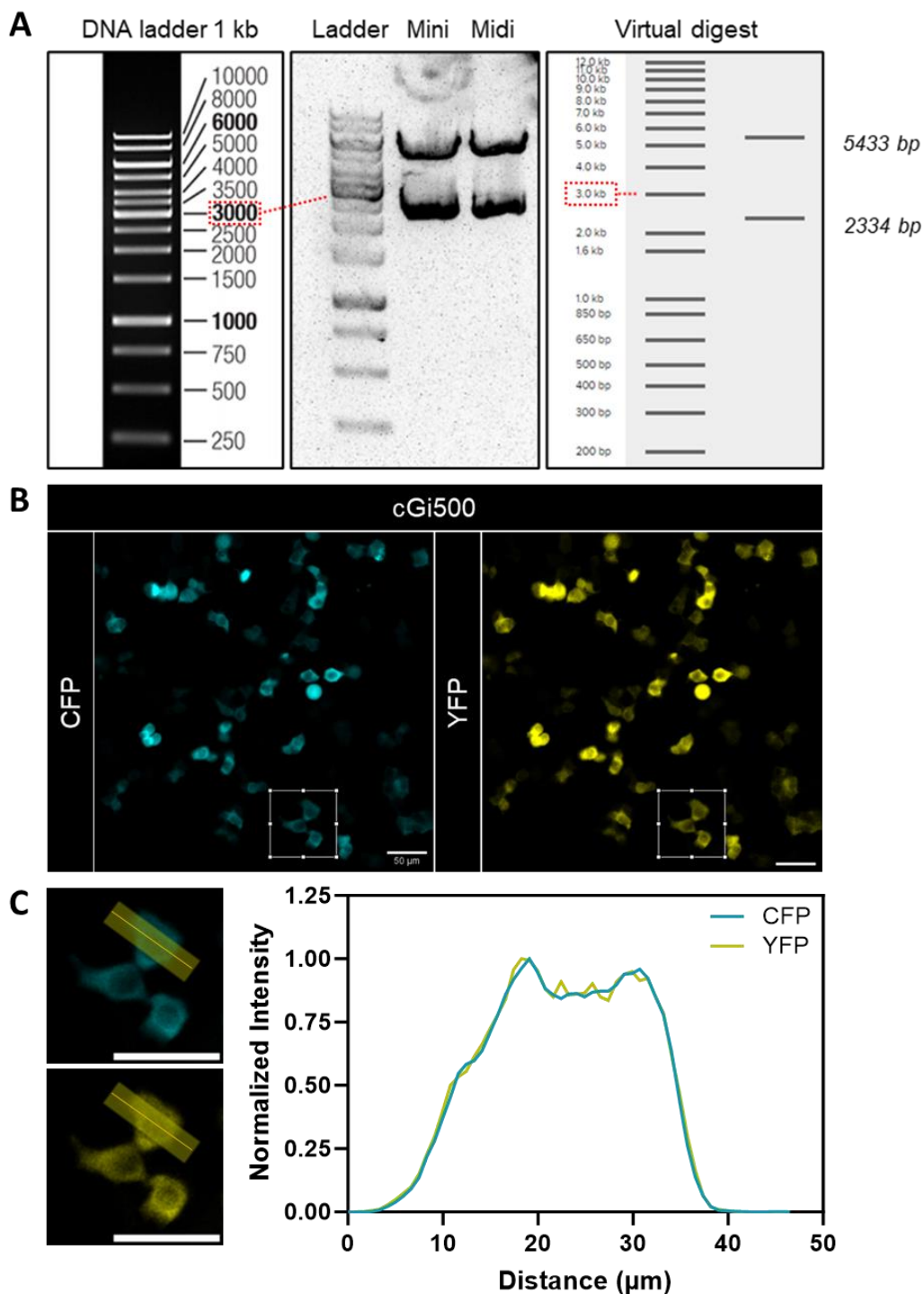


**Figure 8: cGi500 biosensor expression in HEK 293T cells**

(A) EcoRI restriction enzyme digest of mini- & midiprep plasmid DNA encoding cGi500 and virtual digest performed with the online tool Benchling. DNA ladder GeneRuler 1 kb (Figure origin: reference <sup>154</sup>). (B) Representative low-magnification confocal fluorescence images of cGi500-expressing HEK 293T cells. The CFP donor fluorophore is depicted in cyan, while the YFP acceptor fluorophore is represented in yellow. (C) Zoomed inset with diagonally positioned scan line across the cell and corresponding intensity profile plots of CFP and YFP (data was normalized to the highest value). Scale bar: 50  $\mu$ m.

The working principle of the FRET construct was tested through the administration of IBMX, a nonspecific phosphodiesterase (PDE) inhibitor. This substance inhibits endogenous PDE isoforms responsible for cGMP hydrolysis, which results in the accumulation of intracellular cGMP. Time-lapse recordings for live cell imaging of cGi500-transfected HEK 293T cells included acquisition of a stable baseline followed by IBMX exposure, resulting in antiparallel changes in emission intensity of the donor and acceptor fluorophore in response to cGMP accumulation (**Figure 9A**). In particular, the interaction of cGMP with the indicator protein of the sensor (tandem cGMP-binding sites from bovine cGMP-dependent protein kinase type I) positioned between CFP and YFP prompts a conformational change, resulting in a reduction in FRET efficiency. This manifests as an increase in CFP emission and a concurrent decrease in YFP emission. The baseline-normalized CFP/YFP emission ratios ( $\Delta R/R_0$ ) reflect changes in cGMP concentration. Upon the direct addition of IBMX to the imaging buffer-filled well, a rapid increase in cGMP levels was initially observed. However, by the end of the measurement, the response flattened due to the distribution of the added substance (**Figure 9A**). CFP/YFP ratio images visualized changes in subcellular cGMP dynamics after IBMX administration (**Figure 9B**).

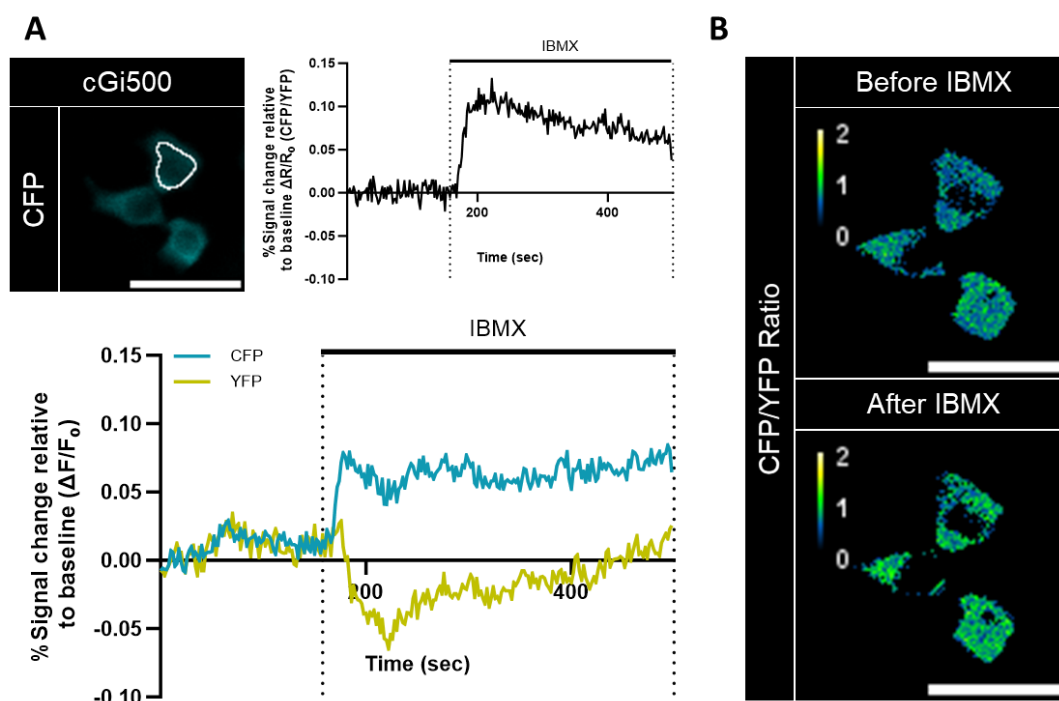


**Figure 9: IBMX-induced cGMP accumulation in cGi500-transfected HEK 293T cell**

(A) Representative CFP emission image of cGi500-expressing HEK 293T cells with superimposed ROI (white). Time-lapse recordings represent baseline-normalized emission intensity changes of the individual CFP (cyan) and YFP (yellow) traces ( $\Delta F/F_0$ ) or the CFP/YFP ratio (black,  $\Delta R/R_0$ ) upon IBMX administration (50  $\mu$ l of 600  $\mu$ M IBMX stock = final concentration 100  $\mu$ M) starting at 160 sec. (B)

CFP/YFP ratio image at frame 5 (10 sec, before IBMX) and frame 120 (240 sec, after IBMX) visualizes an increased FRET response after IBMX administration reflecting intracellular cGMP accumulation. Scale bar: 50  $\mu$ M.

## 4.2 Targeting the NO/sGC/cGMP and NP/pGC/cGMP axis

Transgenic mice expressing the cGMP biosensor exclusively in the cytosol of podocytes (Pod:Cre/cGi500) were euthanized to prepare isolated glomeruli (**Figure 10A**). Line scan analysis across the glomerulus, the branched capillary system, demonstrated the colocalization of the donor and acceptor fluorophore with pixel-precise alignment (**Figure 10B**). A superfusion system facilitated the introduction and removal of test substances, enabling real-time observation of their impact on cGMP signaling due to changes in FRET signal intensity. The isolated glomeruli were superfused with imaging buffer for an 80-second baseline recording followed by the stimulation with test compounds (530 sec) and subsequent wash-out. Regarding the NP/pGC/cGMP axis, the natriuretic peptides ANP and BNP served as ligands for the natriuretic peptide receptors GC-A or GC-B. To stimulate the NO/sGC/cGMP axis, the widely used NO donor SNAP was administered. Its NO-releasing property was induced 10 minutes before the start of measurements by adding the stock solution directly into the imaging buffer (pH 7.4, ambient temperature). All test substances provoked an increase in intracellular cGMP concentration, suggesting the presence of both guanylyl cyclase systems (pGC and sGC) in podocytes (**Figure 10E**). However, ANP induced a stronger response compared to BNP and was chosen for further experiments. The cGMP synthesis induced by SNAP exhibited the most pronounced FRET change in comparison to all other tested substances. Co-stimulation of ANP+SNAP did not demonstrate an additive effect in podocytes, indicating a reciprocal interaction between cGMP-synthesizing systems.

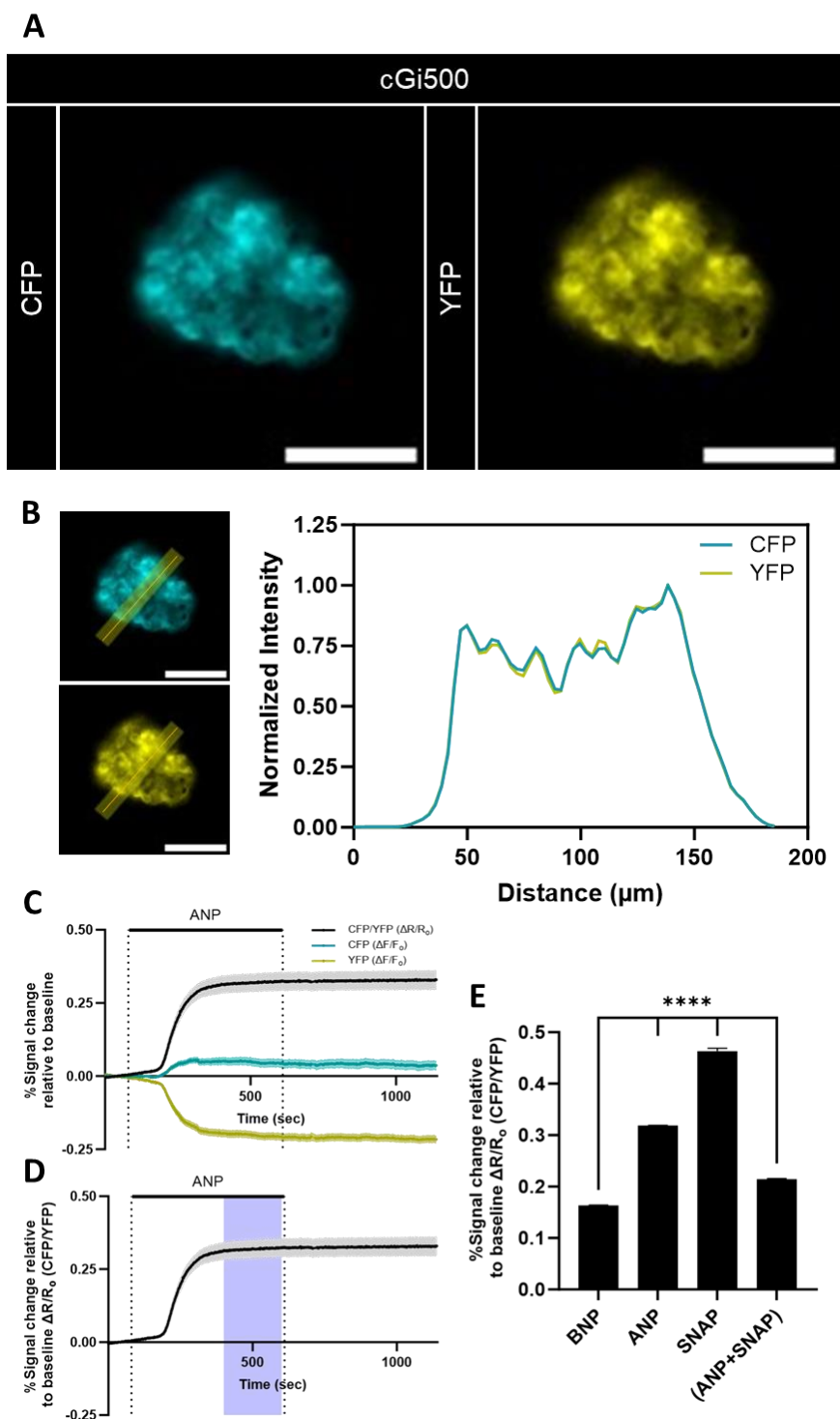


**Figure 10: NP/pGC and NO/sGC induced cGMP synthesis in isolated glomeruli**

(A) Representative confocal fluorescence images of a glomerulus isolated from a transgenic mouse kidney expressing the cGMP biosensor in podocytes (Pod:Cre/cGi500). The CFP donor fluorophore is depicted in a cyan color, while the YFP acceptor fluorophore is represented in yellow. (B) Depiction of the diagonally positioned scan line across the whole glomerulus and corresponding intensity profile plots of CFP and YFP (data was normalized to the highest value). Scale bar: 100  $\mu\text{m}$ . (C) Time-lapse recordings represent baseline-normalized emission intensity changes of the individual CFP (cyan) and YFP (yellow) traces ( $\Delta F/F_0$ ) and the CFP/YFP ratio (black,  $\Delta R/R_0$ ) upon administration of 500 nM ANP



from 80 sec to 610 sec (dotted line). **(D)** Analysis interval (400-600 sec) used in **(E)** is shown in color. **(E)** Bar graphs display the averaged FRET response ( $\Delta R/R_0$ ) for the analysis interval (purple) shown in **(D)**. Data represent mean  $\pm$  SEM after administration of 500 nM BNP (n=21 of 5 mice), 500 nM ANP (n=20 of 3 mice), 250  $\mu$ M SNAP (n=20 of 5 mice) and (500 nM ANP+ 250  $\mu$ M SNAP) (n=28 of 3 mice). One-way ANOVA (Šídák's multiple comparisons test). \*P < 0.05

### 4.3 Investigation of cellular biokinetics of cGMP from synthesis to export

The presence of sGC in podocytes is debated due to inconsistencies in data from different species (mouse,<sup>29</sup> rat,<sup>155</sup> human<sup>80,90</sup>). To ensure that SNAP-induced cGMP synthesis, mediated by NO release and sGC activation in podocytes, is not an artifact introduced by SNAP, another NO donor was tested. Nitroglycerin mobilizes the free radical NO through enzymatic bioactivation,<sup>156</sup> and elicited a cGMP increase in isolated glomeruli from Pod:Cre/cGi500 mice (**Figure 11**). The use of IBMX results in the inhibition of PDE-mediated cGMP degradation, leading to an observable accumulation of the cyclic nucleotide. The relationship between cGMP signaling and calcium signaling was investigated using substances that promote Ca<sup>2+</sup> influx, such as Bradykinin, ATP and Jedi2 (activator for the mechanosensitive ion channel Piezo1). Each of these substances elicited a FRET response. The administration of Probenecid, an inhibitor of organic anion transporter, resulted also in increased cGMP levels, suggesting the existence of a cGMP efflux system in podocytes with a potential contribution to the regulation of cGMP dynamics. A general observation throughout all measurements was that despite the wash-out phase with imaging buffer after each test substance, the FRET response did not return to its baseline level. This observation may be attributed to the damage caused by the isolation process of the glomeruli. Therefore, in the next step, we prepared AKS to preserve the physiological environment and additionally excluded damaged glomeruli from analysis (**see chapter 5**).

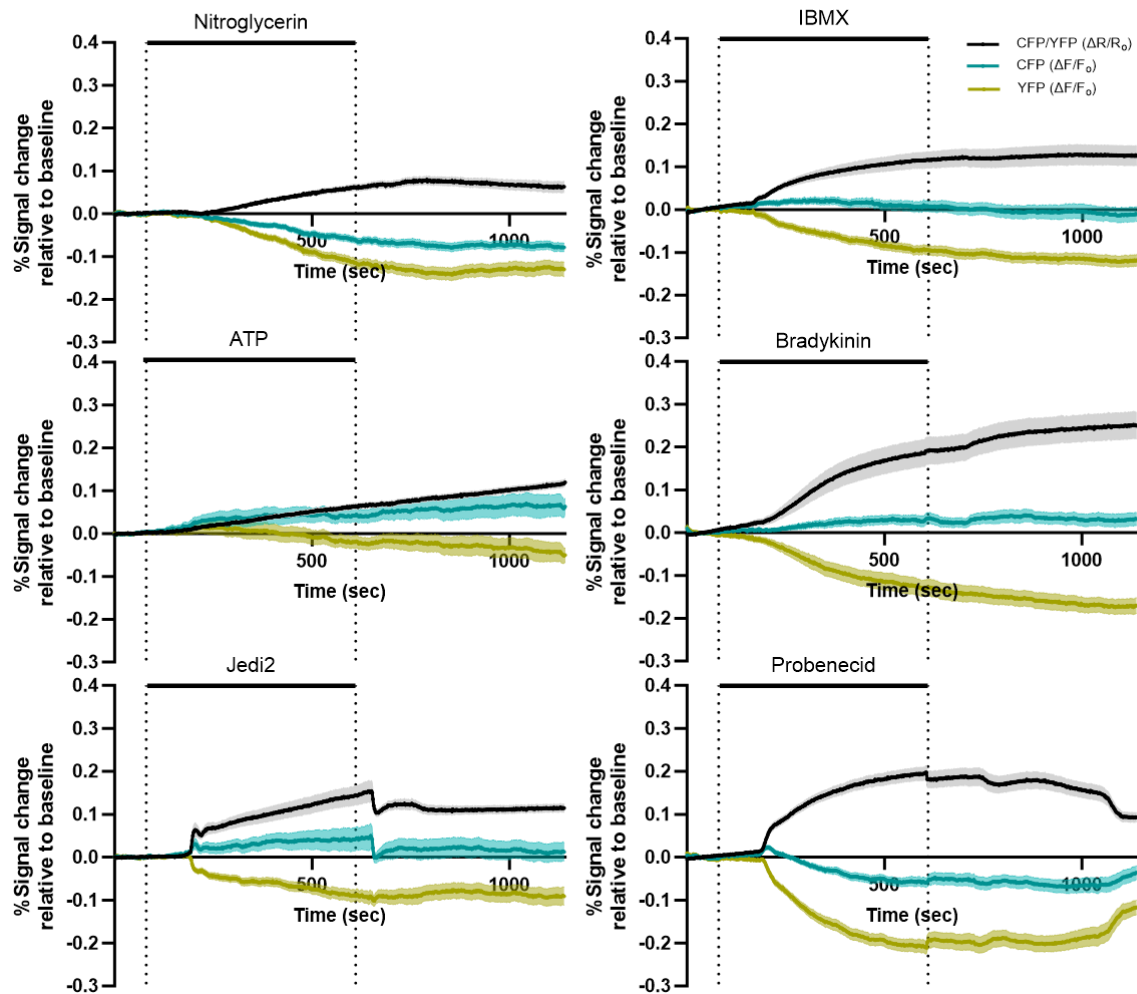


**Figure 11: Elevation of intracellular cGMP following various stimuli in isolated glomeruli**

Time-lapse recordings represent baseline-normalized emission intensity changes of the individual CFP (cyan) and YFP (yellow) traces ( $\Delta F/F_0$ ) and the CFP/YFP ratio (black,  $\Delta R/R_0$ ) upon administration of 750  $\mu\text{M}$  Nitroglycerin ( $n=21$  of 3 mice), 200  $\mu\text{M}$  IBMX ( $n=24$  of 5 mice), 500  $\mu\text{M}$  ATP ( $n=17$  of 3 mice), 25  $\mu\text{M}$  Bradykinin ( $n=11$  of 3 mice), 500  $\mu\text{M}$  Jedi2 ( $n=14$  of 3 mice) and 2 mM Probenecid ( $n=24$  of 4 mice) from 80 sec to 610 sec (dotted line). Data represent mean  $\pm$  SEM.

#### 4.4 Intravital imaging of cGi500-expressing glomeruli failed to demonstrate cGMP responses

The final aim of this thesis was to characterize the two known guanylyl cyclase systems (pGC and sGC) in podocytes and GECs in healthy living animals. Homozygosity of the sensor coincides with higher cGi500 signal intensity in Pod:Cre/cGi500 mice compared to Tie2:Cre/cGi500. Therefore, intravital imaging (IVI) was performed with Pod:Cre/cGi500 mice by administering various concentrated cGMP-elevating agents via bolus injection. Limitations of substance applicability was based on the solvent (e.g. ANP in ddH<sub>2</sub>O, SNAP in 0.5 M HCl, IBMX in DMSO) and the concentration. In addition, targeted stimulation of the cGMP axes led

to vasodilatory effects that caused a significant drop in blood pressure, ultimately resulting in the death of the animal. Higher concentrations of these substances would have been necessary to trigger a sufficient measurable signal-to-noise ratio, as discussed in **chapter 6.6**. Undesired acceptor fluorophore excitation while using two photon-excitation, as well as respiratory artifacts contributed to the difficulties in analyzing the FRET/cGi500 changes. Even a previously described image segmentation approach for FRET/cGi500-mediated cGMP changes in live tissue acquired with a multiphoton microscope could not unmask convincing cGMP responses (**Figure 12**),<sup>142</sup> which is why further IVI attempts were abandoned and open questions were answered *ex vivo* through AKS.

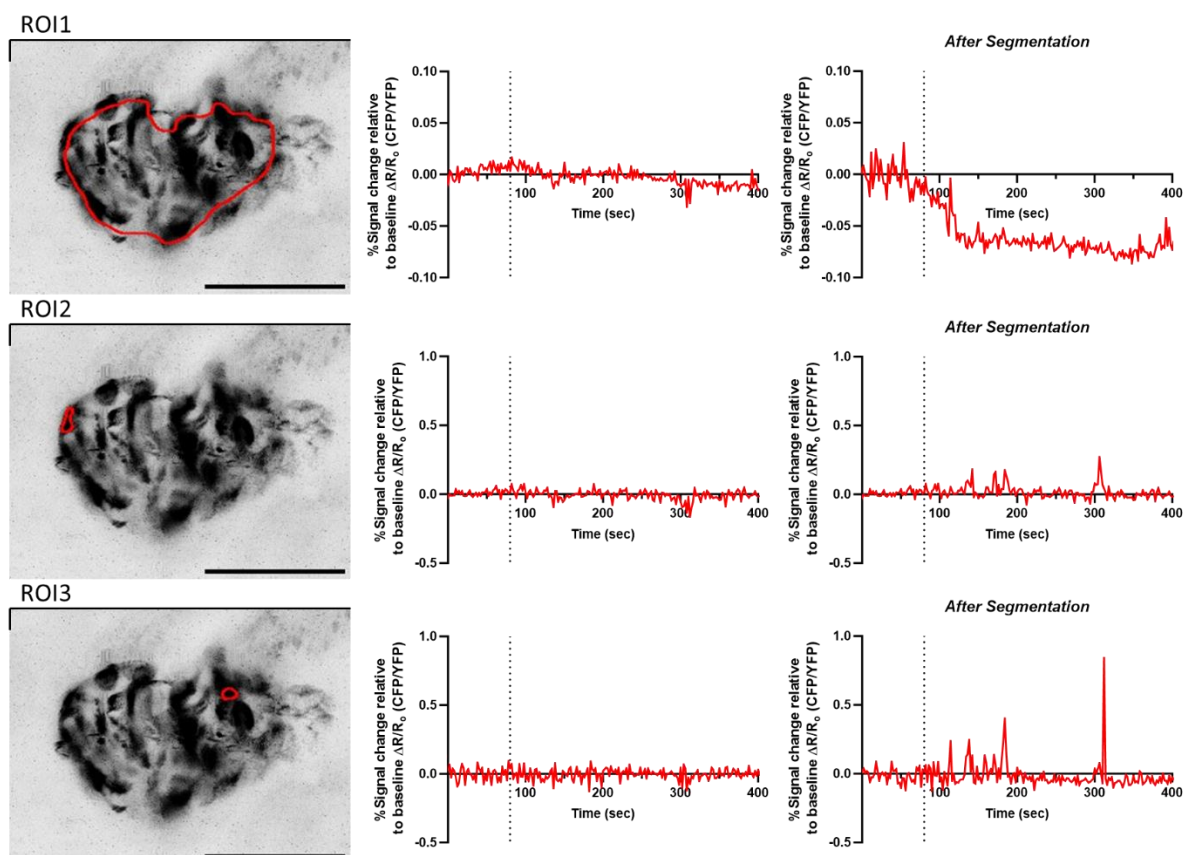


**Figure 12: Imaging of cGi500-expressing podocytes *in vivo* did not show convincing cGMP responses**

Evaluation of *in vivo* FRET/cGMP recordings from cGi500-expressing podocytes (Pod:Cre/cGi500 mouse). Representative image of biosensor expression in podocytes as maximum Z-projection in inverted grayscale with superimposed ROI's covering either the whole glomerulus (ROI1) or distinct podocytes (ROI2+3). Scale bar: 50  $\mu\text{m}$ . Time-lapse recordings represent baseline-normalized emission intensity changes of the CFP/YFP ratio (red,  $\Delta R/R_0$ ) upon bolus injection of 0.03 mg/kg Nitroglycerin (Dashed line: start bolus injection at 80 sec) without applying image segmentation (left) and after image segmentation (right).

## 5 Manuscript

### **Real-time imaging of cGMP signaling shows pronounced differences between glomerular endothelial cells and podocytes**

#### **Author contributions**

Nelli Rutkowski (NR), Frederik Görlitz (FG), Eva Wiesner (EW), Julia Binz-Lotter (JBL), Susanne Feil (SF), Robert Feil (RF), Thomas Benzing (TB), Matthias J. Hackl (MH)

NR - performed the experiments and analyzed the data

EW - performed immunolabeling and STED imaging

FG and JBL - methodology

NR and MH - wrote the manuscript

SF, RF, TB and MH - provided resources and guidance

NR, EW, JBL, SF, RF, MHK - review & editing of the manuscript

*Submitted to Journal of the American Society of Nephrology (JASN), Feb 26 2024*

*Manuscript number: JASN-2024-000272*

*Supplementary Material is provided as Supporting information SI 1. (Appendix)*

This manuscript contributes significantly to our understanding of cyclic guanosine monophosphate (cGMP) signaling within the kidney, particularly in glomerular endothelial cells (GECs) and podocytes. Utilizing the genetically encoded fluorescent biosensor cGi500 expressed in acute kidney slices from transgenic mice, the authors conducted real-time measurements of cGMP dynamics in these specific cell types. Their findings elucidate distinct cGMP responses in GECs and podocytes upon stimulation with the vasoactive substances atrial natriuretic peptide (ANP) or nitric oxide (NO). Furthermore, the discovery of distinct phosphodiesterase (PDE) activities, responsible for cGMP degradation, in each cell type highlights the intricate nature of cGMP regulation within the glomerulus. This comprehensive characterization of cell-specific cGMP signaling pathways paves the way for novel therapeutic strategies targeting kidney diseases, offering potential avenues for more effective interventions.

## **Real-time imaging of cGMP signaling shows pronounced differences between glomerular endothelial cells and podocytes**

Nelli Rutkowski<sup>1,2</sup>, Frederik Görlitz<sup>3</sup>, Eva Wiesner<sup>1,2</sup>, Julia Binz-Lotter<sup>1,2</sup>, Susanne Feil<sup>4</sup>, Robert Feil<sup>4</sup>, Thomas Benzing<sup>1,2</sup>, Matthias J. Hackl<sup>1,2</sup>

- 1 Department II of Internal Medicine and Center for Molecular Medicine Cologne, University of Cologne, Faculty of Medicine and University Hospital Cologne, Cologne, Germany
- 2 University of Cologne, Faculty of Medicine and University Hospital Cologne, Cluster of Excellence Cellular Stress Responses in Aging-associated Diseases (CECAD), Cologne, Germany
- 3 Bio- and Nanophotonics, Department of Microsystem Engineering, University of Freiburg, Freiburg, Germany
- 4 Interfakultäres Institut für Biochemie (IFIB), University of Tübingen, Tübingen, Germany

Correspondence should be addressed to: MH.

Nephrolab Cologne, University Hospital of Cologne, CECAD Research Center

Joseph-Stelzmann-Str. 26, 50931 Cologne, Germany

Phone +49 221/478 84179

Email: matthias.hackl@uk-koeln.de

### **Key points**

1. ANP/pGC and NO/sGC pathways produce cGMP in podocytes and glomerular endothelial cells.
2. ANP induces a long-lasting cGMP elevation in podocytes; endothelial cells show transient responses.
3. Glomerular endothelial cells exhibit broader PDE activity compared to podocytes.

## Abstract

### Background

In recent years, successful clinical trials of drugs elevating cyclic guanosine monophosphate (cGMP) signaling for cardiovascular diseases have renewed interest in cGMP biology within the kidney. However, the role of cGMP signaling in glomerular cell types, especially in endothelial cells and podocytes, remains largely unexplored. The majority of available data relies on cell culture studies and cGMP detection after cell lysis precludes continuous measurements.

### Methods

Acute kidney slices from mice, in which the genetically encoded fluorescent FRET-based cGMP biosensor cGi500 was exclusively expressed in endothelial cells or podocytes, enabled real-time visualization of cGMP. Slices were stimulated with the atrial natriuretic peptide (ANP) or/and SNAP (NO donor) without or with several phosphodiesterase (PDE) inhibitors.

### Results

Application of ANP or SNAP led to an elevation of intracellular cGMP in glomerular endothelial cells (GECs) and podocytes. While GECs exhibited a transient cGMP response upon activation of the soluble or particulate guanylyl cyclase (sGC or pGC) pathway, the cGMP response in podocytes reached a plateau following ANP administration. Simultaneous stimulation with ANP and SNAP led to an additive response in GECs, whereas cGMP levels in podocytes were lower compared to ANP stimulation alone. Administration of PDE inhibitors revealed a broader basal PDE activity in GECs dominated by PDE2a. In podocytes, basal PDE activity was mainly restricted to PDE3 and PDE5 activity.

### Conclusions

Our data demonstrate the existence of the ANP/pGC/cGMP and NO/sGC/cGMP pathways in GECs and podocytes with cell-specific differences regarding cGMP synthesis and degradation. Further insights into cell-specific cGMP signaling could provide new therapeutic options for treating kidney diseases.

## 5.1 Introduction

Recent clinical trials have demonstrated renoprotective effects of enhancing cGMP signaling in patients,<sup>1,2</sup> and ongoing studies are investigating further substances showing renoprotective effects in animal models.<sup>3,4</sup> The second messenger cGMP mediates signal transduction by activation of downstream effector molecules such as protein kinase G (PKG), cyclic nucleotide-gated (CNG) channels or phosphodiesterases (PDE), which degrade cGMP. Two types of guanylyl cyclases catalyze the conversion of guanosine-5'-triphosphate (GTP) to cGMP. These are particulate/membrane-bound receptors with an intracellular guanylyl cyclase domain (pGC-A/B/C) and soluble guanylyl cyclases (sGC) located in the cytosol.<sup>5</sup> Natriuretic peptides, such as atrial natriuretic peptide (ANP), activate the particulate guanylyl cyclase (pGC) signaling cascade via ligand-receptor binding, causing natriuresis, diuresis, suppression of the renin-angiotensin-aldosterone system (RAAS), and an increase in the glomerular filtration rate (GFR).<sup>6-8</sup> The NO/sGC-mediated cGMP synthesis involves nitric oxide synthases (NOS), which generate NO through the conversion of L-arginine to L-citrulline. NO diffuses across cell membranes and activates sGC present in target cells.<sup>5</sup> The NO/sGC/cGMP pathway influences glomerular function by dilating both pre- and post-glomerular arterioles and counteracts the effects of reactive oxygen species (ROS).<sup>9-11</sup> In disease states, cGMP signaling is diminished, suggesting a therapeutic benefit of its restoration. Several approved drugs elevating cGMP signaling became available in recent years.<sup>12,13</sup> Sacubitril inhibits the degradation of ANP,<sup>14,15</sup> whereas riociguat and vericiguat activate sGC and sildenafil and tadalafil inhibit PDE5.<sup>16-19</sup> To date, the role of GECs and podocytes in the renoprotective effect of cGMP signaling remains unclear. Measurements of cGMP levels in podocytes mostly rely on cell culture work, utilizing conventional biochemical techniques such as immunohistochemistry, radioimmunoassays (RIA), and enzyme-linked immunoassays (ELISA).<sup>20-24</sup> However, these techniques require cell lysis and often involve the addition of unspecific PDE inhibitors to enhance sensitivity. This inhibition disrupts cGMP dynamics and precludes a detailed analysis of signaling processes. The development of Förster resonance energy transfer (FRET)-based cGMP biosensors, such as cGi500,<sup>25,26</sup> enables the real-time monitoring of cGMP fluctuations within living cells. Binding of cGMP leads to a conformational change of the indicator protein cGi500, resulting in increased CFP fluorescence (donor) and decreased YFP fluorescence (acceptor). This sensor is capable of visualizing cGMP changes in intact tissue in high spatial and temporal resolution, overcoming some of the hurdles that hampered cGMP research in previous years.<sup>27-29</sup>

Utilizing the cGMP biosensor cGi500 with cell-specific expression, we performed a comparative analysis on GECs and podocytes to investigate cGMP signaling in vital mouse kidney tissue.

## 5.2 Methods

### 5.2.1 *In vitro* characterization of cGi500

The plasmid DNA MH20\_pCMV\_cGi500 (7767 bp, Supplemental Figure 1) encoding the single-chain cGMP biosensor cGi500 was provided by the Feil lab based on the sequence designed<sup>26</sup> by Michael Russwurm.

HEK 293T cells maintained in DMEM (Thermo Fisher Scientific, 31966-021) supplemented with 10% FBS (Thermo Fisher Scientific, 10270106) were transiently transfected by calcium-phosphate mediated DNA transfer. Cells were incubated at 37°C with replacement of the present medium after 7 h with supplemented phenol red free DMEM (Sigma-Aldrich, D1145) using 10% FBS, 1% GlutaMAX™ (Thermo Fisher Scientific, 35050-061) and 1% sodium pyruvate solution (Sigma-Aldrich, S8636). Transfected cells from a 10-cm dish (1x10<sup>7</sup> cells) were harvested and lysed according to a previously published protocol,<sup>26</sup> with minor modifications: Considering temperature and light sensitivity, all preparation steps were performed on ice with avoidance of strong light exposure. Cells were washed twice with 5 ml of ice-cold sterile PBS, followed by 300 µl of freshly prepared ice-cold homogenization buffer (pH 7.4). The adherent cells were scraped off and the lysate was transferred to sterile tubes. A cytosolic fraction was obtained by sonication (5 sec ON, 30 sec OFF, 1 cycle), followed by ultracentrifugation at 100000 g for 30 min at 4°C (Optima MAX-XP, Beckman Coulter, Rotor TLA-55). The volume for 25 µg protein (BCA assay, Thermo Fisher Scientific, 23225) was added to freshly prepared buffer A to achieve a final volume of 300 µl. An ascending cGMP (Sigma-Aldrich, G7504) dilution series (0.01 µM to 100 µM) was then added (2.1 µl) and incubated for 5 min. Fluorescence of the biosensor was recorded using a confocal microscope (LSM Meta 710 Axio Observer, Zeiss) equipped with an EC Plan-Neofluar 10x/0.3 objective and ZEN 2009 software (Zeiss). Intensity changes in the 512 x 512 x 16-bit emission images (mean fluorescence intensity) were analyzed using ImageJ (NIH) to calculate the CFP/YFP emission ratio (FRET ratio). The performed concentration-response curve analysis reflects the concentration-dependent cGMP binding properties of the sensor.

### 5.2.2 Mouse lines

Cell-specific cytosolic expression of the FRET-based biosensor cGi500 was accomplished by crossing the 'floxed' cGi500 sensor line<sup>25</sup> Gt(ROSA)26Sor<sup>tm1(CAG-ECFP/EYFP\*)Feil</sup> (mixed background 129 SV, C57BL/6N, (C57BL6/NRj > 70%)) with Pod:Cre mice<sup>30</sup> to achieve sensor expression in podocytes, and Tie2:Cre mice<sup>31</sup> or Cdh5:Cre mice<sup>32</sup> for expression in GECs. Experiments with Pod:Cre/cGi500 mice were performed with homozygous cGi500 alleles. Experiments with Tie2:Cre/cGi500 mice were performed with the first filial generation of offspring (carrying only one cGi500 allele) due to a reported nonspecific recombination in the



F2 generation.<sup>33,34</sup> Experiments with *Cdh5:Cre* mice were also conducted using the first-generation of offspring. Mice of both sexes, aged 8-27 weeks, were used. Animals were housed under standardized, specific pathogen-free conditions and kept in individually ventilated cage systems (IVC cages type II long) with centrally monitored light periodicity (light/dark cycle 12 h/12 h,  $55 \pm 10\%$  humidity,  $22 \pm 2^\circ\text{C}$  room temperature). Experimental procedures were evaluated and approved by the Landesamt für Natur, Umwelt und Verbraucherschutz (LANUV) NRW (VSG 81-02.04.2018.A351.)

### 5.2.3 Poly-L-lysine coating

To immobilize kidney slices for real-time imaging, coverslips ( $\varnothing$  12 mm, #1.5, Gerhard Menzel) were coated with approximately 700  $\mu\text{l}$  of a 0.1% poly-L-lysine solution (Sigma-Aldrich, P8920) for 1 hour.

### 5.2.4 Acute kidney slices (AKS)

Kidney slices were prepared according to the protocol of Poosti et al.,<sup>35</sup> with the following modifications: On the day of the experiment, 1 L of 1X Krebs-Henseleit buffer (KHB) was prepared, kept cold, and gassed with 95%  $\text{O}_2$ /5%  $\text{CO}_2$  for 30 min using a gas dispersion tube with a fritted disc. Subsequently, the solution was titrated to achieve a pH of 7.42. Mice were euthanized by cervical dislocation and the kidneys were directly transferred to ice-cold 1X KHB, followed by removal of the renal capsule and adherent vessels. The kidneys were embedded in 4% low melt agarose (Bio&SELL, BS20.47.100) and then cut into 250  $\mu\text{m}$  thick tissue sections using a Leica VT1200S vibratome (Leica Microsystems), amplitude: 1.0 mm and cutting speed: 0.20 mm/sec. Protected from light, slices were stored in ice-cold 1X KHB for up to 6 h until imaging.

### 5.2.5 Custom-built perfusion system

The perfusion system included the microscope stage chamber MS4 (Digitimer) connected through the female luer lock (Drifton, LF31) to the tubing Original Perfusor<sup>®</sup> line (B. Braun, 8723060). The respective end of the Perfusor<sup>®</sup> line tubing was inserted into a 1 ml Stripette<sup>®</sup> (Corning, 4011) to provide a stable support for the inlet and outlet. The system was connected to the Masterflex<sup>®</sup> silicone hose (Cole-Parmer, 96400-13) and clamped into the pump head with 2 channels (Masterflex<sup>®</sup> L/S<sup>®</sup> Easy-Load<sup>®</sup> II, Cole-Parmer, 77202-50) of the Masterflex<sup>®</sup> L/S<sup>®</sup> peristaltic pump (Cole-Parmer, 07555-15). The temperature of the buffer was kept constant at 37°C with the Truelife Invio BW Double (Mercateo, 615-Y791972) and was monitored with an external temperature probe LOG200 TC 5005-0204 (Dostmann Electronic). The Perfusor<sup>®</sup> line tubing was wrapped with sealing foam tape (SourcingMap) to avoid temperature loss of the heated buffer.

### 5.2.6 Real-time imaging of AKS

AKS were transferred onto a poly-L-lysine coated coverslip, positioned centrally in the imaging chamber, and secured with the slice anchor SHD-42/10 (Multi Channel Systems MCS, SKU:641419). Thereafter, the slice was allowed to adapt to the pre-tempered 1X KHB (37°C) for 10 min at a continuous flow rate of 1 ml/min using the custom-build perfusion system. Stimulants tested on AKS were: Atrial natriuretic factor (1-28) trifluoroacetate (ANP, Bachem, 01-4030380); Diethylammonium(Z)-1-(N,N-diethylamino)diazene-1-ium-1,2-diolate (DEA NONOate, Biomol, Cay82100-100); S-nitroso-N-acetylpenicillamine (SNAP, Biomol, Cay82250). Prior to DEA NONOate administration, NO release was induced by diluting the stock solution in 1X KHB for 5 min. Prior to SNAP administration, NO release was induced by diluting the stock solution in 1X KHB for 10 min. PDE inhibitors tested were: Avanafil (Hözel Diagnostika, A12619); BAY 60-7550 (Biomol, Cay10011135); Cilostamide (Hözel Diagnostika, A13596); Roflumilast (Hözel Diagnostika, A10804); PF-04449613 (Sigma-Aldrich, PZ0349); 3-Isobutyl-1-methylxanthine (IBMX, Sigma-Aldrich, I5879). Drug exposure and vitality of the tissue was monitored by the delivery and uptake of 1  $\mu$ M Evans Blue (Sigma-Aldrich, E2129) from the administered solution. Real-time cGMP imaging was performed using the TCS SP8 MP-OPO microscope (Leica Microsystems) and an IR Apo L25x/0.95 W objective in conjunction with the LAS X software (Leica). The objective was equipped with an objective heating collar (OBJ-COLLAR-3342, Okolab) adjusted to 37°C, monitored and controlled by a temperature controller (H401-T-CONTROLLER, Okolab). Biosensor excitation was conducted with a diode laser at 448 nm together with a sequential excitation of Evans Blue with the OPSP laser at 552 nm in combination with the TD beam splitter 448/514/552. Due to cGi500 biosensor heterozygosity, real-time imaging of Tie2:Cre/cGi500 and Cdh5:Cre/cGi500 mice was performed with higher laser power compared to homozygous Pod:Cre/cGi500 mice. Simultaneous detection of emission changes was performed at  $480 \pm 25$  nm (CFP),  $535 \pm 20$  nm (YFP) and at  $685 \pm 35$  nm (Evans Blue) with a bidirectional scan at 600 Hz and a line average of 4. Time series were recorded with one frame every 10 sec for 150 frames, starting with a baseline acquisition of 20 frames.

### 5.2.7 FRET imaging data analysis

Sample motion was corrected through the open-source package Galene (realignment mode: warp, points: 10).<sup>36</sup> The reassembled data was further processed using ImageJ (NIH) by superimposing a region of interest (ROI) over the whole glomerulus. Glomeruli showing morphological abnormalities and positive Evans Blue staining, indicating damage, were excluded from analysis (Supplemental Figure 2/3). Baseline normalization (averaged baseline signal: frame 0-20) was applied either to the CFP and YFP emission intensities ( $\Delta F/F_0$ ) or to CFP/YFP emission ratios ( $\Delta R/R_0$ ) (Supplemental Figure 4/5). Relative signal changes in  $\Delta R/R_0$

(%) reflect changes in intracellular cGMP concentration. The depicted curves represent the mean of baseline-normalized CFP/YFP emission ratios (FRET ratio) of all analyzed glomeruli. Scatter plots/Scattered bar plots display the maximal  $\Delta R/R_0$  response (maximal %signal change relative to baseline) in a selected time period of all analyzed glomeruli. Introduced delay in the cGMP/FRET response (lag time) ensued post substance administration, with dependency on the length of the assembled superfusion system hose (inlet). Lag time correction (stimulation intervall + 60 sec) was applied uniformly to all displayed time-lapse recordings with specification of the exact stimulation intervall (w/o correction) in the figure legend.

### 5.2.8 Immunostaining in optically cleared kidney slices

Immunolabeling of cleared kidney slices was based on an adapted protocol by Unnersjö-Jess et al.<sup>37</sup> Freshly prepared AKS of biosensor mice were fixed overnight in 4% PFA (Sigma-Aldrich, P6148) in 1X PBS. The solution was replaced with 1X PBS. Optical clearing was accomplished by immersing the AKS in 1 ml clearing solution (200 mM boric acid (Sigma-Aldrich, B0252), 4% SDS (Sigma-Aldrich, L3771), pH 8.5) at 50°C for 24 h, followed by a washing step with PBS-T for 5 min (1X PBS with 0.1% Triton X-100 (AppliChem, A4975)). Primary antibodies: GFP-Alexa647 (1:100, rabbit, Thermo Fisher Scientific, A-31852),  $\alpha$ -nephrin (1:100, guinea pig, Fitzgerald Industries International, 20R-NP002), CD31/PECAM-1 (1:200, goat, R&D Systems, AF3628). Secondary antibodies: donkey anti-guinea pig Atto594 or donkey anti-goat Atto594 (1:100, coupled in house). Immunolabeling was carried out at 37°C overnight with a PBS-T washing step in between and at the end of antibody incubation. Afterwards, AKS were embedded in a saturated fructose solution (80.2% D-fructose (Sigma-Aldrich, F0127), 0.5% 1-thioglycerol (Sigma-Aldrich, M1753)) and placed in glass-bottom dishes with a cover slip on top for mounting. Samples were imaged using a Leica TCS SP8 gSTED 3X (Leica Microsystems).

### 5.2.9 Statistics analyses

Statistical analysis was performed with GraphPad Prism 10.1.0 (Graphpad Software) utilizing a paired, two-tailed Student's t-test or One-way ANOVA (Tukey's post hoc test or Dunnett T3 post hoc test) to assess differences between groups. Differences between groups were considered statistically significant if  $p < 0.05$  (P value style "GP"). Results are reported as mean  $\pm$  standard error of the mean (SEM).

## 5.3 Results

### 5.3.1 Differential regulation of cGMP pathways in GECs and podocytes

Cell-specific cGi500 expression in GECs and podocytes was confirmed by optical tissue clearing and immunofluorescence labeling of AKS (Supplemental Figure 6). Tie2:Cre/cGi500 and Pod:Cre/cGi500 mice were used to visualize cell-specific changes in the cGMP/FRET response ( $\Delta R/R_0$ ) following the activation of the ANP/pGC/cGMP and the NO/sGC/cGMP pathways in glomeruli of freshly prepared kidney slices (Figure 1). Binding of cGMP to the FRET-based biosensor results in antiparallel intensity changes of the CFP/YFP FRET pair, thereby reporting changes in intracellular cGMP concentration. GECs of Tie2:Cre/cGi500 mice showed a similar maximal cGMP/FRET response after stimulation with 1  $\mu$ M ANP or 1 mM SNAP (NO donor). Compared to the ANP stimulation, SNAP stimulation reached the maximal cGMP/FRET response later and declined earlier (Figure 1B). SNAP was chosen for its longer half-life compared to other NO donors, making it well-suited for image acquisition over longer periods of time. However, high concentrations of SNAP (1 mM) are required to elicit a cGMP increase in tissue slices (Supplemental Figure 7A).<sup>38,39</sup> To address potential unspecific effects of SNAP attributable to its concentration, we applied another NO donor, DEA NONOate, which triggered a transient signal of comparable strength in GECs (Supplemental Figure 8). For Tie2:Cre mouse lines, non-endothelial Cre recombinase activity has been reported.<sup>33,34</sup> To demonstrate endothelial specificity, we repeated the experiments with ANP or/and SNAP and DEA NONOate in Cdh5:Cre/cGi500 mice and obtained similar results (Supplemental Figure 9). Podocytes of Pod:Cre/cGi500 mice showed an increase in cGMP levels after administration of 1 mM SNAP with similar kinetics and a maximal cGMP/FRET response compared to GECs. ANP-triggered cGMP synthesis in podocytes resulted in the highest cGMP/FRET response of all experiments and remained consistently high throughout the measurement period (Figure 1E). This long-lasting plateau was also present with half of the ANP concentration (Supplemental Figure 7B) and receded only after a total recording time of 4250 sec (~ 70 min), as demonstrated in a long-term measurement (Supplemental Figure 10). In GECs, co-stimulation (ANP+SNAP) resulted in an additional elevation of the maximal cGMP/FRET response compared to the response induced by each substance alone (Figure 1C). The time course of signal increase and decrease was comparable to SNAP stimulation (Figure 1B). In podocytes, co-stimulation failed to elicit a synergistic additive effect. The maximal cGMP/FRET response was even lower compared to the stimulation with ANP alone (Figure 1F). After a transient peak, most likely due to the NO release from SNAP, the curve displayed a plateau formation similar to the long-lasting cGMP response after ANP administration alone (Figure 1E).

Overall, our experiments demonstrate clear differences in the activity of the ANP/pGC/cGMP and NO/sGC/cGMP pathways between GECs and podocytes, and indicate a predominant role of the ANP/pGC/cGMP signaling pathway with sustained cGMP elevation in podocytes.

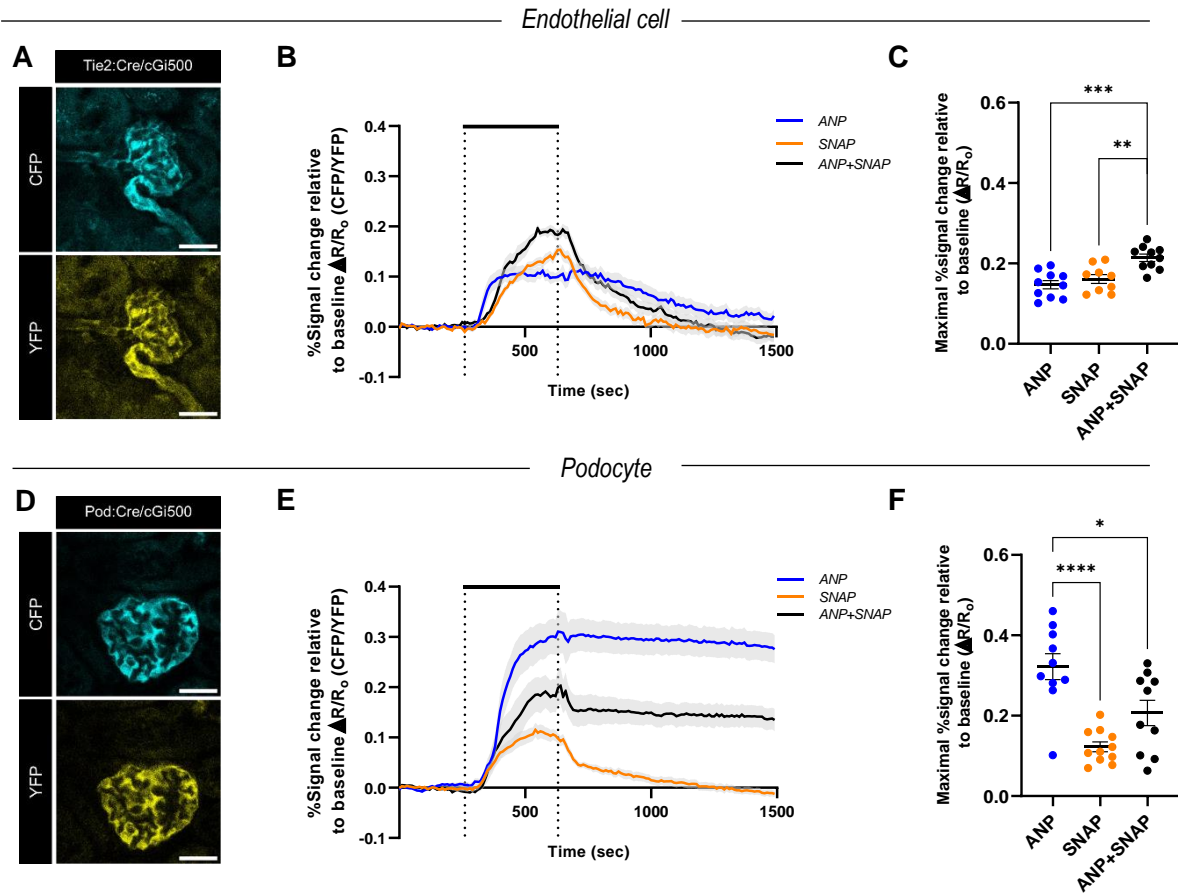


**Figure 1: cGMP response upon stimulation of the ANP/pGC/cGMP and NO/sGC/cGMP pathway in GECs and podocytes**

Acute kidney slices obtained from (A) Tie2:Cre/cGi500 mice or (D) Pod:Cre/cGi500 mice demonstrate cell-specific cGi500 biosensor expression with overlapping CFP/YFP fluorescence patterns in GECs and podocytes. (B, E) AKS were superfused (dotted lines) from 200 sec to 570 sec with 1  $\mu$ M ANP (blue trace), 1 mM SNAP (orange trace), or the combination of both (black trace). Stimulation was followed by a washout phase with 1X KHB (37°C). Time-lapse recordings for each cell type represent the mean of baseline-normalized FRET (CFP/YFP) ratios ( $\Delta R/R_0$ ) of all analyzed glomeruli. Relative signal changes in  $\Delta R/R_0$  (%) reflect changes in intracellular cGMP concentration. (C, F) Scatter dot plots display the maximal  $\Delta R/R_0$  response for each glomerulus derived from the indicated stimulation of (B) Tie2:Cre/cGi500 mice or (E) Pod:Cre/cGi500 mice during the entire measurement period of 1500 sec. Data represent mean  $\pm$  SEM of all analyzed glomeruli of six Tie2:Cre/cGi500 mice ( $n = 10$  for ANP,  $n = 9$  for SNAP,  $n = 10$  for ANP+SNAP) and five Pod:Cre/cGi500 mice ( $n = 10$  for ANP,  $n = 11$  for SNAP,  $n = 10$  for ANP+SNAP). One-way ANOVA, Tukey's post hoc test, \* $P < 0.05$ . Scale bar 25  $\mu$ M.

### **5.3.2 cGMP levels are controlled by a higher PDE activity in GECs compared to podocytes**

The balance of intracellular cGMP concentration within cells or tissues is maintained by the coordinated interplay between cGMP synthesis and its degradation, primarily mediated by phosphodiesterases (PDEs). Therefore, we added the broad-spectrum PDE inhibitor IBMX to the ongoing stimulation with ANP or/and SNAP. In GECs of Tie2:Cre/cGi500 mice, IBMX administration to an ongoing ANP or ANP+SNAP stimulation resulted in a higher additional cGMP/FRET response than the IBMX administration to an ongoing SNAP stimulation (Figure 2A). In contrast, in podocytes of Pod:Cre/cGi500 mice, the addition of IBMX to an ongoing ANP stimulation led only to a minimal additional increase in the cGMP/FRET response (Figure 2B), while the addition of IBMX to SNAP or to ANP+SNAP stimulation resulted in a further increase in cGMP levels. However, in all tested combinations, the additional cGMP/FRET response elicited by IBMX was consistently lower in podocytes compared to GECs, which reached statistical significance for ANP and ANP+SNAP (Figure 2C). This suggests a less pronounced PDE activity in podocytes compared to GECs.

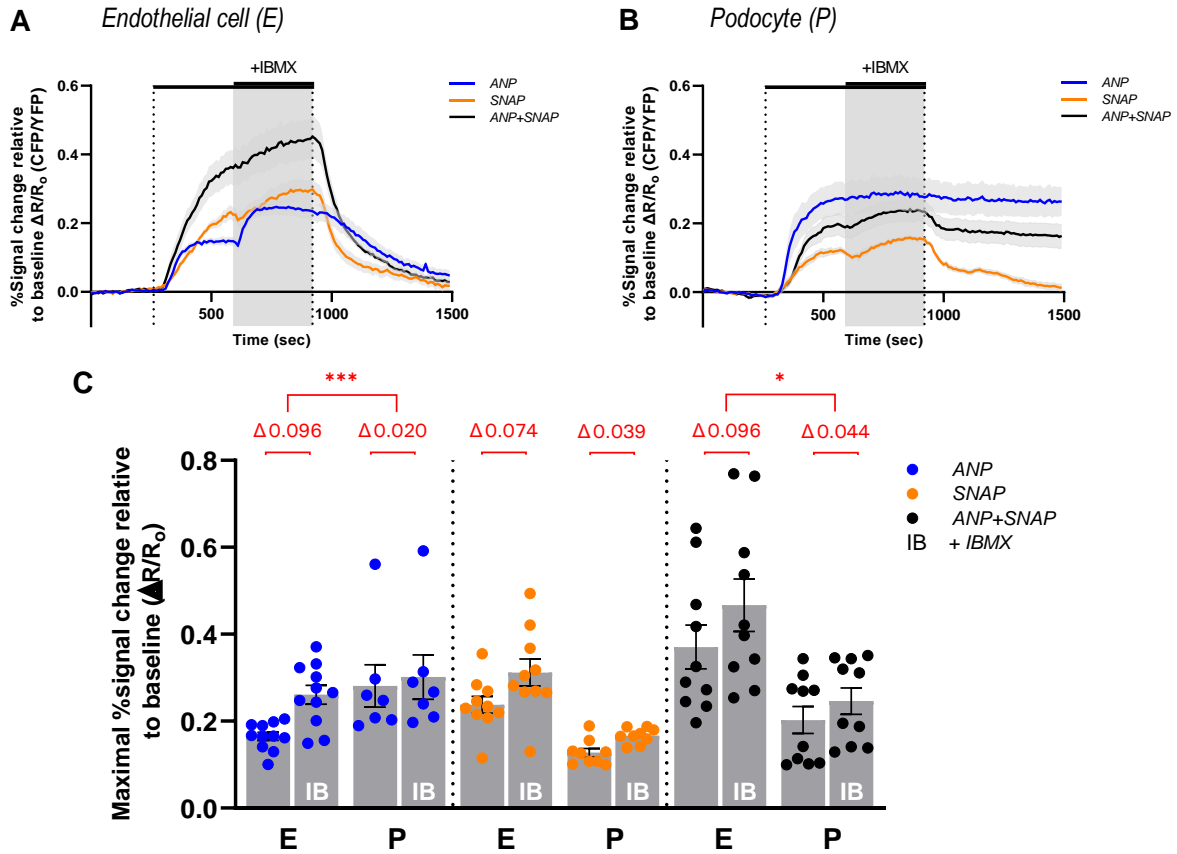


**Figure 2: Addition of the PDE inhibitor IBMX reveals higher PDE activity in GECs compared to podocytes**

Acute kidney slices from (A) Tie2:Cre/cGi500 mice or (B) Pod:Cre/cGi500 mice were superfused (outer dotted lines) from 200 sec to 860 sec with 1  $\mu$ M ANP (blue trace), 1 mM SNAP (orange trace) or the combination of both (black trace). In addition to the ongoing stimulation, 500  $\mu$ M IBMX was administered from 530 sec to 860 sec (gray area). Time-lapse recordings for each cell type represent the mean of baseline-normalized FRET (CFP/YFP) ratios ( $\Delta R/R_0$ ) of all analyzed glomeruli. (C) Comparison of the additional cGMP/FRET response after IBMX administration between GECs and podocytes. Scattered bar plot displays the maximal  $\Delta R/R_0$  response for each glomerulus in the respective measurement interval (w/o IBMX: 260-590 sec; with IBMX: 600-1500 sec). The delta (mean difference, shown in red) between the two time intervals was compared between GECs (E) and podocytes (P). Data represent mean  $\pm$  SEM of all analyzed glomeruli of three Tie2:Cre/cGi500 mice ( $n = 11$  for ANP,  $n = 10$  for SNAP,  $n = 10$  for ANP+SNAP) and four Pod:Cre/cGi500 mice ( $n = 7$  for ANP,  $n = 9$  for SNAP,  $n = 10$  for ANP+SNAP). One-way ANOVA (Brown Forsythe ( $p < 0.0001$ ), Welch test ( $p < 0.0001$ )), Dunnett T3 post hoc test, \* $P < 0.05$ .

### 5.3.3 Predominant PDE2a activity in GECs and PDE3 & PDE5 activity in podocytes

To further analyze PDE activity in GECs and podocytes, we inhibited several PDE isoforms and investigated their effect on cGMP levels without ANP or/and SNAP stimulation. Suitable PDE candidates were identified in proteomics datasets of podocytes<sup>40</sup> and respective PDE inhibitors were applied on AKS of Tie2:Cre/cGi500 mice (Figure 3A) and Pod:Cre/cGi500 mice (Figure 3B). In GECs, inhibition of PDE2a by BAY 60-7550 alone resulted in the highest maximal cGMP/FRET response of all tested substances. The inhibition of all other PDE isoforms tested (PDE3, 4, 5, 9a) also elicited a robust cGMP/FRET response. In contrast, in podocytes PDE3 inhibition by Cilostamide induced the highest cGMP/FRET response of all tested substances, followed by inhibition of PDE5 with Avanafil. The other PDE inhibitors elicited only a minor cGMP/FRET response. This suggests a broader PDE activity in GECs compared to podocytes.

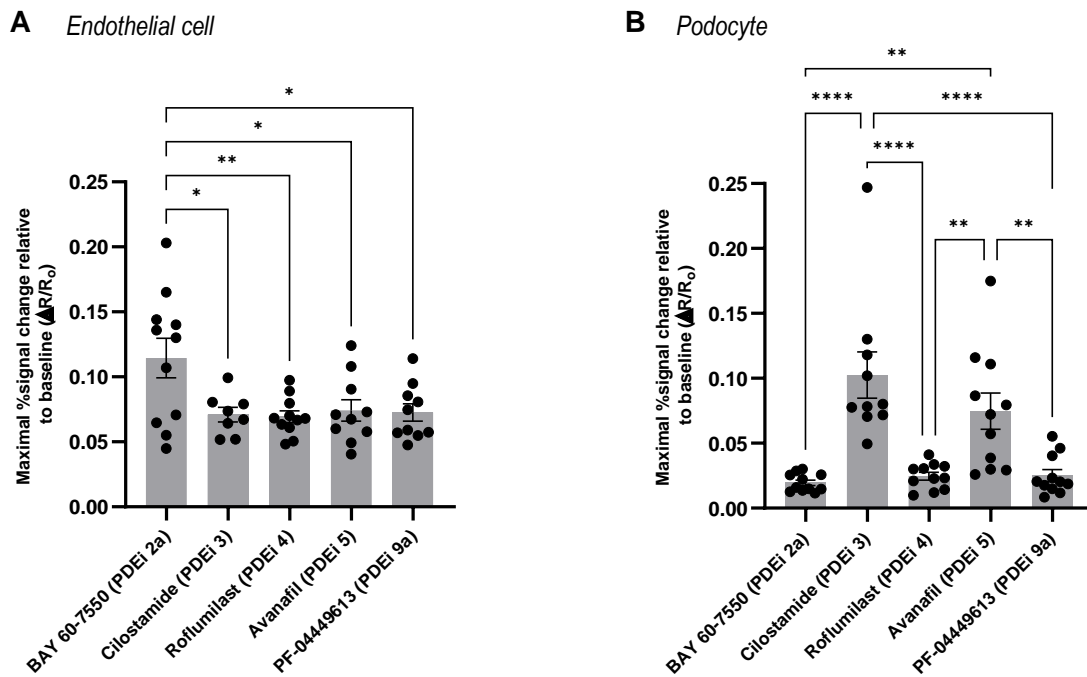


**Figure 3: PDE inhibition reveals predominant PDE2a activity in GECs and PDE3 & PDE5 activity in podocytes**

Acute kidney slices from (A) Tie2:Cre/cGi500 mice or (B) Pod:Cre/cGi500 mice were superfused for 370 sec with 50  $\mu$ M BAY 60-7550, 250  $\mu$ M Cilostamide, 250  $\mu$ M Roflumilast, 250  $\mu$ M Avanafil or 100  $\mu$ M PF-04449613. The primarily inhibited PDE isoform is stated in brackets. Baseline-normalized FRET (CFP/YFP) ratios ( $\Delta R/R_0$ ) of all analyzed glomeruli were calculated. Scattered bar plots display the maximal  $\Delta R/R_0$  response for each compound during the entire measurement period of 1500 sec. Data



represent mean  $\pm$  SEM of all analyzed glomeruli of nine Tie2:Cre/cGi500 mice ( $n = 11$  for BAY 60-7550,  $n = 8$  for Cilostamide,  $n = 11$  for Roflumilast,  $n = 10$  for Avanafil,  $n = 10$  for PF-04449613) and of six Pod:Cre/cGi500 mice ( $n = 11$  for BAY 60-7550,  $n = 10$  for Cilostamide,  $n = 11$  for Roflumilast,  $n = 11$  for Avanafil,  $n = 11$  for PF-04449613). One-way ANOVA, Tukey's post hoc test, \* $P < 0.05$ .

#### **5.3.4 PDE2a inhibition prevents cGMP degradation in GECs, whereas PDE3 & PDE5 inhibition augment the ANP/pGC/cGMP pathway in podocytes**

To investigate the effect of PDE inhibition on the ANP/pGC/cGMP and NO/sGC/cGMP pathways, we applied inhibitors of specific PDE isoforms to an ongoing stimulation with ANP or/and SNAP on AKS of Tie2:Cre/cGi500 mice or Pod:Cre/cGi500 mice. In GECs of Tie2:Cre/cGi500 mice, the administration of BAY 60-7550 (PDE2a inhibitor) resulted only in a minor additional cGMP/FRET response during ANP or/and SNAP stimulation (Figure 4B). However, the increased cGMP levels lasted considerably longer than the cGMP/FRET response after ANP or/and SNAP stimulation without PDE inhibition, as none of the FRET ratios returned back to baseline within the measurement period (Figure 4A). To study the effect of inhibition of specific PDE isoforms in podocytes, we applied Cilostamide (PDE3 inhibitor) or Avanafil (PDE5 inhibitor) on AKS of Pod:Cre/cGi500 mice. Both substances showed a pronounced effect on the ANP and ANP+SNAP stimulation (Figure 4C-F). However, the additional cGMP/FRET response after SNAP stimulation was small for Cilostamide (Figure 4D) and almost absent for Avanafil (Figure 4F). The plateau-like cGMP response seen after ANP and ANP+SNAP stimulation was unaffected by inhibition of PDE3 or PDE5.

Taken together, we were able to demonstrate clear pathway-dependent differences in the activity of PDE isoforms between GECs and podocytes.

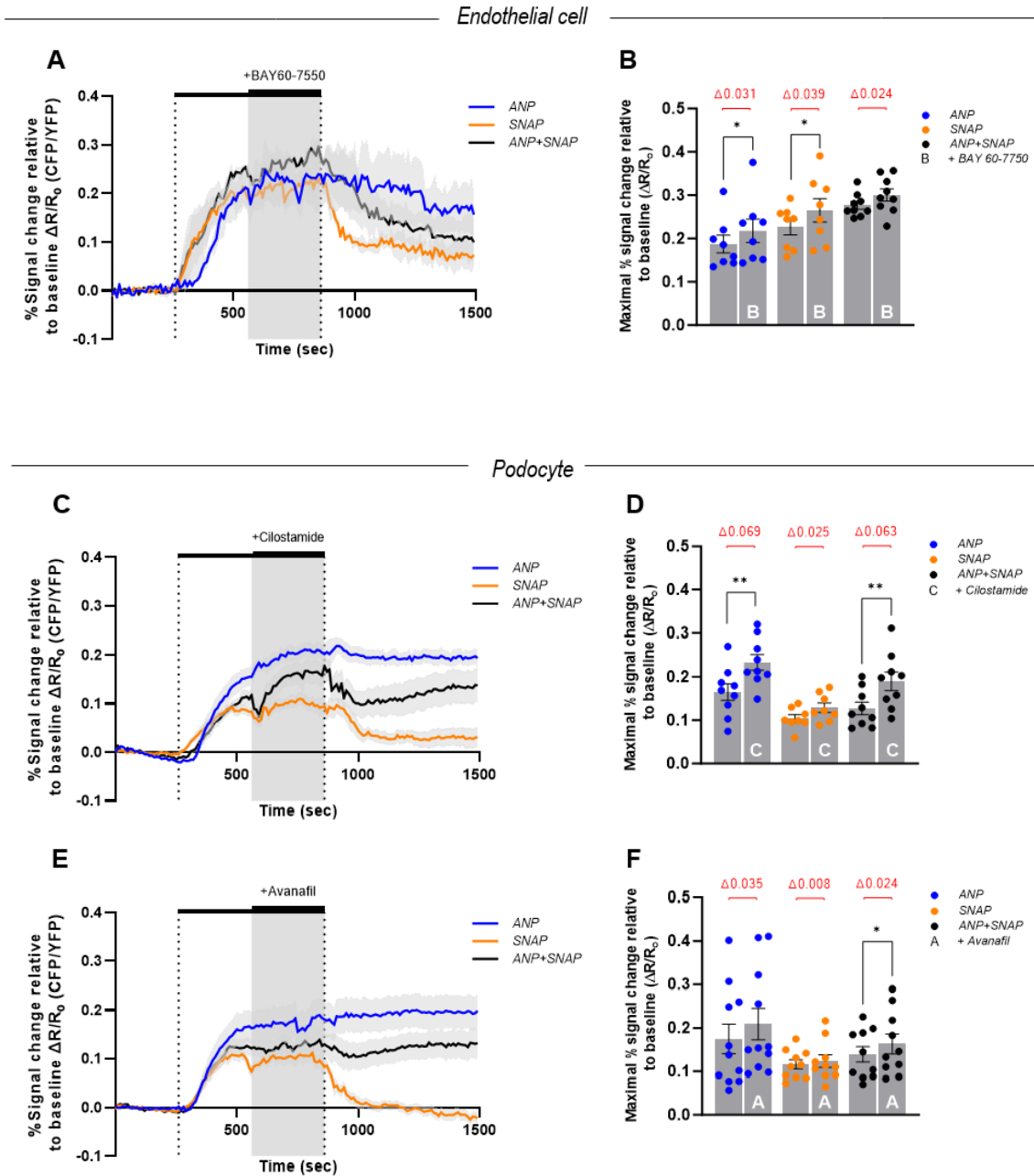


**Figure 4: PDE2a inhibition prevents cGMP degradation in GECs, whereas PDE3 & PDE5 inhibition augment the ANP/pGC/cGMP pathway in podocytes**

Acute kidney slices from (A) Tie2:Cre/cGi500 mice or (C, E) Pod:Cre/cGi500 mice were superfused from 200 sec to 800 sec (outer dotted lines) with 1  $\mu$ M ANP (blue trace), 1 mM SNAP (orange trace) or the combination of both (black trace). In addition to the ongoing stimulation, Tie2:Cre/cGi500 slices were superfused with 50  $\mu$ M BAY 60-7550 and Pod:Cre/cGi500 slices were superfused with 250  $\mu$ M Cilostamide or 250  $\mu$ M Avanafil in the time period from 500 sec to 800 sec (gray area). Time-lapse recordings represent the mean of baseline-normalized FRET (CFP/YFP) ratios ( $\Delta R/R_0$ ) of all analyzed glomeruli. (B, D, F) Scattered bar plots display the maximal  $\Delta R/R_0$  response for each glomerulus in the respective measurement interval (w/o PDE inhibitor: 260-570 sec; with PDE inhibitor: 580-1000 sec) for (B) BAY 60-7550, (D) Cilostamide or (F) Avanafil. The delta (mean difference) between the two time

periods is shown in red. Data represent mean  $\pm$  SEM of all analyzed glomeruli of six Tie2:Cre/cGi500 mice after administration of BAY 60-7550 ( $n = 8$  for ANP,  $n = 8$  for SNAP,  $n = 9$  for ANP+SNAP), eight Pod:Cre/cGi500 mice for Cilostamide ( $n = 9$  for ANP,  $n = 8$  for SNAP,  $n = 9$  for ANP+SNAP) and nine Pod:Cre/cGi500 mice for Avanafil ( $n = 11$  for ANP,  $n = 10$  for SNAP,  $n = 10$  for ANP+SNAP glomeruli of nine mice). Two-tailed paired t-test. \* $P < 0.05$ .

## 5.4 Discussion

To our knowledge, our study is the first, which resolves a cell-specific cGMP response in glomerular cells in vital kidney tissue. For podocytes, we demonstrate an elevation of intracellular cGMP levels provoked by the stimulation of the ANP/pGC/cGMP-axis and NO/sGC/cGMP-axis. These findings contradict the work of Theilig et al. and Wang et al., who were unable to detect SNAP-induced cGMP synthesis in cultured podocytes,<sup>20,21</sup> but are in line with results from other authors.<sup>22,23,41</sup> However, limitations in conventional detection and quantification methods in these publications can hamper the assessment of cGMP dynamics.<sup>28</sup> Additionally, the severe differences in gene expression and morphology between cultured podocytes and podocytes *in vivo* have to be taken into account.<sup>42,43</sup> In agreement with our results, Mundel et al. and Jarry et al. localized sGC in podocytes of kidney tissue.<sup>44,45</sup>

Endothelial cells are known NO suppliers, but there is limited data on endogenous expression of guanylyl cyclases (sGC or pGC) and cGMP signaling in GECs of intact tissue.<sup>23,45-47</sup> Our data provide evidence for the existence of the ANP/pGC/cGMP and NO/sGC/cGMP pathways in GECs. We demonstrate that GECs possess an actively regulated cGMP signaling system, measured with high spatial and temporal resolution in glomeruli embedded in a complex kidney architecture. Compared to conventional assays that rely on a single cGMP endpoint determination, our experimental setup enabled real-time monitoring of cGMP dynamics throughout the study period.

We were able to demonstrate distinct differences in cGMP signaling between GECs and podocytes using the same cGMP biosensor expressed in these cell types. In podocytes, SNAP-induced cGMP synthesis resulted in a transient cGMP/FRET response, similar to ANP or/and SNAP stimulation in GECs. In contrast, the ANP-induced cGMP synthesis in podocytes resulted in a higher and far longer lasting cGMP increase than in GECs. The persistent ANP-triggered cGMP response in podocytes did not decline to baseline level during a total measurement time of 4250 sec ( $\sim 70$  min) (Supplemental Figure 10). Reducing the ANP concentration by 50% resulted in an identically sustained cGMP/FRET response, albeit at a lower level (Supplemental Figure 7B), which argues against a plateau formation due to oversaturation of the sensor. This observation could be explained by delayed internalization of

ligand-receptor complexes of GC-A,<sup>48,49</sup> as podocytes exhibit high expression levels of GC-A.<sup>46</sup> Alternatively, this phenomenon may arise from a positive feedback loop via PKG,<sup>50</sup> or a lower PDE activity, as demonstrated in our experiments. These results suggest an important role of ANP-mediated cGMP synthesis in podocytes, which has been demonstrated in disease states for a podocyte-specific GC-A knockout model. In these mice, a DOCA salt-induced hypertension led to development of proteinuria and foot process effacement.<sup>51</sup> In all of our experiments, the co-stimulation (ANP+SNAP) in podocytes resulted in a lower cGMP increase than the stimulation with ANP alone, whereas it had an additive effect in GECs. Similar results for podocytes regarding a possible mutual regulation of sGC and pGC activity have been published and suggest the avoidance of excessive cGMP concentrations in podocytes.<sup>52,53</sup>

Inhibition of PDE isoforms revealed substantial differences in their activity between GECs and podocytes. In GECs all tested PDE inhibitors (targeting PDE2a, 3, 4, 5 and 9a) increased basal cGMP levels, while inhibition of PDE2a had the strongest effect and delayed cGMP degradation following ANP or/and SNAP stimulation. In podocytes, however, only the PDE3 inhibitor Cilostamide and the PDE5 inhibitor Avanafil resulted in comparable increases of basal cGMP levels. Both substances predominantly augmented the ANP-induced cGMP synthesis without affecting the long-lasting cGMP/FRET response in the washout-phase. As a limitation, the applied PDE inhibitors predominantly inhibit one PDE isoform, but are not completely specific. Hence, it cannot be excluded that these inhibitors partially influence other PDE isoforms. Administration of the unspecific PDE inhibitor IBMX to podocytes resulted only in a small additional accumulation of cGMP levels, with a bigger effect on the NO/sGC/cGMP-pathway. The less pronounced effect of unspecific PDE isoform inhibition by IBMX on cGMP levels compared to specific PDE isoform inhibition might be explained by the unequally effective inhibition of different PDE isoforms by IBMX.<sup>54,55</sup> Taken together, this demonstrates that GECs and podocytes rely on distinct PDE isoforms and their impact varies between the two cGMP pathways, which mandates studying glomerular cGMP signaling with a high spatial and temporal resolution.

The FRET-based cGMP biosensor utilized here was capable of detecting small changes in intracellular cGMP concentrations (EC<sub>50</sub> ~ 532 nM, Supplemental Figure 1) and its functionality has been validated in other *ex vivo* settings.<sup>25,29,56</sup> Further improvement of the FRET sensor could help to increase the signal-to-noise ratio and facilitate cGMP measurements during *in vivo* imaging of the glomerulus. Due to the thickness of AKS and the necessary penetration, we had to apply higher doses of the substances than published for cell culture. Nevertheless, the reported differences between GECs and podocytes were measured, while all surrounding experimental conditions, e.g. the cutting process, the perfusion setup and the imaging protocol, remained unchanged.

Regarding the limitations of this study, our experiments were not designed to elucidate if stimulation of the ANP/pGC/cGMP and NO/sGC/cGMP pathways in GECs and podocytes occur by autocrine or paracrine signaling. Furthermore, we did not investigate downstream targets of the cGMP signaling pathways, which could explain the non-additive effect of ANP+SNAP stimulation or the long-lasting effect of ANP stimulation in podocytes. For these questions, further studies are required and partially ongoing.

Taken together, we demonstrated the presence of the ANP/pGC/cGMP as well as the NO/sGC/cGMP pathway in GECs and podocytes of healthy glomeruli. ANP stimulation resulted in higher and longer lasting cGMP production in podocytes compared to SNAP stimulation and the cGMP response triggered by ANP and/or SNAP in GECs. PDE activity in podocytes is dominated by PDE3 and PDE5, while in GECs all tested isoforms are active and inhibition of PDE2a had the strongest effect.

As cGMP signaling is downregulated in disease states and pharmacological manipulation intends to restore cGMP pathways, further studies with different disease models are warranted to increase our understanding of disease-associated changes in cGMP signaling in glomerular cells.

## Disclosures

All authors have nothing to disclose.

## Acknowledgments

We thank Martin Höhne (Department II of Internal Medicine University Hospital Cologne) and Peter Zentis (CECAD Imaging Facility) for their contribution in data analysis and Katrin Bohl (Department II of Internal Medicine, University Hospital Cologne) for the support in analyzing proteomics data. We also thank Christian Jüngst (CECAD Imaging Facility) for his technical support regarding FRET-based imaging. We thank Dr. Michael Russwurm from the Institute of Pharmacology and Toxicology, Ruhr-University Bochum, Germany for providing the sequence for the cGi500 plasmid. Visual abstract and parts of Supplemental Figure 1 were created using BioRender.com.

## Supporting information (SI 1)

Content: 10 Supplemental figures

Supplemental Figure 1: In vitro characterization of cGi500.

Supplemental Figure 2: Visualization of the cutting process-related damage to glomeruli.

Supplemental Figure 3: Evans Blue interferes at high concentrations with the FRET-based biosensor cGi500.

Supplemental Figure 4: Calculated FRET (CFP/YFP) ratio from CFP and YFP fluorescence traces demonstrates cGMP generation after activation of the ANP/pGC or/and NO/sGC pathway in GECs.

Supplemental Figure 5: Calculated FRET (CFP/YFP) ratio from CFP and YFP fluorescence traces demonstrates cGMP generation after activation of the ANP/pGC or/and NO/sGC pathway in podocytes.

Supplemental Figure 6: Cell-specific expression of the cGMP biosensor in optically cleared AKS.

Supplemental Figure 7: High doses of ANP and SNAP are required to elicit measurable cGi500-mediated cGMP signals.

Supplemental Figure 8: DEA NONOate triggers cGMP synthesis in Tie2:Cre/cGi500 mice.

Supplemental Figure 9: GECs of Cdh5:Cre/cGi500 mice respond similar to Tie2:Cre/cGi500 mice.

Supplemental Figure 10: Long-term measurement of the cGMP/FRET response in podocytes after ANP administration.

## References

1. Voors AA, Gori M, Liu LCY, et al. Renal effects of the angiotensin receptor neprilysin inhibitor LCZ696 in patients with heart failure and preserved ejection fraction. *Eur J Heart Fail.* 2015;17(5):510-517. doi:10.1002/EJHF.232
2. Scheele W, Diamond S, Gale J, et al. Phosphodiesterase Type 5 Inhibition Reduces Albuminuria in Subjects with Overt Diabetic Nephropathy. *J Am Soc Nephrol.* 2016;27(11):3459-3468. doi:10.1681/ASN.2015050473
3. Bénardeau A, Kahnert A, Schomber T, et al. Runcaciguat, a novel soluble guanylate cyclase activator, shows renoprotection in hypertensive, diabetic, and metabolic preclinical models of chronic kidney disease. *Naunyn Schmiedebergs Arch Pharmacol.* 2021;394(12):2363-2379. doi:10.1007/S00210-021-02149-4
4. Reinhart GA, Harrison PC, Lincoln K, et al. The Novel, Clinical-Stage Soluble Guanylate Cyclase Activator BI 685509 Protects from Disease Progression in Models of Renal Injury and Disease. *J Pharmacol Exp Ther.* 2023;384(3):382-392. doi:10.1124/JPET.122.001423
5. Denninger JW, Marletta MA. Guanylate cyclase and the ·NO/cGMP signaling pathway. *Biochimica et Biophysica Acta (BBA) - Bioenergetics.* 1999;1411(2-3):334-350. doi:10.1016/S0005-2728(99)00024-9
6. Chen Y, Burnett JC. Particulate Guanylyl Cyclase A/cGMP Signaling Pathway in the Kidney: Physiologic and Therapeutic Indications. *International Journal of Molecular Sciences* 2018, Vol 19, Page 1006. 2018;19(4):1006. doi:10.3390/IJMS19041006
7. Brignone J, Assersen KB, Jensen M, et al. Protection of kidney function and tissue integrity by pharmacologic use of natriuretic peptides and neprilysin inhibitors. *Pflugers Arch.* 2021;473(4):595-610. doi:10.1007/S00424-021-02555-W
8. Wong PCY, Guo J, Zhang A. The renal and cardiovascular effects of natriuretic peptides. *Adv Physiol Educ.* 2017;41(2):179-185. doi:10.1152/ADVAN.00177.2016
9. Ohishi K, Carmines PK, Inscho EW, Navar LG. EDRF-angiotensin II interactions in rat juxtamedullary afferent and efferent arterioles. *Am J Physiol.* 1992;263(5 Pt 2). doi:10.1152/AJPRENAL.1992.263.5.F900

10. Wennysia IC, Zhao L, Schomber T, et al. Role of soluble guanylyl cyclase in renal afferent and efferent arterioles. *Am J Physiol Renal Physiol.* 2021;320(2):F193-F202. doi:10.1152/AJPRENAL.00272.2020/ASSET/IMAGES/LARGE/AJ-AFLU210002F008.JPEG
  
11. Dolinina J, Sverrisson K, Rippe A, Öberg CM, Rippe B. Nitric oxide synthase inhibition causes acute increases in glomerular permeability in vivo, dependent upon reactive oxygen species. *Am J Physiol Renal Physiol.* 2016;311(5):F984-F990. doi:10.1152/AJPRENAL.00152.2016
  
12. Buglioni A, Burnett JC. New Pharmacological Strategies to Increase cGMP. *Annu Rev Med.* 2016;67:229-243. doi:10.1146/ANNUREV-MED-052914-091923
  
13. Mangmool S, Duangrat R, Parichatikanond W, Kurose H. New Therapeutics for Heart Failure: Focusing on cGMP Signaling. *Int J Mol Sci.* 2023;24(16). doi:10.3390/IJMS241612866
  
14. Murphy SP, Prescott MF, Camacho A, et al. Atrial Natriuretic Peptide and Treatment With Sacubitril/Valsartan in Heart Failure With Reduced Ejection Fraction. *JACC Heart Fail.* 2021;9(2):127-136. doi:10.1016/J.JCHF.2020.09.013
  
15. Polina I, Spicer MJ, Domondon M, et al. Inhibition of neprilysin with sacubitril without RAS blockage aggravates renal disease in Dahl SS rats. *Ren Fail.* 2021;43(1):315-324. doi:10.1080/0886022X.2021.1879856
  
16. Ghofrani HA, D'Armini AM, Grimminger F, et al. Riociguat for the treatment of chronic thromboembolic pulmonary hypertension. *N Engl J Med.* 2013;369(4):319-329. doi:10.1056/NEJMOA1209657
  
17. Kassis-George H, Verlinden NJ, Fu S, Kanwar M. Vericiguat in Heart Failure with a Reduced Ejection Fraction: Patient Selection and Special Considerations. *Ther Clin Risk Manag.* 2022;18:315. doi:10.2147/TCRM.S357422
  
18. Iordache AM, Docea AO, Buga AM, et al. Sildenafil and tadalafil reduce the risk of contrast-induced nephropathy by modulating the oxidant/antioxidant balance in a murine model. *Food Chem Toxicol.* 2020;135. doi:10.1016/J.FCT.2019.111038
  
19. Edmonston D, Sparks M, Rajagopal S, Wolf M. Sildenafil and Kidney Function in Heart Failure with Preserved Ejection Fraction. *Kidney360.* 2023;4(5):631-640. doi:10.34067/KID.0000000000000103



20. Theilig F, Bostanjoglo M, Pavenstädt H, et al. Cellular distribution and function of soluble guanylyl cyclase in rat kidney and liver. *J Am Soc Nephrol.* 2001;12(11):2209-2220. doi:10.1681/ASN.V12112209
21. Wang L, Tang Y, Buckley AF, Spurney RF. Blockade of the natriuretic peptide clearance receptor attenuates proteinuria in a mouse model of focal segmental glomerulosclerosis. *Physiol Rep.* 2021;9(21). doi:10.14814/PHY2.15095
22. Lewko B, Waszkiewicz A, Maryn A, et al. Dexamethasone-dependent modulation of cyclic GMP synthesis in podocytes. *Mol Cell Biochem.* 2015;409(1-2):243. doi:10.1007/S11010-015-2528-6
23. Hart D, Li J, van der Vlag J, Nijenhuis T. Repurposing riociguat to target a novel paracrine nitric oxide-trpc6 pathway to prevent podocyte injury. *Int J Mol Sci.* 2021;22(22). doi:10.3390/IJMS222212485/S1
24. Lewko B, Endlich N, Kriz W, Stepinski J, Endlich K. C-type natriuretic peptide as a podocyte hormone and modulation of its cGMP production by glucose and mechanical stress. *Kidney Int.* 2004;66(3):1001-1008. doi:10.1111/J.1523-1755.2004.00848.X
25. Thunemann M, Wen L, Hillenbrand M, et al. Transgenic mice for cGMP imaging. *Circ Res.* 2013;113(4):365-371. doi:10.1161/CIRCRESAHA.113.301063/-/DC1
26. Russwurm M, Mullershausen F, Friebe A, Jäger R, Russwurm C, Koesling D. Design of fluorescence resonance energy transfer (FRET)-based cGMP indicators: a systematic approach. *Biochem J.* 2007;407(Pt 1):69. doi:10.1042/BJ20070348
27. Feil R, Lehnert M, Stehle D, Feil S. Visualising and understanding cGMP signals in the cardiovascular system. *Br J Pharmacol.* 2022;179(11):2394-2412. doi:10.1111/BPH.15500
28. Russwurm M, Koesling D. Measurement of cGMP-generating and -degrading activities and cGMP levels in cells and tissues: Focus on FRET-based cGMP indicators. *Nitric Oxide.* 2018;77:44-52. doi:10.1016/J.NIOX.2018.04.006
29. Stehle D, Xu MZ, Schomber T, et al. Novel soluble guanylyl cyclase activators increase glomerular cGMP, induce vasodilation and improve blood flow in the murine kidney. *Br J Pharmacol.* 2022;179(11):2476-2489. doi:10.1111/BPH.15586

30. Moeller MJ, Sanden SK, Soofi A, Wiggins RC, Holzman LB. Podocyte-specific expression of cre recombinase in transgenic mice. *Genesis*. 2003;35(1):39-42. doi:10.1002/GENE.10164
31. Kisanuki YY, Hammer RE, Miyazaki J ichi, Williams SC, Richardson JA, Yanagisawa M. Tie2-Cre Transgenic Mice: A New Model for Endothelial Cell-Lineage Analysis in Vivo. *Dev Biol*. 2001;230(2):230-242. doi:10.1006/DBIO.2000.0106
32. Alva JA, Zovein AC, Monvoisin A, et al. VE-Cadherin-Cre-recombinase transgenic mouse: a tool for lineage analysis and gene deletion in endothelial cells. *Dev Dyn*. 2006;235(3):759-767. doi:10.1002/DVDY.20643
33. Heffner CS, Herbert Pratt C, Babiuk RP, et al. Supporting conditional mouse mutagenesis with a comprehensive cre characterization resource. *Nature Communications* 2012 3:1. 2012;3(1):1-9. doi:10.1038/ncomms2186
34. Payne S, Val S De, Neal A. Endothelial-Specific Cre Mouse Models: Is Your Cre CREdible? *Arterioscler Thromb Vasc Biol*. 2018;38(11):2550. doi:10.1161/ATVBAHA.118.309669
35. Poosti F, Pham BT, Oosterhuis D, et al. Precision-cut kidney slices (PCKS) to study development of renal fibrosis and efficacy of drug targeting ex vivo. *Dis Model Mech*. 2015;8(10):1227-1236. doi:10.1242/DMM.020172
36. Warren SC, Nobis M, Magenau A, et al. Removing physiological motion from intravital and clinical functional imaging data. *Elife*. 2018;7. doi:10.7554/ELIFE.35800
37. Unnersjö-Jess D, Scott L, Blom H, Brismar H. Super-resolution stimulated emission depletion imaging of slit diaphragm proteins in optically cleared kidney tissue. *Kidney Int*. 2016;89(1):243-247. doi:10.1038/KI.2015.308
38. Ferrero R, Rodriguez-Pascual F, Miras-Portugal MT, Torres M. Comparative effects of several nitric oxide donors on intracellular cyclic GMP levels in bovine chromaffin cells: correlation with nitric oxide production. *Br J Pharmacol*. 1999;127(3):779-787. doi:10.1038/SJ.BJP.0702607
39. Boulton CL, Irving AJ, Southam E, Potier B, Garthwaite J, Collingridge GL. The nitric oxide--cyclic GMP pathway and synaptic depression in rat hippocampal slices. *Eur J Neurosci*. 1994;6(10):1528-1535. doi:10.1111/J.1460-9568.1994.TB00543.X

40. Rinschen MM, Gödel M, Grahammer F, et al. A Multi-layered Quantitative In Vivo Expression Atlas of the Podocyte Unravels Kidney Disease Candidate Genes. *Cell Rep.* 2018;23(8):2495-2508. doi:10.1016/J.CELREP.2018.04.059
41. Golos M, Lewko B, Bryl E, et al. Effect of angiotensin II on ANP-dependent guanylyl cyclase activity in cultured mouse and rat podocytes. *Kidney Blood Press Res.* 2002;25(5):296-302. doi:10.1159/000066790
42. Yaoita E, Yoshida Y, Nameta M, Takimoto H, Fujinaka H. Induction of interdigitating cell processes in podocyte culture. *Kidney Int.* 2018;93(2):519-524. doi:10.1016/J.KINT.2017.06.031
43. Chittiprol S, Chen P, Petrovic-Djergovic D, Eichler T, Ransom RF. Marker expression, behaviors, and responses vary in different lines of conditionally immortalized cultured podocytes. *Am J Physiol Renal Physiol.* 2011;301(3). doi:10.1152/AJPRENAL.00234.2011
44. Mundel P, Bachmann S, Kriz W, Gambaryan S, Koesling D. Immunolocalization of soluble guanylyl cyclase subunits in rat kidney. *Histochem Cell Biol.* 1995;103(1):75-79. doi:10.1007/BF01464478
45. Jarry A, Renaudin K, Denis MG, et al. Expression of NOS1 and soluble guanylyl cyclase by human kidney epithelial cells: morphological evidence for an autocrine/paracrine action of nitric oxide. *Kidney Int.* 2003;64(1):170-180. doi:10.1046/J.1523-1755.2003.00078.X
46. Heintz ES, Broecker KAE, Lehrmann C, et al. Localization of natriuretic peptide receptors A, B, and C in healthy and diseased mouse kidneys. *Pflugers Arch.* 2023;475(3):343-360. doi:10.1007/S00424-022-02774-9
47. Green DF, Duruibe VA, Blyden G, Laskey RE, Bourgoignie JJ. Uptake of atrial natriuretic peptide and production of cGMP in cultured human glomerular endothelial cells. *J Am Soc Nephrol.* 1994;5(4):1091-1098. doi:10.1681/ASN.V541091
48. Mani I, Garg R, Tripathi S, Pandey KN. Rapid Internalization and Trafficking of GC-A/NPRA via Endo-lysosomal Compartments with Concurrent Generation of cGMP in Mouse Mesangial Cells: Role of FQQI Motif. *The FASEB Journal.* 2016;30(S1):967.19-967.19. doi:10.1096/FASEBJ.30.1\_SUPPLEMENT.967.19

49. Somanna NK, Mani I, Tripathi S, Pandey KN. Clathrin-dependent internalization, signaling, and metabolic processing of guanylyl cyclase/natriuretic peptide receptor-A. *Mol Cell Biochem.* 2018;441(1-2):135-150. doi:10.1007/S11010-017-3180-0
50. Castro LR V, Schittl J, Fischmeister R. Feedback control through cGMP-dependent protein kinase contributes to differential regulation and compartmentation of cGMP in rat cardiac myocytes. *Circ Res.* 2010;107(10):1232-1240. doi:10.1161/CIRCRESAHA.110.226712
51. Staffel J, Valletta D, Federlein A, et al. Natriuretic peptide receptor guanylyl cyclase - A in podocytes is renoprotective but dispensable for physiologic renal function. *Journal of the American Society of Nephrology.* 2017;28(1):260-277. doi:10.1681/ASN.2015070731/-DCSUPPLEMENTAL
52. Lewko B, Wendt U, Szczepanska-Konkel M, Stepinski J, Drewnowska K, Angielski S. Inhibition of endogenous nitric oxide synthesis activates particulate guanylyl cyclase in the rat renal glomeruli. *Kidney Int.* 1997;52(3):654-659. doi:10.1038/KI.1997.379
53. Stepinski J, Wendt U, Lewko B, Angielski S. Co-operation between particulate and soluble guanylyl cyclase systems in the rat renal glomeruli. *Journal of Physiology and Pharmacology.* 2000;51(3).
54. Tulsian NK, Sin VJE, Koh HL, Anand GS. Development of Phosphodiesterase-Protein-Kinase Complexes as Novel Targets for Discovery of Inhibitors with Enhanced Specificity. *Int J Mol Sci.* 2021;22(10). doi:10.3390/IJMS22105242
55. Lavan BE, Lakey T, Houslay MD. Resolution of soluble cyclic nucleotide phosphodiesterase isoenzymes, from liver and hepatocytes, identifies a novel IBMX-insensitive form. *Biochem Pharmacol.* 1989;38(22):4123-4136. doi:10.1016/0006-2952(89)90694-1
56. Peters S, Paolillo M, Mergia E, et al. cGMP Imaging in Brain Slices Reveals Brain Region-Specific Activity of NO-Sensitive Guanylyl Cyclases (NO-GCs) and NO-GC Stimulators. *Int J Mol Sci.* 2018;19(8). doi:10.3390/IJMS19082313

## 6 Discussion

*The following discussion encompasses all compiled data, incorporating the results from the submitted manuscript (Chapter 5).*

### 6.1 cGMP signaling in podocytes

#### 6.1.1 Evidence for pGC-mediated cGMP synthesis in podocytes

Although podocytes may not exhibit fully developed foot processes or cell-specific markers, the use of conditionally immortalized podocyte cell lines from various species (mouse, rat, human) expressing the temperature-sensitive mutant of the SV40 T-antigen is common practice and formed the basis for cGMP research in podocytes.<sup>157,158</sup> Species-dependent differences manifest in the absence of essential key enzymes for the cGMP signaling cascade, such as sGC and its subunits, resulting in a lack of cGMP response upon stimulation.<sup>29,69,72</sup> As the data on the existence of guanylyl cyclase systems in this cell type are contradicting, we addressed this question by isolating glomeruli of transgenic mice (Pod:Cre/cGi500) expressing the cGMP biosensor exclusively in podocytes. The NP/pGC/cGMP pathway was stimulated by two different natriuretic peptides, ANP and BNP, which function as ligands for the natriuretic peptide receptors GC-A and GC-B. The interaction between ligands and receptor resulted in different cGMP responses, as evidenced by a stronger FRET/cGMP response elicited by 500 nM ANP compared to 500 nM BNP. In addition, AKS of Pod:Cre/cGi500 mice also demonstrated an ANP-evoked FRET/cGMP response (**Chapter 5, Fig. 1**). Previous studies conducted on cultured podocytes are in line with our results, demonstrating cGMP synthesis upon ANP stimulation.<sup>29,68,69,72,159,160</sup> The design of the cGi500 sensor did not allow for differentiation between cGMP pools synthesized by GC-A or GC-B activity. However, podocytes highly express GC-A mRNA and foot processes exhibit ANP-binding sites.<sup>52,65,67,161</sup> In addition, GC-A has shown a higher affinity towards ANP ( $\text{ANP} \geq \text{BNP}$ ), whereas GC-B preferentially binds CNP (not tested).<sup>162,163</sup> Therefore, we hypothesize, that GC-A is the receptor responsible for the cGMP synthesis after ANP and BNP administration. The importance of GC-A expression in renal tissue was demonstrated by a GC-A knockout model, in which GC-A protected against aldosterone-induced glomerular injury.<sup>164</sup> Furthermore, podocyte-specific knockout mice lacking GC-A (Podo-GC-A-KO) exhibited substantial albuminuria and glomerular damage following mineralocorticoid deoxycorticosterone acetate (DOCA) treatment or high salt-diet (6% NaCl diet and aldosterone).<sup>63,165</sup>

Isolated glomeruli and AKS of Pod:Cre/cGi500 mice showed a persistent elevated FRET/cGMP response following ANP administration throughout the entire measurement period. This observation was also made in AKS when using half the amount of ANP (**Supplemental Fig. 7**), which excludes sensor saturation as a potential cause for the prolonged signal. The signal declined slowly over a period of more than 1 hour, demonstrated in a long-term recording (**Supplemental Fig. 10**). As previously described in the **chapter 5.4**, the prolonged ANP-evoked cGMP synthesis could be maintained due to delayed internalization of ligand-receptor complexes of GC-A or delayed desensitization of the receptor by ligand-induced dephosphorylation or activation of PKC.<sup>166–169</sup> PKC is a downstream target of ANGII/AT1 signaling and plays a crucial role as mediator of the suppressive function on the GC-A receptor, emphasizing the counter-regulatory crosstalk between the RAAS and NP systems.<sup>86,159</sup> In addition, a positive feedback loop involving PKG or lower PDE activity, which would delay cGMP degradation, or a combination of the mentioned mechanism could be possible.<sup>170</sup> The plasma half-life for ANP/GC-A ligand-receptor binding ranges within 2 minutes,<sup>171,172</sup> prompting the hypothesis that signal termination occurs via circulating mediators in the plasma. Given that neither isolated glomeruli nor AKS are directly connected to the bloodstream, addressing this question would necessitate *in vivo* imaging. Due to the limitations preventing *in vivo* imaging with the biosensor cGi500 (discussed in **chapter 6.6**), the utilization of a more sensitive cGMP biosensor with enhanced signal-to-noise ratio could offer a potential solution.

To our knowledge, our data provides the first evidence of a long-lasting cGMP response following stimulation of the ANP/pGC/cGMP axis in podocytes. Conventional methods quantify cGMP levels after cell lysis using antibody-based techniques such as radioimmunoassay (RIA) or enzyme-linked immunosorbent assay (ELISA), which results in a loss of temporal resolution. The utilization of the FRET-based cGMP biosensor cGi500 demonstrates superiority over conventional biochemical methods in this context, enabling real-time monitoring of cGMP dynamics. This finding is particularly important in the context of reduced cGMP levels observed in disease, which are intended to be addressed through pharmacological treatment. A mutation in the ANP gene (mutant-ANP = MANP) was found to be more resistant to neprilysin-induced proteolytic degradation.<sup>173</sup> Pre-clinical results, including the first in-human study of MANP, suggest that this resistance may lead to prolonged effects in lowering blood pressure and suppressing aldosterone through GC-A activation.<sup>174,175</sup> Thus, a long-lasting ANP/GC-A/cGMP response in podocytes represents a potential target for novel therapeutic strategies and should be examined further for its clinical relevance in kidney diseases. However, our study was not designed to elucidate downstream effector molecules responsible for the prolonged response after ANP/pGC/cGMP axis stimulation in podocytes. Regarding the functional role of ANP stimulation, studies conducted with cultured rat podocytes suggest induced PKG $\alpha$

dimerization, cytoskeletal alterations, and increased albumin permeability.<sup>84,176</sup> This implies a potential influence on podocyte morphology, affecting foot processes and slit pore size, and ultimately glomerular permeability. However, this hypothesis has to be confirmed utilizing *ex vivo* or *in vivo* models.

### 6.1.2 Evidence for sGC-mediated cGMP synthesis in podocytes

To date, data on NO-related processes in isolated glomeruli have been limited to NO detection following stimulation with vasoactive substances such as ANGII,<sup>88,177</sup> while the localization of NO production remains speculative. Sharma et al. demonstrated glomerular cGMP production after BAY 41-2272 exposure, a NO-independent activator of sGC, but could not identify the specific cell type responsible.<sup>178</sup> Furthermore, data regarding the existence of a NO/sGC/cGMP pathway in podocytes is contradictory. Studies by Theilig et al. and Wang et al. failed to demonstrate a SNAP-mediated cGMP response in cultured podocytes.<sup>29,72</sup> To investigate whether podocytes from isolated glomeruli are capable of responding to stimulation of the NO/sGC/cGMP axis, SNAP was added through the perfusion system. SNAP, an NO donor, spontaneously releases the free radical NO under physiological conditions, triggered a robust FRET/cGMP response in cGi500-expressing podocytes, thereby indicating the existence of the NO/sGC/cGMP signaling pathway. To account for the possibility that SNAP stimulation exerts a paracrine effect on podocytes, another NO donor was used. Nitroglycerin generates NO through enzymatic bioactivation,<sup>179</sup> elicited also a FRET/cGMP response and provides additional evidence for NO/sGC-mediated cGMP synthesis in podocytes of isolated glomeruli. In addition, SNAP administration on AKS of Pod:Cre/cGi500 mice displayed a FRET/cGMP response, albeit to a lesser extent in terms of intensity (**Chapter 5, Fig. 1**). The signal profile was transient, which is in line with our expectations arising from the short half-life of NO in the range of a few milliseconds.<sup>180,181</sup> Without a connection to the blood stream, NO scavengers such as hemoglobin are not available to modulate fluctuating NO concentrations. As a result, the cGMP response observed in our experiments endures for an extended period and may potentially be terminated by desensitization of sGC.<sup>182</sup> Other studies are in agreement with our data, showing an increased cGMP concentration after SNAP administration.<sup>68,80,159,160</sup> Moreover, they also demonstrate that ANP consistently stimulates higher levels of cGMP production compared to cGMP synthesis elicited by SNAP. Increased cGMP levels following SNAP, as well as the sGC stimulator Riociguat, were able to decrease Adriamycin-induced TRPC6 expression and reduce podocyte injury, indicating a protective effect of this signaling pathway for podocytes.<sup>80</sup> Mundel et al. and Jarry et al. localized sGC in podocytes of kidney tissue and Hart et al. provided evidence for sGC subunit expression in a human podocyte cell line.<sup>80,90,155</sup> Our experimental setup did not allow for identification of the sGC subunit ( $\alpha 1$ ,  $\beta 1$ ,  $\alpha 2$ , and  $\beta 2$ ) configuration present in podocytes, additional experiments are required for this

purpose. The results obtained from antibody pull-down, Western blot analysis or immunolabeling, should be critically evaluated. The presence of sGC subunits does not necessarily imply functionality, and vice versa. Furthermore, evidence suggest a dynamic equilibrium between mature functional heterodimers and immature sGC forms.<sup>183</sup> During stress conditions, active sGC forms can transition to immature forms,<sup>184</sup> while sGC stimulators/activators hold therapeutic potential for restoring diminished cGMP responses resulting from this transition.<sup>185</sup> Thus, the relative levels of mature sGC heterodimer and immature sGC (sGC $\beta$ 1 subunit-Hsp90 complex) before and after stimulation should be assessed, as NO can promote the maturation process and can activate sGC $\beta$ 2 subunits without a second sGC subunit partner.<sup>183,186</sup>

Additionally, the administration of SNAP, a compound releasing NO spontaneously, can exert its influence on all cell types within isolated glomeruli and AKS. Spatial confinement of NO release can be achieved for single-cell studies using the photocaged NO donor (Npm-photocaged) NONOate, which has already been tested with cGi500-expressing vascular smooth muscle cells (VSMCs).<sup>187</sup> UV irradiation can induce cellular toxicity, whereas two-photon microscopy (2PE microscopy) offers advantages for the utilization of such NO donors. This method restricts excitation to a focal plane, unlike confocal microscopy where excitation occurs throughout the focus, requiring a pinhole for optical sectioning.<sup>188</sup> The photocaged NO donor Cupferron (CP) O-alkylated with anthracene (CPA), exhibited negligible photo-activated cell toxicity when coupled with 2PE microscopy,<sup>189</sup> thus presenting a promising option for future experiments. Our experiments were not designed to identify the NO-producing cell in the glomerulus, as both mesangial cells and glomerular endothelial cells possess NOS activity.<sup>80,190,191</sup> One way to test the influence of NO on podocytes is to use eNOS knockout mice (eNOS-KO mice). Endothelial NOS is mostly expressed in endothelial cells and deficiency of eNOS has been associated with podocyte loss and injury, emphasizing endothelial-podocyte interaction.<sup>93,94</sup>

In summary, our study provides evidence for the presence and functionality of both guanylyl cyclase pathways (sGC and pGC) in podocytes of isolated glomeruli and kidney slices from Pod:Cre/cGi500 mice, in which the synthesis of cGMP stimulated by ANP predominated.



### 6.1.3 Suppressed global cGMP levels after simultaneous activation of sGC & pGC-pathways in podocytes

After providing evidence for the existence of the sGC and pGC pathways in podocytes, we elucidated a potential reciprocal regulation between these two signaling pathways. Simultaneous co-stimulation with ANP+SNAP in isolated glomeruli from Pod:Cre/cGi500 mice resulted in a smaller FRET/cGMP response compared to the stimulation with ANP or SNAP alone. Co-stimulation in AKS confirmed this outcome, whereas only ANP stimulation exhibited a higher FRET/cGMP response in comparison (**Chapter 5, Fig. 1**). These findings align with the work of Lewko et al., but contradict the results observed in a later study (2015).<sup>68,160</sup> In the study carried out in 2015, co-stimulation in cultured mouse and rat podocytes resulted either in equivalent or even higher cGMP levels compared to ANP stimulation alone. However, in both studies, cGMP measurements were conducted using a radioimmunoassay after the addition of the unspecific PDE-inhibitor IBMX. In contrast, our experimental approach enabled us to monitor cGMP dynamics with temporal resolution and without inhibiting cGMP degradation. In AKS of Pod:Cre/cGi500 mice, the signal profile after co-stimulation revealed a direct inhibition of the global cGMP concentration that, as we hypothesize, is controlled by a potential negative feedback mechanism preferentially lowering ANP/pGC-controlled cGMP level (**Chapter 5, Fig. 1**). The reached FRET/cGMP response was higher compared to the response induced by SNAP, but lower than the response induced by ANP. The time course of the co-stimulation exhibited similarities with the individual stimulation by SNAP and ANP, presenting a progressively developing signal (peak) that then declined and transitioned into the characteristic prolonged plateau seen with ANP stimulation alone. This implies that both guanylyl cyclase (GC) systems operate concurrently, preventing excessively high cGMP levels even shortly after simultaneous stimulation of sGC and pGC. The absence of an additive effect is seen in all other test combinations with ANP+SNAP, suggesting that podocytes strictly regulate their cGMP homeostasis through intrinsic inhibition with a ceiling on the maximum intracellular cGMP level. However, sequential stimulation with ANP and SNAP, and vice versa, could elucidate which signaling pathway exerts a stronger influence on the other. Both Lewko et al. and Stepinski et al. discussed a mutual compensation between the two GC systems, where the suppressor effect of ANGII or the inhibition of the NOS system (also in a time-dependent manner) can exert influence.<sup>68,160,192,193</sup> Additionally, global cGMP levels can be diminished through elimination pathways like PDE-mediated hydrolysis or cGMP extrusion. Both options will be discussed in the subsequent sections. Besides PDE activity, our study was not designed to identify additional downstream effector molecules responsible for the hypothesized reciprocal interaction between sGC and pGC following co-stimulation with ANP+SNAP in podocytes.

## 6.2 Phosphodiesterase (PDE) activity in podocytes

The intracellular cGMP concentration is regulated by its synthesis and degradation. Degradation is mediated by PDEs, which cleave the 3', 5'-cyclic phosphate moiety of cGMP to produce the corresponding purine nucleotide GTP. Conventional techniques for assessing cGMP levels in isolated glomeruli involve the addition of the nonspecific PDE inhibitor IBMX as pretreatment prior to stimulation.<sup>194–196</sup> This approach stops dynamic cellular processes influenced by cGMP degradation, facilitating comparisons before and after stimulation of this pathway. We administered IBMX to elucidate the impact of PDE inhibition on basal cGMP levels in podocytes of isolated glomeruli from Pod:Cre/cGi500 mice, which resulted in a progressively increasing FRET/cGMP response. Subsequently, the impact of PDE inhibition on stimulated sGC or/and pGC signaling was tested. AKS of Pod:Cre/cGi500 mice were subjected to stimulation with ANP and/or SNAP, with the addition of IBMX during the course of stimulation (**Chapter 5, Fig. 2**). IBMX administration potentiated the FRET/cGMP response triggered by co-stimulation with ANP+SNAP the most, suggesting that the reduction in global cGMP concentration (discussed in **Chapter 6.1.3**) is partly influenced by enhanced PDE activity. IBMX administration on SNAP-evoked cGMP levels had a greater effect than on ANP-evoked cGMP level, indicating higher PDE activity after sGC activation. The prolonged cGMP response observed with ANP or ANP+SNAP stimulation was not influenced by PDE inhibition. These findings imply that cGMP pools synthesized by ANP/pGC exhibit less susceptibility to degradation by PDEs, which we hypothesize is based on the localization of the NP receptor family members (GC-A/B and NPR-C) on the cell body and/or foot processes. This hypothesis finds support in the detection of pGC activity in foot processes and the presence of ANP binding sites.<sup>197–199</sup> This suggests compartmentalization of cGMP pools, in addition to transmembrane-associated pGC activity and sGC localization in the cytosol. Furthermore, the spatial distribution of PDEs within the cell is a crucial factor to consider, as the majority of the PDEs would accumulate in the cell body to regulate the overall intracellular cGMP concentration. As a result, pGC/cGMP pools generated at the membrane, especially in the foot processes, may experience slower degradation. The lack of evidence on the abundance, localization, and activity or potential subcellular trafficking of PDEs following stimulation of the two cGMP signaling pathways in podocytes, leaves this hypothesis unanswered. However, it remains possible that the hydrolysis of ANP/pGC-synthesized cGMP pools would primarily depend on PDEs with a slow degradation rate. Different degradation rates are described for members of the PDE4 family and cAMP activity.<sup>200,201</sup> This would result in a prolonged cGMP response, indicating that enzymatic kinetics play a more significant role than the subcellular localization of PDEs with restricted cGMP accessibility. Of note, individual PDE isoforms are not equally effectively inhibited by IBMX,<sup>202,203</sup> highlighting the need to assess the inhibition of selected PDE isoforms on AKS.

### 6.2.1 PDE3 and PDE5 predominate in podocytes

Evidence regarding the profile of specific PDE isoforms within podocytes is primarily based on proteomics data. These datasets hint towards a subset of PDE isoforms that require further examination to elucidate their enzymatic activity. Building upon the findings of Rinschen et al. and corroborating literature on podocyte-specific and renal expression,<sup>66,72</sup> our selection included PDE2a, 3, 4, 5, and 9a. Commercially available inhibitors targeting these PDE isoforms were applied on AKS of Pod:Cre/cGi500 mice to assess their impact on cGMP signaling under basal conditions (**Chapter 5, Fig. 3**). Notably, the inhibition of PDE3 by Cilostamide elicited the highest FRET/cGMP response, followed by PDE5 inhibition with Avanafil. Avanafil was chosen as a potent PDE5 inhibitor due to its higher selectivity against other PDE isoforms compared to Sildenafil, a well-established PDE5 inhibitor.<sup>204</sup>

Subsequently, the impact of specific PDE inhibition on stimulated sGC or/and pGC signaling was tested. AKS of Pod:Cre/cGi500 mice were subjected to stimulation with ANP and/or SNAP, with the addition of Cilostamide (PDE3 inhibitor) or Avanafil (PDE5 inhibitor) during the course of stimulation (**Chapter 5, Fig. 4**). PDE3 inhibition potentiated the FRET/cGMP response triggered by ANP the most, followed by ANP+SNAP, indicating a preference for the ANP/pGC/cGMP axis. PDE3 hydrolyzes cAMP and cGMP: In the presence of elevated cGMP concentrations, cAMP hydrolysis by PDE3 is inhibited, leading to intracellular cAMP accumulation.<sup>205</sup> The interplay between cAMP and cGMP may function as a mechanistic regulator for cytoskeletal alterations, impacting foot processes and slit pore size, as postulated by Sharma et al.<sup>176</sup> Additionally, evidence suggests that cAMP promotes the assembly of cell-cell contacts among podocytes and prevents podocyte apoptosis.<sup>206–208</sup>

PDE5 inhibition during an ongoing stimulation with the trinary test set ANP or/and SNAP revealed a similar FRET/cGMP response to that observed with PDE3 inhibition, albeit to a lesser extent. Avanafil potentiated the synthesized cGMP pools following ANP and ANP+SNAP stimulation the most, while showing only a marginal impact on SNAP stimulation (**Chapter 5, Fig. 4**). PDE5 binds cGMP with high specificity. PDE5 inhibition in podocytes has demonstrated renoprotective effects in various kidney disease models.<sup>79,209–211</sup> Furthermore, research has linked PDE5 inhibition with podocyte motility,<sup>81</sup> and with the (e)NOS/NO/sGC/cGMP pathway that protects against podocyte damage.<sup>79,80</sup> Although PDE5 appears to be highly associated with the NO/sGC/cGMP axis, our data demonstrate a preference for pGC-synthesized cGMP pools. The possibility that the ANP/pGC/cGMP pathway may influence PDE5 activity is supported by the work of Polzin et al., where increased levels of PDE5 and PKG-II were observed in kidneys of corin knockout mice.<sup>71</sup> Corin is a transmembrane serine/threonine protease responsible for the conversion of pro-ANP to active

ANP.<sup>212</sup> Regarding the limitation of this study, we tested a subset of PDE isoforms using commercially available inhibitors, which results in a biased approach. These inhibitors are not completely specific, thus interference with other PDE isoforms cannot be excluded.

Taken together, PDE3 and PDE5 preferentially influence ANP/pGC-generated cGMP pools in podocytes. Specific PDE isoforms are targeted for the pharmacological elevation of diminished cGMP signaling in diseases, emphasizing the need to investigate their activity in podocytes.

### **6.3 Inhibition of cGMP extrusion increases intracellular cGMP levels in podocytes**

In addition to PDE-mediated hydrolysis, intracellular cGMP concentration can be regulated through cGMP efflux. Previous studies suggest the release of cGMP following stimulation of the ANP/pGC/cGMP axis in podocytes, as well as the extrusion of cGMP by ATP-binding cassette (ABC) transporters.<sup>160,213–217</sup> Moreover, probenecid, an inhibitor of the organic anion transporter OAT1, was able to induce cGMP accumulation in cultured rat podocytes,<sup>160</sup> providing evidence for an active transport by the organic anion transporter family. By administering probenecid to isolated glomeruli from Pod:Cre/cGi500 mice, we were able to demonstrate cGMP efflux at basal conditions. This was shown by an increase in the FRET/cGMP response in podocytes. A subsequent stimulation with ANP and/or SNAP could uncover potential differences in the degree of released cGMP and whether this elimination pathway partially accounts for the non-additive cGMP response after co-stimulation with ANP+SNAP seen in our experiments. Lewko et al. tested the effect of probenecid on ANP or/and SNAP stimulation in cultured rat podocytes, showing an increased cGMP accumulation after ANP+SNAP stimulation compared to ANP and SNAP alone.<sup>160</sup> These results are in line with our hypothesis, however, experiments utilizing isolated glomeruli or AKS should be conducted to further elucidate these findings.

Currently, there is no available data regarding the functional role of cGMP extrusion by podocytes, as well as the specific cell type targeted by this process. However, it is conceivable that cells downstream within the tubular system could be the next potential target and respond to extracellular cGMP as a component of a paracrine signaling cascade, which traverses the cell membrane. This assumption is supported by the fact that cultured renal proximal tubule (RPT) cells responded to the addition of the membrane-permeable analogue 8-Br-cGMP with an increase in intracellular cGMP levels.<sup>218</sup> Additionally, several studies confirm the presence of sGC in this cell type.<sup>29,105,219,220</sup> Furthermore, RPTs responded to the addition of 8-Br-cGMP, the NO donor sodium nitroprusside (SNP), or co-incubation with endothelial cells (stimuli-activated) with decreased Na<sup>+</sup>/K<sup>+</sup>-ATPase activity and transcellular Na<sup>+</sup> transport.<sup>221</sup> *In vivo*

experiments involving the infusion of Texas red-conjugated cGMP into the renal cortical interstitium revealed that interstitial cGMP inhibits renal tubular Na<sup>+</sup> uptake without affecting hemodynamic parameters such as RBF and GFR. Infusion of conjugated-cGMP into the renal artery induced renal vasodilation and increased glomerular filtration, leading to a comparable level of natriuresis.<sup>222</sup> This data strongly suggests that cGMP release is involved in paracrine signaling, and the resulting effect depends on the local microenvironment.

#### **6.4 Calcium (Ca<sup>2+</sup>)-dependent mechanisms trigger cGMP release in podocytes**

The morphology, structure, and viability of podocytes are affected by calcium (Ca<sup>2+</sup>) signaling.<sup>223</sup> Despite being distinct cellular signaling pathways, calcium and cGMP signaling exhibit interactive relationships that mutually regulate each other through diverse mechanisms (e.g. cGMP hydrolysis by Ca<sup>2+</sup>/calmodulin-dependent PDE1).<sup>224</sup> Notably, GECs respond to Bradykinin or ATP by eliciting an increase in intracellular calcium levels ([Ca<sup>2+</sup>]<sub>i</sub>) and triggering both NO-in/dependent cGMP production in e.g. mesangial cells.<sup>225,226</sup> To assess the responsiveness of podocytes to stimuli that trigger calcium-dependent mechanisms, we tested the effect of Bradykinin and ATP on isolated glomeruli from Pod:Cre/cGi500 mice. Both compounds triggered a progressively evolving FRET/cGMP response that endured throughout the wash-out phase without returning to baseline levels. These data suggest that ligand-receptor binding may exert a direct effect on podocytes, thereby increasing cGMP levels. Alternatively, an indirect paracrine signaling, potentially involving eNOS/NO/sGC/cGMP signaling, could exert influence. Studies indicate the expression of bradykinin receptors and a bradykinin-induced increase in [Ca<sup>2+</sup>]<sub>i</sub> in cultured podocytes.<sup>227-230</sup> Furthermore, P2 receptors (comprising P2X and P2Y receptor subtypes) have been identified on both cultured podocytes and isolated glomeruli.<sup>231</sup> These receptors mediate an ATP-triggered Ca<sup>2+</sup> influx,<sup>232</sup> primarily through the metabotropic receptor subtypes P2Y1 and P2Y2.<sup>232,233</sup> A recent intravital multiphoton microscopy imaging study postulated a role for P2 receptors and transient receptor potential canonical 6 (TRPC6) channels in mechanical and metabolic sensing, emphasizing the significance of calcium-dependent mechanisms in podocytes.<sup>234</sup> In this context, both cGMP-synthesizing guanylyl cyclase systems (sGC and pGC) have been associated with a suppressive role on TRPC6 expression, in which Adriamycin-treated eNOS-KO mice and DOCA-treated podocyte-specific GC-A KO (Podo-GC-A-KO) mice showed an enhanced expression of glomerular TRPC6.<sup>63,80</sup> Furthermore, Sonneveld et al. postulated a connection between PDE5/cGMP/PKG-I signaling and the binding of PPAR-γ to the TRPC6 promoter, thereby reducing TRPC6-mediated Ca<sup>2+</sup> influx and ultimately mitigating podocyte injury.<sup>79</sup> Increased intracellular calcium levels in podocytes have been demonstrated to enhance cell motility,<sup>235,236</sup> albumin permeability, and are associated with podocyte injury,<sup>237</sup> accentuating

the need to investigate both calcium and cGMP signaling in health and disease. As damage to podocytes of isolated glomeruli cannot be avoided, we discontinued experiments with this method to differentiate whether NO-in/dependent mechanisms played a role in ATP-/bradykinin-evoked cGMP synthesis in podocytes. Instead, we plan to utilize whole-body eNOS-KO mice along with the calcium indicator GCaMP3 and the cGMP biosensor cGi500 used in this study, to resolve a potential endothelial-podocyte cross talk *ex vivo* and *in vivo*.

PIEZO1 is a mechanosensitive ion channel protein that plays a functional role in stretch-induced  $\text{Ca}^{2+}$  influx and ATP release.<sup>238</sup> Conditional endothelial cell-specific deletion of PIEZO1 has been demonstrated to influence eNOS expression in this cell type, suggesting the capability to detect and adjust to variations in shear stress induced by blood flow, consequently inducing vasodilation.<sup>239,240</sup> The presence of PIEZO channels has been confirmed on GECs as well as podocytes,<sup>241,242</sup> and mechanical stress has been shown to modulate cGMP production in conditionally immortalized mouse podocytes.<sup>69</sup> To investigate whether cGMP is a component of the PIEZO1-mediated mechanotransduction pathway in podocytes, isolated glomeruli were treated with Jedi2 (PIEZO1 activator), which elicited a cGMP response in podocytes from Pod:Cre/cGi500 mice. Further experiments are required to validate these findings and to elucidate the signaling cascade in greater detail.

In summary, our data suggest a connection between calcium-dependent mechanisms and cGMP signaling in podocytes, implicating their involvement in mechanosensation, and pointing towards a potential stimulus-driven endothelial-podocyte crosstalk.

## 6.5 cGMP signaling in glomerular endothelial cells (GECs)

### 6.5.1 Evidence for sGC-/pGC-mediated cGMP synthesis

Endothelial cells serve as a link between the circulatory system and tissues, regulating vasotonus through local mechanisms such as the secretion of nitric oxide via a calcium-calmodulin-mediated activation.<sup>243,244</sup> GECs exhibit a remarkably flattened morphology and transcellular fenestrations.<sup>245</sup> They express eNOS and respond to NOS agonists (such as L-arginine) by releasing nitric oxide (NO).<sup>80,246,247</sup> The production of NO plays a crucial role in renal hemodynamics, maintaining the integrity of the capillary protein permeability barrier, counteracting the generation of reactive oxygen species (ROS) through the NO/sGC/cGMP pathway.<sup>41,248</sup> However, little is known about whether GECs possess intrinsic cGMP dynamics. To address this question, kidney slices from Tie2:Cre/cGi500 mice expressing the cGMP biosensor exclusively in the cytosol of endothelial cells were exposed to cGMP-elevating agents. The NP/pGC/cGMP system was stimulated by ANP, while the NO/sGC/cGMP system was activated with the NO donors SNAP or DEA NONOate. Both stimulations resulted in an

increase in intracellular cGMP concentration with similar signal strength, and co-stimulation (ANP+SNAP) revealed an additive effect (**Chapter 5, Fig. 1, Supplemental Fig. 8**).

The cGMP response initiated in GECs after ANP stimulation is anticipated to result from the binding of the ligand to its receptor. Our findings are in line with the expression pattern of GC-A, GC-B and the NP-clearance receptor-C (NPR-C) on glomerular endothelial cells,<sup>52</sup> and with the work of Green et al. demonstrating a dose-dependent accumulation of cGMP following ANP administration in cultured human GECs.<sup>249</sup> The receptor selectivity of GC-A and GC-B for the natriuretic peptide family (ANP, BNP, CNP) in GECs remains uncertain, as does the hierarchy for cGMP production. The biological role of renal endothelial GC-A and GC-B is still unknown, but there are reports suggesting an influence of ANP on endothelial permeability and in renal inflammation.<sup>250–252</sup> Furthermore, mice with endothelial-restricted deletion of the GC-A gene proved that endothelial GC-A is indeed crucial for the ANP-induced acute increase in capillary permeability to macromolecules.<sup>75</sup> The design of the sensor precludes making conclusions regarding the specific NP receptor (GC-A or GC-B) involved in ANP-mediated cGMP synthesis in GECs. The NP-receptors GC-A and GC-B exhibit a high degree of structural similarity,<sup>253,254</sup> posing challenges for the targeted blockade of a specific receptor. The GC-A positive allosteric modulator (PAM), MUF-651, is a promising development, enhances ANP-mediated cGMP generation in HEK cells while demonstrating low affinity towards GC-B.<sup>255</sup> The utilization of this modulator has the potential to confirm the existence of an ANP/GC-A/pGC/cGMP signaling cascade within GECs.

In GECs of Tie2:Cre/cGi00 mice, stimulation with SNAP or DEA NONOate resulted in an elevation of intracellular cGMP levels, indicating that GECs are not only capable of producing NO but are also responsive to it. This implies that this cell type has the ability to induce cGMP synthesis in a sGC-dependent manner. The expression of two subunits of sGC (sGC $\alpha$ 2 and sGC $\beta$ 2) was shown in cultured human GECs.<sup>80</sup> Based on our knowledge, this study represents the first documentation of a functional NO/sGC/cGMP pathway in GECs. Our experimental setup lacks the capability to distinguish between the induced cGMP synthesis from different sGC subunit configurations. Studies examining sGC subunit expression in diverse cell types, including endothelial cells, have predominantly concentrated on systemic vasculature or non-renal tissues.<sup>29,30,256</sup> These investigations suggest that the sGC $\alpha$ 1 $\beta$ 1 heterodimer is the prevailing form. Further research is necessary to provide conclusive evidence regarding the sGC subunit expression present in glomerular endothelial cells and the function of NO/sGC/cGMP signaling in this cell type. Building upon Stehle et al.'s study, future experiments could integrate an sGC activator, such as BAY-543, known to induce cGMP generation under conditions of oxidative stress in glomeruli of kidney slices from cGi500 biosensor mice.<sup>92</sup> Moving away from real-time monitoring of cGMP dynamics *ex vivo*,

additional immunolabeling, Western blots or single cell proteomic analysis could provide a clearer picture about sGC expression in GECs. We investigated the impact of exogenous NO delivered to GECs through spontaneous release from NO donors. However, the study did not investigate whether endogenously produced NO via calcium-dependent or- independent activation of eNOS within the cell induces a different cGMP response or any response at all. This question could be addressed by using agents known to induce calcium-dependent eNOS activation, such as agonists like acetylcholine, bradykinin, or carbachol.

Evidence for an actively regulated cGMP system in GECs is almost non-existent in the literature, as even the presence of guanylyl cyclases is not well-documented. We claim to be the first to provide such data using real-time cGMP measurements in living kidney tissue. However, further investigation is required to elucidate the specific role of cGMP in GECs.

### **6.5.2 GECs exhibit high basal PDE activity, with PDE2a being the predominant isoform**

In our experiments, GECs exhibited a higher basal PDE activity compared to podocytes with a predominance of the PDE2a isoform (**Chapter 5, Fig. 3**). Stimulation with ANP and/or SNAP in addition with IBMX administration demonstrated a stronger PDE influence on the ANP/pGC-generated cGMP pools (**Chapter 5, Fig. 2**), while PDE2a showed no preference towards one cGMP signaling pathway (**Chapter 5, Fig. 4**). These findings align with the study conducted by Sadhu et al., who reported positive PDE2a immunostaining in capillary endothelial cells within the glomerulus of human renal tissue.<sup>257</sup> Expressed in GECs, PDE2 could potentially influence signaling pathways mediated by cAMP and cGMP, based on its capability to hydrolyze both. This assumption would support the work of Surapisitchat et al., suggesting a concentration-dependent influence of cGMP on endothelial permeability via PDE2 and PDE3 activity.<sup>258</sup> At lower concentrations, cGMP inhibits PDE3, which increases the local cAMP pool and decreases permeability. Conversely, at higher concentrations, cGMP activates PDE2, which leads to a decrease in the cAMP level and reverses the effect. Differential expression of PDE2 and PDE3 may serve as a regulatory mechanism between physiological and pathological cGMP levels, thereby fine-tuning endothelial permeability.<sup>259</sup> When interpreting data on endothelial cells, it should be noted that the relative expression levels of PDEs vary among different endothelial cell beds.<sup>260</sup> Additionally, the activity of PDE isoforms changes significantly in cultured endothelial cells between passages and in response to phenotypic alterations, as demonstrated in resting BAEC exhibiting cobblestone morphology compared to spindle-shaped proliferating BAEC.<sup>261</sup> This phenotypic heterogeneity of endothelial cells is rarely acknowledged in drug development.<sup>262,263</sup> Recent efforts utilizing single-cell mRNA sequencing aim to address this issue by identifying marker genes for GECs.<sup>264</sup> This could provide the



foundation for establishing knockout models specifically targeting intraglomerular endothelial cells or for the development of Cre mouse lines. However, the biosensor cGi500 was able to reveal a functional cGMP signaling in GECs, wherein PDE activity influenced the regulation of global cGMP levels.

## 6.6 Evaluating cGi500 biosensor performance for cGMP imaging: Strengths and Limitations

### 6.6.1 Comparison of cGi500 with other cGMP biosensors

As the majority of cGMP signaling-related studies are based on sample preparation from cultured cell lines, we first transfected HEK 293T cells with the MH20\_pCMV\_cGi500 plasmid encoding the monomolecular FRET-based cGMP biosensor cGi500 (**Supplemental Fig. 1**). Following the preparation of homogenates, in which the sensor was dissolved in solution, we performed a dose-response curve analysis by introducing ascending ligand concentrations ranging from 0.01  $\mu\text{M}$  to 100  $\mu\text{M}$  cGMP. The analysis revealed a half-maximal effective concentration (EC<sub>50</sub>) of  $\sim 532$  nM (**Supplemental Fig. 1**), which reflects the cGMP binding affinity of the sensor. This result closely corresponds to the postulated EC<sub>50</sub> value of 500 nM determined by Russwurm et al.<sup>139</sup> In comparison to other cGMP biosensors, cGi500 demonstrates superiority in terms of cGMP affinity, dynamic range and spatial distribution. The cGMP biosensor cGES-DE5 utilizes the same FRET pair as cGi500 (CFP/YFP), but exhibits a lower affinity for cGMP compared to cGi500, with an EC<sub>50</sub> of  $1.5 \pm 0.2$   $\mu\text{M}$ .<sup>138,265</sup> In contrast, the biosensor Yellow PfPKG exhibits a higher cGMP affinity (EC<sub>50</sub> of 22 nM) and displays stronger FRET ratio changes upon stimulation compared to cGi500.<sup>138</sup> However, Yellow PfPKG has a smaller dynamic range than cGi500, saturating at lower cGMP concentrations while cGi500 can detect higher concentrations. Despite these limitations, PfPKG displays a nonuniform distribution pattern, which restricts its function to certain subcellular areas. By replacing the FRET pair CFP/YFP, the new developed cGMP biosensors surpassed cGi500 in terms of sensitivity and selectivity (cAMP/cGMP), but they have not been fully evaluated in an *ex vivo* setting. Among these, the cGMP biosensor Cygnus stands out, allowing for triple-parameter fluorescence imaging of cAMP, cGMP, and  $\text{Ca}^{2+}$ , albeit with significant spectral bleed-through (a contaminant in FRET signaling).<sup>266</sup> Furthermore, attempts have been made to combine two FRET sensors (TagRFP/mPlum and ECFP/Venus) with fluorescence lifetime imaging (FLIM) to avoid spectral crosstalk.<sup>267</sup> Nevertheless, ratiometric FRET-based biosensors, such as cGi500, simultaneously capture two fluorescence intensities, rendering them less susceptible to motion artifacts in the Z-plane. This characteristic enables their utilization in both *ex vivo* and *in vivo* experiments.

### 6.6.2 Signal intensity

The functionality of the sensor was assessed *in vitro* by conducting real-time measurements on cGi500-transfected HEK 293T cells following IBMX stimulation. An accumulation of intracellular cGMP was observed, evident by the increase in donor (CFP) fluorescence and the decrease in acceptor fluorescence (YFP). The modest change in the CFP/YFP emission ratio (maximal  $\Delta R/R_0 \sim 0.10\%$ ), fell within the range documented for primary cultures of cerebellar granule neurons (CGNs) or vascular smooth muscle cells (VSMCs) derived from cGi500-indicator mice ( $\Delta R/R_0 \sim 0.60\%$ ).<sup>140,268</sup> However, during the transition from *in vitro* to *ex vivo* or *in vivo* settings, the intensity of cGi500-mediated cGMP responses (maximal  $\Delta R/R_0$ ) decreases,<sup>140,142</sup> a trend that was also noticeable in our study. An observation that is primarily attributed to the small FRET changes associated with the CFP/YFP fluorophore combination.<sup>269</sup> Although this FRET pair is widely used, its application comes with difficulties in detection due to a narrow FRET dynamic range (**Supplemental Fig. 11**) and a low signal-to-noise ratio. This aspect is particularly challenging in tissues with high background autofluorescence signals, as observed in the kidney.<sup>270,271</sup> Increasing the excitation laser power improves the distinction of the signal from the background, but it simultaneously induces sensor photobleaching. This fact poses a challenge in time-lapse recordings, as significant photobleaching was observed in cGi500 heterozygous Tie2:Cre/cGi500 mice (**Supplemental Fig. 4**). Furthermore, processes such as phototoxic CFP excitation or the conversion of YFP into cyan fluorescent protein-like species can play a role.<sup>272,273</sup>

Considering the accessibility of the substance to the target cell is another factor to take into account. While isolated glomeruli are superfused with solution from all angles, the formation of concentration gradients in AKS will affect the strength of FRET signals when glomeruli are detected in deeper tissue layers. In an effort to address challenges associated with substance delivery to the target cell, we tried to evaluate cGMP dynamics through an intravital imaging (IVI) approach using two-photon microscopy. In this context, diminished FRET/cGMP responses are expected due to the undesirable excitation of the acceptor fluorophore using two-photon excitation. Following the experimental guidelines for IVI by Thunemann et al. and conducting an excitation scan of cGi500-transfected HEK 293T homogenates (**Supplemental Fig. 11**),<sup>142</sup> we chose a two-photon excitation at 860 nm. This decision was motivated by the fact that renal cells exhibit lower autofluorescence at higher wavelengths.<sup>269,271</sup> In addition, it leads to decreased light scattering in biological tissue, ultimately resulting in an increased penetration depth. Unfortunately, we were unable to obtain reliable FRET/cGi500 signals through an image segmentation pipeline intended to enhance the signal-to-noise ratio. This challenge was compounded by difficulties in applying the substance in terms of concentration and its systematic effect on blood pressure. Furthermore, it is feasible that podocytes maintain

a very low cGMP level, which precludes the detection of high cGMP concentrations after stimulation.

Each FRET pair has its advantages and disadvantages, however, there is still no existing FRET system available for *in vivo* imaging of the kidney. Therefore, conducting *ex vivo* experiments with AKS represents the next best option for studying mechanisms under conditions that closely mimics the physiological environment.

### 6.6.3 Isolated glomeruli vers. AKS

Time-lapse recordings of isolated glomeruli from Pod:Cre/cGi500 mice displayed different signal profiles during the washout phase. However, none of these responses returned to baseline level during a measurement period of 19 min. In contrast, certain FRET/cGi500 responses in AKS returned to baseline level within 19 minutes (**Chapter 5, Figure 1 - 4**), and cGi500-mediated cGMP responses in cells or tissues typically display a transient pattern.<sup>140,143</sup> These differences could be attributed to the depth of the imaging chamber utilized for isolated glomeruli. Notably, the flow rate in experiments involving isolated glomeruli and AKS remained unchanged. Consequently, a deeper chamber recess might lead to prolonged washout times of the substances from the imaging chamber. Another explanation for the observations made with isolated glomeruli could be cell damage caused by the preparation process. Each step of glomeruli isolation (sieving, collagenase treatment, Dynabeads perfusion) contributes to podocyte damage, as demonstrated by Kindt et al. through staining with membrane-impermeable DNA-binding propidium iodide (PI).<sup>274</sup> In this context, it has been demonstrated that isolated glomeruli respond to ANGII stimulation with an increase in cytosolic calcium.<sup>275</sup> However, the proportion of reactive podocytes showing an ANGII-mediated calcium signal in *in vivo* experiments was remarkably low.<sup>151</sup> Emphasizing that podocytes behave differently due to induced damage from the isolation process compared with a more close-to-native scenario. Moreover, externally applied mechanical forces can lead to apoptotic cell death.<sup>276</sup> Cells undergoing apoptosis experience a phenomenon known as intracellular acidification, characterized by a significant decrease in intracellular pH.<sup>277</sup> The FRET acceptor YFP is highly pH-sensitive,<sup>278</sup> with acidic pH values causing changes in absorption and emission properties, potentially influencing FRET responses. The addition of HEPES to the imaging buffer aims to attenuate pH fluctuations caused by external sources. However, it cannot compensate for alterations in intracellular pH resulting from cell damage. In contrast to isolated glomeruli, experiments with AKS are more reliable as damaged glomeruli were excluded from analysis through vital staining with Evans Blue (**Supplemental Fig. 2 - 3**). The imaging setup also included real-time cGMP measurements performed at physiological temperature (37°C), which

was not implemented in experiments with isolated glomeruli. In summary, the utilization of AKS bridges the gap between *in vitro* and *in vivo* settings.

## 7 Conclusion and perspectives

Numerous hormones and vasoactive substances have the potential to influence cGMP-synthesizing systems, thereby affecting glomerular ultrafiltration.<sup>279</sup> The presence of an intrinsically regulated cGMP system, influenced by vasoactive substances, within cells of the glomerular filtration barrier remains uncertain. The work presented here, aims to resolve the discrepancies surrounding the presence of both cGMP signaling pathways in podocytes and GECs, utilizing the FRET-based cGMP biosensor cGi500 in a cell-specific approach. Real-time cGMP imaging on cGi500-transfected HEK 293T cells (sensor characterization) was followed by experiments involving isolated glomeruli and prepared AKS of transgenic mice. These experiments provided evidence for the existence of both guanylyl cyclase systems (sGC and pGC) in podocytes and GECs, including cell-specific differences. Podocytes showed a predominance of the ANP/pGC/cGMP pathway and a stringent regulation of global cGMP levels. To counteract excessively high cGMP peaks, this cell type may utilize mechanisms such as intrinsic inhibition of sGC/pGC, increased PDE activity, or cGMP efflux. Compared to GECs, basal PDE activity was lower in podocytes, wherein PDE3 & PDE5 were the most active isoforms. In contrast to podocytes, GECs showed no preference towards one specific cGMP pathway. However, the additive effect following co-stimulation was only observed in this cell type, suggesting an absence of a ceiling on the maximum intracellular cGMP concentration, as assumed for podocytes. GECs exhibited a high basal PDE activity, wherein PDE2a was the most active isoform. This result indicates a strong reliance on the elimination pathway mediated by cGMP-degrading PDEs to regulate global cGMP levels.

These cell-specific differences raise speculation that pathway-dependent cGMP synthesis could trigger diverse functions and, due to the close association of cGMP with the actin cytoskeleton, could impact cell morphology and, consequently, glomerular filtration. Furthermore, we hypothesize a cross-talk between podocytes and GECs, as the eNOS/NO/sGC/cGMP pathway is described to modulate vasotonus and podocytes express key molecules of a contractile apparatus. In this context, our data highlights mechanotransduction and calcium signaling as additional mechanisms to affect this intercellular communication. These aspects will be addressed in future experiments utilizing eNOS-KO mice, which express GCaMP3 (Ca<sup>2+</sup> sensor) or cGi500 (cGMP sensor) exclusively in podocytes or endothelial cells.

Taken together, our data provide new insights into cell-specific cGMP signaling in podocytes and GECs, laying a foundation for the development of cGMP-elevating drugs that target specific glomerular cell types. Ongoing research will continue to unravel the intricate details of cGMP signaling in renal physiology and pathology.

## Publications

Wiesner E, Binz-Lotter J, Hackl A, Unnersjö-Jess D, Rutkowski N, Benzing T, Hackl MJ: Correlation of calcium multiphoton with ultrastructural STED imaging of the slit diaphragm in the same glomerulus. bioRxiv [Preprint]. 2023 Sep. doi: <https://doi.org/10.1101/2023.09.27.559730>.

### Participation in conferences, congresses etc.

- 9th International Conference on cGMP: Generators, Effectors and Therapeutic Implications 2019, Mainz, DE

Poster\_\_Rutkowski N, Binz J, Benzing T, Hackl M: Hyperosmotic stress induces cGMP release in podocytes.

Meeting abstract published: No authors listed: Meeting abstracts from the 9th International Conference on cGMP: Generators, Effectors and Therapeutic Implications. J Transl Med. 2019 Aug 15;17(Suppl 2):254. doi: 10.1186/s12967-019-1994-0.

- CMMC SYMPOSIUM, 25 Years of Progress in Molecular Medicine: From Basic Research to Clinical Application 2021, Köln, DE

Poster\_\_Rutkowski N, Görlitz F, Höhne M, Benzing T, Hackl MJ: FRET-based visualization of compartmentalized cGMP signalling in podocytes.

- 13th International Podocyte Conference 2021, Manchester, UK

Presentation\_\_Rutkowski N, Görlitz F, Höhne M, Benzing T, Hackl M: FRET-based visualization of compartmentalized cGMP signalling in podocytes.

Meeting abstract published: Brix SR, Kanigicherla DAK, Wallace D, Desai T, Lennon R: The 13th International Podocyte Conference. Glomerular Dis. 2022 Apr; 2(Suppl 1): 1–78. doi: 10.1159/000525410.

- American Society of Nephrology (ASN) Kidney Week 2022, Orlando, US

Poster\_\_Rutkowski N, Görlitz F, Höhne M, Schermer B, Benzing T, Hackl M: FRET-based visualization of cGMP signaling in glomerular endothelial cells and podocytes.

- The 14th Biennial International Podocyte Conference 2023, Philadelphia, US

Poster\_\_Rutkowski N, Görlitz F, Höhne M, Schermer B, Benzing T, Hackl M: FRET-based visualization of cGMP signaling in glomerular endothelial cells and podocytes.

# Aknowledgements

An erster Stelle möchte ich meine aufrichtige Dankbarkeit und tiefste Bewunderung für Dr. Matthias Hackl zum Ausdruck bringen. Unter seiner Anleitung habe ich im Laufe der Jahre nicht nur meine persönlichen Stärken weiterentwickelt, sondern auch meine Schwächen erkannt und daran gearbeitet. Seine fachlich fundierte Unterstützung und außergewöhnlich disziplinierte Arbeitsmoral haben mich nachhaltig beeindruckt.

Als nächstes möchte ich meinen Dank an Prof. Thomas Benzing und Prof. Bernhard Schermer aussprechen, dass sie mir die Möglichkeit gegeben haben, meine Doktorarbeit im Nephrolab durchzuführen und jeden wissenschaftlichen Gedanken in die Tat umsetzen zu können.

In diesem Zusammenhang möchte ich den Mitarbeitern des Nephrolabs und der Imaging Facility meinen aufrichtigen Dank aussprechen. Insbesondere danke ich Dr. Lena Ebert für ihren fachkundigen Rat und Emilia Kieckhöfer für ihre wertvolle Unterstützung.

Abschließend möchte ich meiner Familie und meinen Freunden meinen tiefsten Dank aussprechen. Meine Eltern, Helene und Nikolai Rutkowski, haben mir Disziplin und Durchhaltevermögen vermittelt, Eigenschaften, die mich bis zu diesem Punkt getragen haben. Zusätzlich bin ich meinen Eltern für meine Schwester Julia Rutkowski dankbar, die stets an meiner Seite stand und mir eine emotionale Stütze in vielen schweren Zeiten war.

Ein Mensch, der mir in außerordentlichem Maße geholfen hat, mein Lebensziel zu verwirklichen, ist Nikolaj Zilke. Ohne seine Unterstützung während meiner Studienzeit und seine Rücksichtnahme in vielen Belangen wäre ich nicht bis zu diesem Punkt gelangt. Ich danke dir von Herzen für alles, was du im Laufe der Jahre für mich getan hast.

Des Weiteren kann ich einfach nicht genug in Worte fassen, welchen unschätzbaren Wert Carina Feierabend in meinem Leben hat. Carina, ich danke dir von Herzen für deine wertvolle Zeit, deine ungeteilte Aufmerksamkeit und vor allem für deine unerschütterliche Freundschaft.

# Erklärung

Hiermit versichere ich an Eides statt, dass ich die vorliegende Dissertation selbstständig und ohne die Benutzung anderer als der angegebenen Hilfsmittel und Literatur angefertigt habe. Alle Stellen, die wörtlich oder sinngemäß aus veröffentlichten und nicht veröffentlichten Werken dem Wortlaut oder dem Sinn nach entnommen wurden, sind als solche kenntlich gemacht. Ich versichere an Eides statt, dass diese Dissertation noch keiner anderen Fakultät oder Universität zur Prüfung vorgelegen hat; dass sie - abgesehen von unten angegebenen Teilpublikationen und eingebundenen Artikeln und Manuskripten - noch nicht veröffentlicht worden ist sowie, dass ich eine Veröffentlichung der Dissertation vor Abschluss der Promotion nicht ohne Genehmigung des Promotionsausschusses vornehmen werde. Die Bestimmungen dieser Ordnung sind mir bekannt. Darüber hinaus erkläre ich hiermit, dass ich die Ordnung zur Sicherung guter wissenschaftlicher Praxis und zum Umgang mit wissenschaftlichem Fehlverhalten der Universität zu Köln gelesen und sie bei der Durchführung der Dissertation zugrundeliegenden Arbeiten und der schriftlich verfassten Dissertation beachtet habe und verpflichte mich hiermit, die dort genannten Vorgaben bei allen wissenschaftlichen Tätigkeiten zu beachten und umzusetzen. Ich versichere, dass die eingereichte elektronische Fassung der eingereichten Druckfassung vollständig entspricht.

## Teilpublikationen:

**Rutkowski N**, Görlitz F, Wiesner E, Binz-Lotter J, Feil S, Feil R, Benzing T, Hackl MJ: Real-time imaging of cGMP signaling shows pronounced differences between glomerular endothelial cells and podocytes.

Submitted to Journal of the American Society of Nephrology (JASN), Feb 26 2024

Manuscript number: JASN-2024-000272

Nelli Rutkowski

Köln, den 12-Dec-24



## Bibliography

1. Pollak MR, Quaggin SE, Hoenig MP, Dworkin LD. The glomerulus: the sphere of influence. *Clin J Am Soc Nephrol*. 2014;9(8):1461-1469. doi:10.2215/CJN.09400913
2. Shiraishi M, Wang X, Walsh MP, Kargacin G, Loutzenhiser K, Loutzenhiser R. Myosin heavy chain expression in renal afferent and efferent arterioles: relationship to contractile kinetics and function. *FASEB J*. 2003;17(15):2284-2286. doi:10.1096/FJ.03-0096FJE
3. Ito S, Abe K. Contractile properties of afferent and efferent arterioles. In: *Clinical and Experimental Pharmacology and Physiology*. Vol 24. Clin Exp Pharmacol Physiol; 1997:532-535. doi:10.1111/j.1440-1681.1997.tb01241.x
4. Arkill KP, Qvortrup K, Starborg T, et al. Resolution of the three dimensional structure of components of the glomerular filtration barrier. *BMC Nephrol*. 2014;15(1). doi:10.1186/1471-2369-15-24
5. Arakawa M. A Scanning Electron Microscope Study of the Human Glomerulus. *Am J Pathol*. 1971;64(2):457. /pmc/articles/PMC2047570/?report=abstract. Accessed January 30, 2024.
6. Kocylowski MK, Aypek H, Bildl W, et al. A slit-diaphragm-associated protein network for dynamic control of renal filtration. *Nature Communications 2022 13:1*. 2022;13(1):1-15. doi:10.1038/s41467-022-33748-1
7. Fukasawa H, Bornheimer S, Kudlicka K, Farquhar MG. Slit Diaphragms Contain Tight Junction Proteins. *J Am Soc Nephrol*. 2009;20(7):1491. doi:10.1681/ASN.2008101117
8. Albrecht M, Sticht C, Wagner T, et al. The crosstalk between glomerular endothelial cells and podocytes controls their responses to metabolic stimuli in diabetic nephropathy. *Sci Rep*. 2023;13(1). doi:10.1038/S41598-023-45139-7
9. 't Hart DC, Yildiz D, Palacio-Castañeda V, et al. Co-Culture of Glomerular Endothelial Cells and Podocytes in a Custom-Designed Glomerulus-on-a-Chip Model Improves the Filtration Barrier Integrity and Affects the Glomerular Cell Phenotype. *Biosensors (Basel)*. 2023;13(3). doi:10.3390/BIOS13030339

10. Eremina V, Baelde HJ, Quaggin SE. Role of the VEGF-A Signaling Pathway in the Glomerulus: Evidence for Crosstalk between Components of the Glomerular Filtration Barrier. *Nephron Physiol.* 2007;106(2):p32-p37. doi:10.1159/000101798
11. Guan F, Villegas G, Teichman J, Mundel P, Tufro A. Autocrine VEGF-A system in podocytes regulates podocin and its interaction with CD2AP. *Am J Physiol Renal Physiol.* 2006;291(2):422-428. doi:10.1152/AJPRENAL.00448.2005/ASSET/IMAGES/LARGE/ZH20080644260005.JPEG
12. Ferrara N, Carver-Moore K, Chen H, et al. Heterozygous embryonic lethality induced by targeted inactivation of the VEGF gene. *Nature* 1996 380:6573. 1996;380(6573):439-442. doi:10.1038/380439a0
13. Eremina V, Sood M, Haigh J, et al. Glomerular-specific alterations of VEGF-A expression lead to distinct congenital and acquired renal diseases. *J Clin Invest.* 2003;111(5):707-716. doi:10.1172/JCI17423
14. Fridén V, Oveland E, Tenstad O, et al. The glomerular endothelial cell coat is essential for glomerular filtration. *Kidney Int.* 2011;79(12):1322-1330. doi:10.1038/KI.2011.58
15. Finch NC, Fawaz SS, Neal CR, et al. Reduced Glomerular Filtration in Diabetes Is Attributable to Loss of Density and Increased Resistance of Glomerular Endothelial Cell Fenestrations. *J Am Soc Nephrol.* 2022;33(6):1120-1136. doi:10.1681/ASN.2021030294
16. Ermert K, Buhl EM, Klinkhammer BM, Floege J, Boor P. Reduction of Endothelial Glycocalyx on Peritubular Capillaries in Chronic Kidney Disease. *Am J Pathol.* 2023;193(2):138-147. doi:10.1016/J.AJPATH.2022.11.003
17. Grishman E, Churg J. Focal glomerular sclerosis in nephrotic patients: An electron microscopic study of glomerular podocytes. *Kidney Int.* 1975;7(2):111-122. doi:10.1038/KI.1975.16
18. Roselli S, Heidet L, Sich M, et al. Early Glomerular Filtration Defect and Severe Renal Disease in Podocin-Deficient Mice. *Mol Cell Biol.* 2004;24(2):550. doi:10.1128/MCB.24.2.550-560.2004

19. Trimarchi H. Mechanisms of Podocyte Detachment, Podocyturia, and Risk of Progression of Glomerulopathies. *Kidney Diseases*. 2020;6(5):324-329. doi:10.1159/000507997
20. Ashman DF, Lipton R, Melicow MM, Price TD. Isolation of adenosine 3', 5'-monophosphate and guanosine 3', 5'-monophosphate from rat urine. *Biochem Biophys Res Commun*. 1963;11(4):330-334. doi:10.1016/0006-291X(63)90566-7
21. Beavo JA, Brunton LL. Cyclic nucleotide research -- still expanding after half a century. *Nat Rev Mol Cell Biol*. 2002;3(9):710-718. doi:10.1038/NRM911
22. Krishnan SM, Kraehling JR, Eitner F, Bénardeau A, Sandner P. The Impact of the Nitric Oxide (NO)/Soluble Guanylyl Cyclase (sGC) Signaling Cascade on Kidney Health and Disease: A Preclinical Perspective. *International Journal of Molecular Sciences* 2018, Vol 19, Page 1712. 2018;19(6):1712. doi:10.3390/IJMS19061712
23. Ignarro LJ, Buga GM, Wood KS, Byrns RE, Chaudhuri G. Endothelium-derived relaxing factor produced and released from artery and vein is nitric oxide. *Proc Natl Acad Sci U S A*. 1987;84(24):9265. doi:10.1073/PNAS.84.24.9265
24. Carvajal JA, Germain AM, Huidobro-Toro JP, Weiner CP. Molecular Mechanism of cGMP-Mediated Smooth Muscle Relaxation. *J Cell Physiol*. 2000;184:409-420. doi:10.1002/1097-4652
25. Sanadi DR, Gibson DM, Ayengar P, Jacob M.  $\alpha$ -KETOGLUTARIC DEHYDROGENASE: V. GUANOSINE DIPHOSPHATE IN COUPLED PHOSPHORYLATION. *Journal of Biological Chemistry*. 1956;218(1):505-520. doi:10.1016/S0021-9258(18)65913-7
26. Denninger JW, Marletta MA. Guanylate cyclase and the  $\cdot$ NO/cGMP signaling pathway. *Biochimica et Biophysica Acta (BBA) - Bioenergetics*. 1999;1411(2-3):334-350. doi:10.1016/S0005-2728(99)00024-9
27. Ignarro LJ, Byrns RE, Buga GM, Wood KS. Endothelium-derived relaxing factor from pulmonary artery and vein possesses pharmacologic and chemical properties identical to those of nitric oxide radical. *Circ Res*. 1987;61(6):866-879. doi:10.1161/01.RES.61.6.866
28. Kobiałka M, Gorczyca W. Particulate guanylyl cyclases: multiple mechanisms of activation. *Acta Biochim Pol*. 2000;47(3):517-528.

29. Theilig F, Bostanjoglo M, Pavenstädt H, et al. Cellular distribution and function of soluble guanylyl cyclase in rat kidney and liver. *Journal of the American Society of Nephrology*. 2001;12(11):2209-2220. doi:10.1681/ASN.V12112209
30. Budworth J, Meillerais S, Charles I, Powell K. Tissue distribution of the human soluble guanylate cyclases. *Biochem Biophys Res Commun*. 1999;263(3):696-701. doi:10.1006/BBRC.1999.1444
31. Sharma VS, Magde D. Activation of Soluble Guanylate Cyclase by Carbon Monoxide and Nitric Oxide: A Mechanistic Model. *Methods*. 1999;19(4):494-505. doi:10.1006/METH.1999.0892
32. Kang Y, Liu R, Wu JX, Chen L. Structural insights into the mechanism of human soluble guanylate cyclase. *Nature*. 2019;574(7777):206-210. doi:10.1038/S41586-019-1584-6
33. Dai Y, Faul EM, Ghosh A, Stuehr DJ. NO rapidly mobilizes cellular heme to trigger assembly of its own receptor. *Proc Natl Acad Sci U S A*. 2022;119(4). doi:10.1073/PNAS.2115774119/-DCSUPPLEMENTAL
34. Montfort WR, Wales JA, Weichsel A. Structure and Activation of Soluble Guanylyl Cyclase, the Nitric Oxide Sensor. *Antioxid Redox Signal*. 2017;26(3):107-121. doi:10.1089/ARS.2016.6693/ASSET/IMAGES/LARGE/FIGURE9.JPEG
35. Kennedy CRJ. Nitrate, nitrite, and nitric oxide find a home in the kidney by offsetting Angiotensin ii-mediated hypertension. *Hypertension*. 2015;65(1):31-33. doi:10.1161/HYPERTENSIONAHA.114.04349
36. Gao X, Yang T, Liu M, et al. NADPH oxidase in the renal microvasculature is a primary target for blood pressure-lowering effects by inorganic nitrate and nitrite. *Hypertension*. 2015;65(1):161-170. doi:10.1161/HYPERTENSIONAHA.114.04222
37. Lundberg JO, Govoni M. Inorganic nitrate is a possible source for systemic generation of nitric oxide. *Free Radic Biol Med*. 2004;37(3):395-400. doi:10.1016/j.freeradbiomed.2004.04.027
38. Benjamin N, O'Driscoll F, Dougall H, et al. Stomach NO synthesis. *Nature* 1994 368:6471. 1994;368(6471):502-502. doi:10.1038/368502a0

39. Stuehr DJ, Misra S, Dai Y, Ghosh A. Maturation, inactivation, and recovery mechanisms of soluble guanylyl cyclase. *Journal of Biological Chemistry*. 2021;296:100336. doi:10.1016/J.JBC.2021.100336
40. Lundberg JO, Weitzberg E. Nitric oxide signaling in health and disease. *Cell*. 2022;185(16):2853-2878. doi:10.1016/J.CELL.2022.06.010
41. Sharma M, McCarthy ET, Savin VJ, Lianos EA. Nitric oxide preserves the glomerular protein permeability barrier by antagonizing superoxide. *Kidney Int*. 2005;68(6):2735-2744. doi:10.1111/J.1523-1755.2005.00744.X
42. Krishnan SM, Kraehling JR, Eitner F, Bénardeau A, Sandner P. The Impact of the Nitric Oxide (NO)/Soluble Guanylyl Cyclase (sGC) Signaling Cascade on Kidney Health and Disease: A Preclinical Perspective. *Int J Mol Sci*. 2018;19(6). doi:10.3390/IJMS19061712
43. Baylis C, Qiu C. Importance of nitric oxide in the control of renal hemodynamics. *Kidney Int*. 1996;49(6):1727-1731. doi:10.1038/KI.1996.256
44. Kurtz A, Götz KH, Hamann M, Kieninger M, Wagner C. Stimulation of renin secretion by NO donors is related to the cAMP pathway. *Am J Physiol*. 1998;274(4). doi:10.1152/AJPRENAL.1998.274.4.F709
45. Schweda F, Friis U, Wagner C, Skott O, Kurtz A. Renin release. *Physiology (Bethesda)*. 2007;22(5):310-319. doi:10.1152/PHYSIOL.00024.2007
46. Yan Y, Zhou A, Carrell RW, Read RJ. Structural basis for the specificity of renin-mediated angiotensinogen cleavage. *J Biol Chem*. 2019;294(7):2353. doi:10.1074/JBC.RA118.006608
47. Navar LG. Intrarenal Renin-Angiotensin System in Regulation of Glomerular Function. *Curr Opin Nephrol Hypertens*. 2014;23(1):38. doi:10.1097/01.MNH.0000436544.86508.F1
48. Sachse A, Wolf G. Angiotensin II-induced reactive oxygen species and the kidney. *Journal of the American Society of Nephrology*. 2007;18(9):2439-2446. doi:10.1681/ASN.2007020149

49. Kuhn M. Molecular Physiology of Membrane Guanylyl Cyclase Receptors. *Physiol Rev.* 2016;96(2):751-804. doi:10.1152/PHYSREV.00022.2015
50. Carrithers SL, Taylor B, Cai WY, et al. Guanylyl cyclase-C receptor mRNA distribution along the rat nephron. *Regul Pept.* 2000;95(1-3):65-74. doi:10.1016/S0167-0115(00)00139-7
51. Carrithers SL, Hill MJ, Johnson BR, et al. Renal effects of uroguanylin and guanylin in vivo. *Braz J Med Biol Res.* 1999;32(11):1337-1344. doi:10.1590/S0100-879X1999001100003
52. Heintz ES, Broecker KAE, Lehrmann C, et al. Localization of natriuretic peptide receptors A, B, and C in healthy and diseased mouse kidneys. *Pflugers Arch.* 2023;475(3):343-360. doi:10.1007/S00424-022-02774-9
53. Schulz S, Wedel BJ, Matthews A, Garbers DL. The cloning and expression of a new guanylyl cyclase orphan receptor. *J Biol Chem.* 1998;273(2):1032-1037. doi:10.1074/JBC.273.2.1032
54. Marin-Grez M, Fleming JT, Steinhausen M. Atrial natriuretic peptide causes pre-glomerular vasodilatation and post-glomerular vasoconstriction in rat kidney. *Nature* 1986 324:6096. 1986;324(6096):473-476. doi:10.1038/324473a0
55. Burnett JC, Opgenorth TJ, Granger JP. The renal action of atrial natriuretic peptide during control of glomerular filtration. *Kidney Int.* 1986;30(1):16-19. doi:10.1038/KI.1986.144
56. Burnett JC, Granger JP, Opgenorth TJ. Effects of synthetic atrial natriuretic factor on renal function and renin release. *Am J Physiol.* 1984;247(5 Pt 2). doi:10.1152/AJPRENAL.1984.247.5.F863
57. Hunt PJ, Richards AM, Espiner EA, Nicholls MG, Yandle TG. Bioactivity and metabolism of C-type natriuretic peptide in normal man. *J Clin Endocrinol Metab.* 1994;78(6):1428-1435. doi:10.1210/JCEM.78.6.8200946
58. Dean AD, Matti Vehaskari V, Ritter D, Greenwald JE. Distribution and regulation of guanylyl cyclase type B in the rat nephron. *Am J Physiol.* 1996;270(2 Pt 2). doi:10.1152/AJPRENAL.1996.270.2.F311

59. Zakeri R, Burnett JC, Sangaralingham SJ. Urinary C-Type Natriuretic Peptide: An Emerging Biomarker for Heart Failure and Renal Remodeling. *Clin Chim Acta*. 2015;0:108. doi:10.1016/J.CCA.2014.12.009
60. Cataliotti A, Giordano M, De Pascale E, et al. CNP production in the kidney and effects of protein intake restriction in nephrotic syndrome. *Am J Physiol Renal Physiol*. 2002;283(3). doi:10.1152/AJPRENAL.00372.2001
61. Jin X, Zhang Y, Li X, Zhang J, Xu D. C-type natriuretic peptide ameliorates ischemia/reperfusion-induced acute kidney injury by inhibiting apoptosis and oxidative stress in rats. *Life Sci*. 2014;117(1):40-45. doi:10.1016/J.LFS.2014.09.023
62. Potter LR. Natriuretic Peptide Metabolism, Clearance and Degradation. *FEBS J*. 2011;278(11):1808. doi:10.1111/J.1742-4658.2011.08082.X
63. Staffel J, Valletta D, Federlein A, et al. Natriuretic peptide receptor guanylyl cyclase - A in podocytes is renoprotective but dispensable for physiologic renal function. *Journal of the American Society of Nephrology*. 2017;28(1):260-277. doi:10.1681/ASN.2015070731/-/DCSUPPLEMENTAL
64. Sexton PM, Zhuo J, Mendelsohn FAO. Localization and regulation of renal receptors for angiotensin II and atrial natriuretic peptide. *Tohoku J Exp Med*. 1992;166(1):41-56. doi:10.1620/TJEM.166.41
65. Frees A, Assersen KB, Jensen M, et al. Natriuretic peptides relax human intrarenal arteries through natriuretic peptide receptor type-A recapitulated by soluble guanylyl cyclase agonists. *Acta Physiologica*. 2021;231(3):e13565. doi:10.1111/APHA.13565
66. Rinschen MM, Gödel M, Grahammer F, et al. A Multi-layered Quantitative In Vivo Expression Atlas of the Podocyte Unravels Kidney Disease Candidate Genes. *Cell Rep*. 2018;23(8):2495-2508. doi:10.1016/J.CELREP.2018.04.059
67. Zhao J, Ardaillou N, Lu CY, et al. Characterization of C-type natriuretic peptide receptors in human mesangial cells. *Kidney Int*. 1994;46(3):717-725. doi:10.1038/KI.1994.326
68. Lewko B, Waszkiewicz A, Maryn A, et al. Dexamethasone-dependent modulation of cyclic GMP synthesis in podocytes. *Mol Cell Biochem*. 2015;409(1-2):243. doi:10.1007/S11010-015-2528-6

69. Lewko B, Endlich N, Kriz W, Stepinski J, Endlich K. C-type natriuretic peptide as a podocyte hormone and modulation of its cGMP production by glucose and mechanical stress. *Kidney Int.* 2004;66(3):1001-1008. doi:10.1111/J.1523-1755.2004.00848.X
70. Dong L, Wang H, Dong N, Zhang C, Xue B, Wu Q. Localization of corin and atrial natriuretic peptide expression in human renal segments. *Clin Sci (Lond).* 2016;130(18):1655. doi:10.1042/CS20160398
71. Polzin D, Kaminski HJ, Kastner C, et al. Impaired renal corin expression contributes to sodium retention in proteinuric kidney diseases. *Kidney Int.* 2010;78(7):650. doi:10.1038/KI.2010.197
72. Wang L, Tang Y, Buckley AF, Spurney RF. Blockade of the natriuretic peptide clearance receptor attenuates proteinuria in a mouse model of focal segmental glomerulosclerosis. *Physiol Rep.* 2021;9(21). doi:10.14814/PHY2.15095
73. John SWM, Krege JH, Oliver PM, et al. Genetic Decreases in Atrial Natriuretic Peptide and Salt-Sensitive Hypertension. *Science (1979).* 1995;267(5198):679-681. doi:10.1126/SCIENCE.7839143
74. Lopez MJ, Wong SKF, Kishimoto I, et al. Salt-resistant hypertension in mice lacking the guanylyl cyclase-A receptor for atrial natriuretic peptide. *Nature.* 1995;378(6552):65-68. doi:10.1038/378065A0
75. Sabrane K, Kruse MN, Fabritz L, et al. Vascular endothelium is critically involved in the hypotensive and hypovolemic actions of atrial natriuretic peptide. *J Clin Invest.* 2005;115(6):1666-1674. doi:10.1172/JCI23360
76. Reiser J, Polu KR, Möller CC, et al. TRPC6 is a glomerular slit diaphragm-associated channel required for normal renal function. *Nat Genet.* 2005;37(7):739. doi:10.1038/NG1592
77. Möller CC, Wei C, Altintas MM, et al. Induction of TRPC6 channel in acquired forms of proteinuric kidney disease. *J Am Soc Nephrol.* 2007;18(1):29-36. doi:10.1681/ASN.2006091010
78. Ning B, Guo C, Kong A, et al. Calcium Signaling Mediates Cell Death and Crosstalk with Autophagy in Kidney Disease. *Cells.* 2021;10(11). doi:10.3390/CELLS10113204



79. Sonneveld R, Hoenderop JG, Isidori AM, et al. Sildenafil Prevents Podocyte Injury via PPAR-  $\gamma$ -Mediated TRPC6 Inhibition. *J Am Soc Nephrol.* 2017;28(5):1491-1505. doi:10.1681/ASN.2015080885
80. Hart D, Li J, van der Vlag J, Nijenhuis T. Repurposing riociguat to target a novel paracrine nitric oxide-trpc6 pathway to prevent podocyte injury. *Int J Mol Sci.* 2021;22(22). doi:10.3390/IJMS222212485/S1
81. Hall G, Rowell J, Farinelli F, et al. Phosphodiesterase 5 inhibition ameliorates angiotensin II-induced podocyte dysmotility via the protein kinase G-mediated downregulation of TRPC6 activity. *Am J Physiol Renal Physiol.* 2014;306(12). doi:10.1152/AJPRENAL.00212.2013
82. Drenckhahn D, Franke RP. Ultrastructural organization of contractile and cytoskeletal proteins in glomerular podocytes of chicken, rat, and man. *Lab Invest.* 1988;59(5):673-682. <https://europepmc.org/article/med/3141719>. Accessed February 7, 2024.
83. Kriz W, Hackenthal E, Nobiling R, Sakai T, Elger M. A role for podocytes to counteract capillary wall distension. *Kidney Int.* 1994;45(2):369-376. doi:10.1038/KI.1994.47
84. Piwkowska A, Rogacka D, Jankowski M, Kocbuch K, Angielski S. Hydrogen peroxide induces dimerization of protein kinase G type I $\alpha$  subunits and increases albumin permeability in cultured rat podocytes. *J Cell Physiol.* 2012;227(3):1004-1016. doi:10.1002/JCP.22810
85. Hsu HH, Hoffmann S, Endlich N, et al. Mechanisms of angiotensin II signaling on cytoskeleton of podocytes. *J Mol Med.* 2008;86(12):1379-1394. doi:10.1007/S00109-008-0399-Y/FIGURES/8
86. Ma X, Iyer SR, Ma X, et al. Evidence for Angiotensin II as a Naturally Existing Suppressor for the Guanylyl Cyclase A Receptor and Cyclic GMP Generation. *Int J Mol Sci.* 2023;24(10):8547. doi:10.3390/IJMS24108547/S1
87. Semenikhina M, Bohovyk R, Klemens CA, et al. RAS-mediated nitric oxide signaling in podocytes. *The FASEB Journal.* 2022;36(S1). doi:10.1096/FASEBJ.2022.36.S1.R3999
88. Palygin O, Ilatovskaya D V., Levchenko V, Endres BT, Geurts AM, Staruschenko A. Nitric oxide production by glomerular podocytes. *Nitric Oxide.* 2018;72:24. doi:10.1016/J.NIOX.2017.11.005

89. Searles CD, Ide L, Davis ME, Cai H, Weber M. Actin cytoskeleton organization and posttranscriptional regulation of endothelial nitric oxide synthase during cell growth. *Circ Res.* 2004;95(5):488-495. doi:10.1161/01.RES.0000138953.21377.80
90. Jarry A, Renaudin K, Denis MG, et al. Expression of NOS1 and soluble guanylyl cyclase by human kidney epithelial cells: morphological evidence for an autocrine/paracrine action of nitric oxide. *Kidney Int.* 2003;64(1):170-180. doi:10.1046/J.1523-1755.2003.00078.X
91. Semenikhina M, Stefanenko M, Spires DR, Ilatovskaya D V., Palygin O. Nitric-Oxide-Mediated Signaling in Podocyte Pathophysiology. *Biomolecules.* 2022;12(6). doi:10.3390/BIOM12060745
92. Stehle D, Xu MZ, Schomber T, et al. Novel soluble guanylyl cyclase activators increase glomerular cGMP, induce vasodilation and improve blood flow in the murine kidney. *Br J Pharmacol.* 2022;179(11):2476-2489. doi:10.1111/BPH.15586
93. Ueda S, Ozawa S, Mori K, et al. eNOS deficiency causes podocyte injury with mitochondrial abnormality. *Free Radic Biol Med.* 2015;87:181-192. doi:10.1016/J.FREERADBIOMED.2015.06.028
94. Nakayama T, Sato W, Yoshimura A, et al. Endothelial von Willebrand factor release due to eNOS deficiency predisposes to thrombotic microangiopathy in mouse aging kidney. *American Journal of Pathology.* 2010;176(5):2198-2208. doi:10.2353/ajpath.2010.090316
95. Mangmool S, Duangrat R, Parichatikanond W, Kurose H. New Therapeutics for Heart Failure: Focusing on cGMP Signaling. *International Journal of Molecular Sciences* 2023, Vol 24, Page 12866. 2023;24(16):12866. doi:10.3390/IJMS241612866
96. Schlossmann J, Schinner E. cGMP becomes a drug target. *Naunyn Schmiedebergs Arch Pharmacol.* 2012;385(3):243-252. doi:10.1007/S00210-012-0730-6
97. Lukowski R, Feil R. Recent developments in cGMP research: From mechanisms to medicines and back. *Br J Pharmacol.* 2022;179(11):2321-2327. doi:10.1111/BPH.15824

98. Shen K, Johnson DW, Gobe GC. The role of cGMP and its signaling pathways in kidney disease. *Am J Physiol Renal Physiol.* 2016;311(4):F671-F681. doi:10.1152/AJPRENAL.00042.2016
99. Chen Y, Burnett JC. Particulate Guanylyl Cyclase A/cGMP Signaling Pathway in the Kidney: Physiologic and Therapeutic Indications. *International Journal of Molecular Sciences* 2018, Vol 19, Page 1006. 2018;19(4):1006. doi:10.3390/IJMS19041006
100. Cheng J, Grande JP. Cyclic Nucleotide Phosphodiesterase (PDE) Inhibitors: Novel Therapeutic Agents for Progressive Renal Disease. <https://doi.org/10.3181/00379727-207-2320038>. January 2007. doi:10.3181/00379727-207-2320038
101. Buglioni A, Burnett JC. New Pharmacological Strategies to Increase cGMP. <https://doi.org/10.1146/annurev-med-052914-091923>. 2016;67:229-243. doi:10.1146/ANNUREV-MED-052914-091923
102. Friebe A, Kraehling JR, Russwurm M, Sandner P, Schmidtko A. The 10th International Conference on cGMP 2022: recent trends in cGMP research and development—meeting report. *Naunyn-Schmiedeberg's Archives of Pharmacology* 2023 396:8. 2023;396(8):1669-1686. doi:10.1007/S00210-023-02484-8
103. van Kraaij SJW, Gal P, Borghans LGJM, et al. First-in-human trial to assess safety, tolerability, pharmacokinetics, and pharmacodynamics of zagociguat (CY6463), a CNS-penetrant soluble guanylyl cyclase stimulator. *Clin Transl Sci.* 2023;16(8):1381. doi:10.1111/CTS.13537
104. Reinhart GA, Harrison PC, Lincoln K, et al. The Novel, Clinical Stage Soluble Guanylate Cyclase Activator BI 685509 Protects from Disease Progression in Models of Renal Injury and Disease. *Journal of Pharmacology and Experimental Therapeutics.* 2022;384(3):382-392. doi:10.1124/JPET.122.001423
105. Balzer MS, Pavkovic M, Frederick J, et al. Treatment effects of soluble guanylate cyclase modulation on diabetic kidney disease at single-cell resolution. *Cell Rep Med.* 2023;4(4). doi:10.1016/J.XCRM.2023.100992
106. Egom EEA. Natriuretic Peptide Clearance Receptor (NPR-C) Pathway as a Novel Therapeutic Target in Obesity-Related Heart Failure With Preserved Ejection Fraction (HFpEF). *Front Physiol.* 2021;12:674254. doi:10.3389/FPHYS.2021.674254/BIBTEX

107. De Nicola L, Bellizzi V, Minutolo R, et al. Randomized, double-blind, placebo-controlled study of arginine supplementation in chronic renal failure. *Kidney Int.* 1999;56(2):674-684. doi:10.1046/J.1523-1755.1999.00582.X
108. Li X, Zhuge Z, Carvalho LRR, et al. Inorganic nitrate and nitrite ameliorate kidney fibrosis by restoring lipid metabolism via dual regulation of AMP-activated protein kinase and the AKT-PGC1 $\alpha$  pathway. *Redox Biol.* 2022;51. doi:10.1016/J.REDOX.2022.102266
109. Omori K, Kotera J. Overview of PDEs and their regulation. *Circ Res.* 2007;100(3):309-327. doi:10.1161/01.RES.0000256354.95791.F1
110. Galiè N, Ghofrani HA, Torbicki A, et al. Sildenafil Citrate Therapy for Pulmonary Arterial Hypertension. <https://doi.org/10.1056/NEJMoa050010>. 2005;353(20):2148-2157. doi:10.1056/NEJMoa050010
111. Rwin I, Oldstein G, Ue OFL, et al. Oral Sildenafil in the Treatment of Erectile Dysfunction. <https://doi.org/10.1056/NEJM199805143382001>. 1998;338(20):1397-1404. doi:10.1056/NEJM199805143382001
112. Ala M, Mohammad Jafari R, Dehpour AR. Sildenafil beyond erectile dysfunction and pulmonary arterial hypertension: Thinking about new indications. *Fundam Clin Pharmacol.* 2021;35(2):235-259. doi:10.1111/FCP.12633
113. ElHady AK, El-Gamil DS, Abdel-Halim M, Abadi AH. Advancements in Phosphodiesterase 5 Inhibitors: Unveiling Present and Future Perspectives. *Pharmaceuticals.* 2023;16(9). doi:10.3390/PH16091266/S1
114. Coskuner ER, Ozkan B. Reno-protective effects of Phosphodiesterase 5 inhibitors. *Clin Exp Nephrol.* 2021;25(6):585-597. doi:10.1007/S10157-021-02051-6
115. Abdel-Rahman DM, Messiha BAS, Ali FEM, Azouz AA. Regulation of renal nitric oxide and eNOS/iNOS expression by tadalafil participates in the mitigation of amphotericin B-induced renal injury: Down-regulation of NF- $\kappa$ B/iNOS/caspase-3 signaling. *Naunyn Schmiedeberg's Arch Pharmacol.* 2023. doi:10.1007/S00210-023-02787-W
116. Pofi R, Fiore D, De Gaetano R, et al. Phosphodiesterase-5 inhibition preserves renal hemodynamics and function in mice with diabetic kidney disease by modulating miR-22 and BMP7. *Scientific Reports* 2017 7:1. 2017;7(1):1-12. doi:10.1038/srep44584

117. Nio Y, Ookawara M, Yamasaki M, et al. Ameliorative effect of phosphodiesterase 4 and 5 inhibitors in deoxycorticosterone acetate-salt hypertensive uni-nephrectomized KKAY mice. *FASEB J*. 2020;34(11):14997-15014. doi:10.1096/FJ.202001084R
118. Tardi NJ, Reiser J. The Use of Sildenafil for Glomerular Disease. *J Am Soc Nephrol*. 2017;28(5):1329-1331. doi:10.1681/ASN.2017020171
119. Soderling SH, Bayuga SJ, Beavo JA. Identification and Characterization of a Novel Family of Cyclic Nucleotide Phosphodiesterases. *Journal of Biological Chemistry*. 1998;273(25):15553-15558. doi:10.1074/JBC.273.25.15553
120. Lee DI, Zhu G, Sasaki T, et al. Phosphodiesterase 9A controls nitric-oxide-independent cGMP and hypertrophic heart disease. *Nature* 2015 519:7544. 2015;519(7544):472-476. doi:10.1038/nature14332
121. Meibom D, Micus S, Andreevski AL, et al. BAY-7081: A Potent, Selective, and Orally Bioavailable Cyanopyridone-Based PDE9A Inhibitor. *J Med Chem*. 2022;65(24):16420-16431. doi:10.1021/ACS.JMEDCHEM.2C01267/SUPPL\_FILE/JM2C01267\_SI\_002.CSV
122. Kim D, Aizawa T, Wei H, et al. Angiotensin II increases phosphodiesterase 5A expression in vascular smooth muscle cells: A mechanism by which angiotensin II antagonizes cGMP signaling. *J Mol Cell Cardiol*. 2005;38(1):175. doi:10.1016/J.YJMCC.2004.10.013
123. Xie X, Liu Y, Perkovic V, et al. Renin-Angiotensin System Inhibitors and Kidney and Cardiovascular Outcomes in Patients With CKD: A Bayesian Network Meta-analysis of Randomized Clinical Trials. *Am J Kidney Dis*. 2016;67(5):728-741. doi:10.1053/J.AJKD.2015.10.011
124. Zhang Y, He D, Zhang W, et al. ACE Inhibitor Benefit to Kidney and Cardiovascular Outcomes for Patients with Non-Dialysis Chronic Kidney Disease Stages 3–5: A Network Meta-Analysis of Randomised Clinical Trials. *Drugs*. 2020;80(8):797. doi:10.1007/S40265-020-01290-3
125. JJ M, M P, AS D, et al. Angiotensin-neprilysin inhibition versus enalapril in heart failure. *N Engl J Med*. 2014;371(11):132-133. doi:10.1056/NEJMOA1409077

126. Sekar RB, Periasamy A. Fluorescence resonance energy transfer (FRET) microscopy imaging of live cell protein localizations. *J Cell Biol.* 2003;160(5):629. doi:10.1083/JCB.200210140
127. Soleja N, Manzoor O, Khan I, Ahmad A, Mohsin M. Role of green fluorescent proteins and their variants in development of FRET-based sensors. *J Biosci.* 2018;43(4):763-784. doi:10.1007/S12038-018-9783-0/FIGURES/3
128. Bajar BT, Wang ES, Zhang S, Lin MZ, Chu J. A Guide to Fluorescent Protein FRET Pairs. *Sensors (Basel).* 2016;16(9). doi:10.3390/S16091488
129. Schmidt PM. Biochemical Detection of cGMP From Past to Present: An Overview. *Handb Exp Pharmacol.* 2009;191(191):195-228. doi:10.1007/978-3-540-68964-5\_10
130. Russwurm M, Koesling D. Measurement of cGMP-generating and -degrading activities and cGMP levels in cells and tissues: Focus on FRET-based cGMP indicators. *Nitric Oxide.* 2018;77:44-52. doi:10.1016/J.NIOX.2018.04.006
131. Jäger R, Groneberg D, Lies B, Bettaga N, Kümmel M, Friebe A. Radioimmunoassay for the quantification of cGMP levels in cells and tissues. *Methods Mol Biol.* 2013;1020:63-72. doi:10.1007/978-1-62703-459-3\_4
132. Huang KT, Lin TJ, Hsu MH. Determination of cyclic GMP concentration using a gold nanoparticle-modified optical fiber. *Biosens Bioelectron.* 2010;26(1):11-15. doi:10.1016/J.BIOS.2010.04.050
133. Gorbe A, Giricz Z, Szunyog A, et al. Role of cGMP-PKG signaling in the protection of neonatal rat cardiac myocytes subjected to simulated ischemia/reoxygenation. *Basic Res Cardiol.* 2010;105(5):643-650. doi:10.1007/S00395-010-0097-0
134. Sprenger JU, Nikolaev VO. Biophysical Techniques for Detection of cAMP and cGMP in Living Cells. *International Journal of Molecular Sciences 2013, Vol 14, Pages 8025-8046.* 2013;14(4):8025-8046. doi:10.3390/IJMS14048025
135. Niino Y, Hotta K, Oka K. Simultaneous Live Cell Imaging Using Dual FRET Sensors with a Single Excitation Light. *PLoS One.* 2009;4(6):6036. doi:10.1371/JOURNAL.PONE.0006036

136. Bhargava Y, Hampden-Smith K, Chachlaki K, et al. Improved genetically-encoded, FlincG-type fluorescent biosensors for neural cGMP imaging. *Front Mol Neurosci*. 2013;6(SEP). doi:10.3389/FNMOL.2013.00026/ABSTRACT
137. Matsuda S, Harada K, Ito M, et al. Generation of a cGMP Indicator with an Expanded Dynamic Range by Optimization of Amino Acid Linkers between a Fluorescent Protein and PDE5 $\alpha$ . *ACS Sens*. 2017;2(1):46-51. doi:10.1021/ACSSENSORS.6B00582/ASSET/IMAGES/LARGE/SE-2016-00582S\_0004.JPEG
138. Calamera G, Li D, Ulsund AH, et al. FRET-based cyclic GMP biosensors measure low cGMP concentrations in cardiomyocytes and neurons. *Communications Biology* 2019 2:1. 2019;2(1):1-12. doi:10.1038/s42003-019-0641-x
139. Russwurm M, Mullershausen F, Friebe A, Jäger R, Russwurm C, Koesling D. Design of fluorescence resonance energy transfer (FRET)-based cGMP indicators: a systematic approach. *Biochem J*. 2007;407(Pt 1):69. doi:10.1042/BJ20070348
140. Thunemann M, Wen L, Hillenbrand M, et al. Transgenic mice for cGMP imaging. *Circ Res*. 2013;113(4):365-371. doi:10.1161/CIRCRESAHA.113.301063/-/DC1
141. Giesen J, Füchtbauer EM, Füchtbauer A, Funke K, Koesling D, Russwurm M. AMPA Induces NO-Dependent cGMP Signals in Hippocampal and Cortical Neurons via L-Type Voltage-Gated Calcium Channels. *Cereb Cortex*. 2020;30(4):2128-2143. doi:10.1093/CERCOR/BHZ227
142. Thunemann M, Schmidt K, de Wit C, et al. Correlative intravital imaging of cGMP signals and vasodilation in mice. *Front Physiol*. 2014;5(OCT):110349. doi:10.3389/FPHYS.2014.00394/BIBTEX
143. Peters S, Paolillo M, Mergia E, et al. cGMP Imaging in Brain Slices Reveals Brain Region-Specific Activity of NO-Sensitive Guanylyl Cyclases (NO-GCs) and NO-GC Stimulators. *Int J Mol Sci*. 2018;19(8). doi:10.3390/IJMS19082313
144. Moeller MJ, Sanden SK, Soofi A, Wiggins RC, Holzman LB. Podocyte-specific expression of cre recombinase in transgenic mice. *Genesis*. 2003;35(1):39-42. doi:10.1002/GENE.10164

145. Kisanuki YY, Hammer RE, Miyazaki J ichi, Williams SC, Richardson JA, Yanagisawa M. Tie2-Cre Transgenic Mice: A New Model for Endothelial Cell-Lineage Analysis in Vivo. *Dev Biol.* 2001;230(2):230-242. doi:10.1006/DBIO.2000.0106
146. Alva JA, Zovein AC, Monvoisin A, et al. VE-Cadherin-Cre-recombinase transgenic mouse: a tool for lineage analysis and gene deletion in endothelial cells. *Dev Dyn.* 2006;235(3):759-767. doi:10.1002/DVDY.20643
147. Payne S, Val S De, Neal A. Endothelial-Specific Cre Mouse Models: Is Your Cre CREdible? *Arterioscler Thromb Vasc Biol.* 2018;38(11):2550. doi:10.1161/ATVBAHA.118.309669
148. Heffner CS, Herbert Pratt C, Babiuk RP, et al. Supporting conditional mouse mutagenesis with a comprehensive cre characterization resource. *Nature Communications 2012 3:1.* 2012;3(1):1-9. doi:10.1038/ncomms2186
149. Truett GE, Heeger P, Mynatt RL, Truett AA, Walker JA, Warman ML. Preparation of PCR-quality mouse genomic DNA with hot sodium hydroxide and tris (HotSHOT). *Biotechniques.* 2000;29(1):52-54. doi:10.2144/00291BM09
150. Takemoto M, Asker N, Gerhardt H, et al. A new method for large scale isolation of kidney glomeruli from mice. *Am J Pathol.* 2002;161(3):799-805. doi:10.1016/S0002-9440(10)64239-3
151. Binz-Lotter J, Jüngst C, Rinschen MM, et al. Injured Podocytes Are Sensitized to Angiotensin II-Induced Calcium Signaling. *J Am Soc Nephrol.* 2020;31(3):532-542. doi:10.1681/ASN.2019020109
152. Kardash E, Bandemer J, Raz E. Imaging protein activity in live embryos using fluorescence resonance energy transfer biosensors. *Nat Protoc.* 2011;6(12):1835-1846. doi:10.1038/NPROT.2011.395
153. Warren SC, Nobis M, Magenau A, et al. Removing physiological motion from intravital and clinical functional imaging data. *Elife.* 2018;7. doi:10.7554/ELIFE.35800
154. GeneRuler 1 kb DNA-Leiter. <https://www.thermofisher.com/order/catalog/product/de/de/SM0311>. Accessed February 22, 2024.



155. Mundel P, Bachmann S, Kriz W, Gambaryan S, Koesling D. Immunolocalization of soluble guanylyl cyclase subunits in rat kidney. *Histochem Cell Biol.* 1995;103(1):75-79. doi:10.1007/BF01464478
156. Bennett BM, Leitman DC, Schröder H, Kawamoto JH, Nakatsu K, Murad F. Relationship between biotransformation of glyceryl trinitrate and cyclic GMP accumulation in various cultured cell lines. *Journal of Pharmacology and Experimental Therapeutics.* 1989;250(1).
157. Yaoita E, Yoshida Y, Nameta M, Takimoto H, Fujinaka H. Induction of interdigitating cell processes in podocyte culture. *Kidney Int.* 2018;93(2):519-524. doi:10.1016/J.KINT.2017.06.031
158. Chittiprol S, Chen P, Petrovic-Djergovic D, Eichler T, Ransom RF. Marker expression, behaviors, and responses vary in different lines of conditionally immortalized cultured podocytes. *Am J Physiol Renal Physiol.* 2011;301(3). doi:10.1152/AJPRENAL.00234.2011
159. Golos M, Lewko B, Bryl E, et al. Effect of angiotensin II on ANP-dependent guanylyl cyclase activity in cultured mouse and rat podocytes. *Kidney Blood Press Res.* 2002;25(5):296-302. doi:10.1159/000066790
160. Lewko B, Gołos M, Latawiec E, Angielski S, Stepinski J. Regulation of cGMP synthesis in cultured podocytes by vasoactive hormones. *J Physiol Pharmacol.* 2006;57(4):599-610. <https://europepmc.org/article/med/17229984>. Accessed February 28, 2024.
161. Koseki C, Kanai Y, Hayashi Y, Ohnuma N, Imai M. Intrarenal Localization of Receptors for  $\alpha$ -Rat Atrial Natriuretic Polypeptide: An Autoradiographic Study with [125I]-Labeled Ligand Injected in Vivo into the Rat Aorta. *The Japanese Journal of Pharmacology.* 1986;42(1):27-33. doi:10.1254/JJP.42.27
162. Suga SI, Nakao K, Hosoda K, et al. Receptor selectivity of natriuretic peptide family, atrial natriuretic peptide, brain natriuretic peptide, and C-type natriuretic peptide. *Endocrinology.* 1992;130(1):229-239. doi:10.1210/ENDO.130.1.1309330
163. Lopez MJ, Garbers DL, Kuhn M. The guanylyl cyclase-deficient mouse defines differential pathways of natriuretic peptide signaling. *J Biol Chem.* 1997;272(37):23064-23068. doi:10.1074/JBC.272.37.23064

164. Ogawa Y, Mukoyama M, Yokoi H, et al. Natriuretic peptide receptor guanylyl cyclase-A protects podocytes from aldosterone-induced glomerular injury. *Journal of the American Society of Nephrology*. 2012;23(7):1198-1209. doi:10.1681/ASN.2011100985/-/DCSUPPLEMENTAL
165. Kato Y, Mori K, Kasahara M, et al. Natriuretic peptide receptor guanylyl cyclase-A pathway counteracts glomerular injury evoked by aldosterone through p38 mitogen-activated protein kinase inhibition. *Sci Rep*. 2017;7. doi:10.1038/SREP46624
166. Mani I, Garg R, Tripathi S, Pandey KN. Rapid Internalization and Trafficking of GC-A/NPRA via Endo-lysosomal Compartments with Concurrent Generation of cGMP in Mouse Mesangial Cells: Role of FQQL Motif. *The FASEB Journal*. 2016;30(S1):967.19-967.19. doi:10.1096/FASEBJ.30.1\_SUPPLEMENT.967.19
167. Somanna NK, Mani I, Tripathi S, Pandey KN. Clathrin-dependent internalization, signaling, and metabolic processing of guanylyl cyclase/natriuretic peptide receptor-A. *Mol Cell Biochem*. 2018;441(1-2):135-150. doi:10.1007/S11010-017-3180-0
168. Potter LR, Garbers DL. Dephosphorylation of the guanylyl cyclase-A receptor causes desensitization. *Journal of Biological Chemistry*. 1992;267(21):14531-14534. doi:10.1016/S0021-9258(18)42069-8
169. Potter LR, Garbers DL. Protein kinase C-dependent desensitization of the atrial natriuretic peptide receptor is mediated by dephosphorylation. *Journal of Biological Chemistry*. 1994;269(20):14636-14642. doi:10.1016/S0021-9258(17)36672-3
170. Castro LR V, Schittl J, Fischmeister R. Feedback control through cGMP-dependent protein kinase contributes to differential regulation and compartmentation of cGMP in rat cardiac myocytes. *Circ Res*. 2010;107(10):1232-1240. doi:10.1161/CIRCRESAHA.110.226712
171. Yandle TG, Richards AM, Nicholls MG, Cuneo R, Espiner EA, Livesey JH. Metabolic clearance rate and plasma half life of alpha-human atrial natriuretic peptide in man. *Life Sci*. 1986;38(20):1827-1833. doi:10.1016/0024-3205(86)90137-2
172. Nakao K, Sugawara A, Morii N, et al. The pharmacokinetics of alpha-human atrial natriuretic polypeptide in healthy subjects. *Eur J Clin Pharmacol*. 1986;31(1):101-103. doi:10.1007/BF00870995

173. Dickey DM, Yoder AR, Potter LR. A familial mutation renders atrial natriuretic Peptide resistant to proteolytic degradation. *J Biol Chem.* 2009;284(29):19196-19202. doi:10.1074/JBC.M109.010777
174. Dzhoyashvili NA, Iyer SR, Chen HH, Burnett JC. MANP (M-Atrial Natriuretic Peptide) Reduces Blood Pressure and Furosemide-Induced Increase in Aldosterone in Hypertension. *Hypertension.* 2022;79(4):750-760. doi:10.1161/HYPERTENSIONAHA.121.18837
175. Chen HH, Wan SH, Iyer SR, et al. First-in-Human Study of MANP: A Novel ANP (Atrial Natriuretic Peptide) Analog in Human Hypertension. *Hypertension.* 2021;78(6):1859-1867. doi:10.1161/HYPERTENSIONAHA.121.17159
176. Sharma R, Lovell HB, Wiegmann TB, Savin VJ. Vasoactive substances induce cytoskeletal changes in cultured rat glomerular epithelial cells. *Journal of the American Society of Nephrology.* 1992;3(5):1131-1138. doi:10.1681/ASN.V351131
177. Craven PA, Studer RK, DeRubertis FR. Impaired nitric oxide release by glomeruli from diabetic rats. *Metabolism.* 1995;44(6):695-698. doi:10.1016/0026-0495(95)90178-7
178. Sharma M, Zhou Z, Miura H, et al. ADMA injures the glomerular filtration barrier: role of nitric oxide and superoxide. *Am J Physiol Renal Physiol.* 2009;296(6):F1386. doi:10.1152/AJPRENAL.90369.2008
179. Chen Z, Zhang J, Stamler JS. From the Cover: Identification of the enzymatic mechanism of nitroglycerin bioactivation. *Proc Natl Acad Sci U S A.* 2002;99(12):8306. doi:10.1073/PNAS.122225199
180. Condorelli P, George SC. In vivo control of soluble guanylate cyclase activation by nitric oxide: a kinetic analysis. *Biophys J.* 2001;80(5):2110-2119. doi:10.1016/S0006-3495(01)76184-X
181. Ballou DP, Zhao Y, Brandish PE, Marletta MA. Revisiting the kinetics of nitric oxide (NO) binding to soluble guanylate cyclase: The simple NO-binding model is incorrect. *Proc Natl Acad Sci U S A.* 2002;99(19):12097-12101. doi:10.1073/PNAS.192209799/ASSET/D887A33B-4D01-4E8E-8FA9-AA12ACBFECFD/ASSETS/GRAPHIC/PQ1922097003.JPEG

182. Sayed N, Baskaran P, Ma X, Van Den Akker F, Beuve A. Desensitization of soluble guanylyl cyclase, the NO receptor, by S-nitrosylation. *Proc Natl Acad Sci U S A*. 2007;104(30):12312-12317. doi:10.1073/PNAS.0703944104
183. Ghosh A, Stasch JP, Papapetropoulos A, Stuehr DJ. Nitric Oxide and Heat Shock Protein 90 Activate Soluble Guanylate Cyclase by Driving Rapid Change in Its Subunit Interactions and Heme Content. *J Biol Chem*. 2014;289(22):15259. doi:10.1074/JBC.M114.559393
184. Dai Y, Stuehr DJ. Inactivation of soluble guanylyl cyclase in living cells proceeds without loss of haem and involves heterodimer dissociation as a common step. *Br J Pharmacol*. 2022;179(11):2505. doi:10.1111/BPH.15527
185. Pereira DA, Silveira THR, Calmasini FB, Silva FH. Soluble guanylate cyclase stimulators and activators: new horizons in the treatment of priapism associated with sickle cell disease. *Front Pharmacol*. 2024;15. doi:10.3389/FPHAR.2024.1357176
186. Koglin M, Vehse K, Budaeus L, Scholz H, Behrends S. Nitric Oxide Activates the  $\beta$ 2 Subunit of Soluble Guanylyl Cyclase in the Absence of a Second Subunit. *Journal of Biological Chemistry*. 2001;276(33):30737-30743. doi:10.1074/JBC.M102549200
187. Stroppel AS, Paolillo M, Ziegler T, Feil R, Stafforst T. Npom-Protected NONOate Enables Light-Triggered NO/cGMP Signalling in Primary Vascular Smooth Muscle Cells. *ChemBioChem*. 2018;19(12):1312-1318. doi:10.1002/CBIC.201700683
188. Benninger RKP, Piston DW. Two-Photon Excitation Microscopy for the Study of Living Cells and Tissues. *Current protocols in cell biology / editorial board, Juan S Bonifacino* . [et al]. 2013;0 4(SUPPL.59):Unit. doi:10.1002/0471143030.CB0411S59
189. Thomsen H, Marino N, Conoci S, Sortino S, Ericson MB. Confined photo-release of nitric oxide with simultaneous two-photon fluorescence tracking in a cellular system. *Sci Rep*. 2018;8(1). doi:10.1038/S41598-018-27939-4
190. Furusu A, Miyazaki M, Abe K, et al. Expression of endothelial and inducible nitric oxide synthase in human glomerulonephritis. *Kidney Int*. 1998;53(6):1760-1768. doi:10.1046/j.1523-1755.1998.00907.x
191. Shultz PJ, Archer SL, Rosenberg ME. Inducible nitric oxide synthase mRNA and activity in glomerular mesangial cells. *Kidney Int*. 1994;46(3):683-689. doi:10.1038/KI.1994.321

192. Stepinski J, Wendt U, Lewko B, Angielski S. Co-operation between particulate and soluble guanylyl cyclase systems in the rat renal glomeruli. *Journal of Physiology and Pharmacology*. 2000;51(3).
193. Lewko B, Wendt U, Szczepanska-Konkel M, Stepinski J, Drewnowska K, Angielski S. Inhibition of endogenous nitric oxide synthesis activates particulate guanylyl cyclase in the rat renal glomeruli. *Kidney Int*. 1997;52(3):654-659. doi:10.1038/KI.1997.379
194. Woodard GE, Zhao J, Rosado JA, Brown J. Patterning of renal cGMP production by the natriuretic peptide receptor type A and blood pressure in spontaneously hypertensive rats. *Regul Pept*. 2004;119(1-2):45-51. doi:10.1016/J.REGPEP.2003.12.002
195. Rivas-Cabanero L, Montero A, López-Novoa JM. Nitric Oxide-dependent Cyclic GMP Synthesis by Isolated Rat Glomeruli. *Endothelium*. 1994;1(4):259-261. doi:10.3109/10623329409100964
196. Wang Y, Krämer S, Loof T, et al. Enhancing cGMP in experimental progressive renal fibrosis: Soluble guanylate cyclase stimulation vs. phosphodiesterase inhibition. *Am J Physiol Renal Physiol*. 2006;290(1):167-176. doi:10.1152/AJPRENAL.00197.2005/ASSET/IMAGES/LARGE/ZH20010641870007.JPEG
197. Mizukawa K, Ogura T, Yamamoto I, et al. Localization of receptors for atrial natriuretic polypeptide (ANP) in the glomerulus: in vitro electron microscopic autoradiographical investigation using <sup>125</sup>I-labeled ANP. *Regul Pept*. 1988;21(1-2):167-172. doi:10.1016/0167-0115(88)90100-0
198. Bianchi C, Gutkowska J, Thibault G, Garcia R, Genest J, Cantin M. Distinct localization of atrial natriuretic factor and angiotensin II binding sites in the glomerulus. *American Journal of Physiology - Renal Fluid and Electrolyte Physiology*. 1986;251(4 (20/4)). doi:10.1152/AJPRENAL.1986.251.4.F594
199. Rambotti MG, Saccardi C, Spreca A. Evidence for particulate guanylate cyclase in rat kidney after stimulation by atrial natriuretic factor. An ultracytochemical study. *Histochem J*. 1990;22(9):469-474. doi:10.1007/BF01007230/METRICS
200. Paes D, Hermans S, van den Hove D, Vanmierlo T, Prickaerts J, Carlier A. Computational investigation of the dynamic control of cAMP signaling by PDE4 isoform types. *Biophys J*. 2022;121(14):2693-2711. doi:10.1016/J.BPJ.2022.06.019

201. Kyurkchieva E, Baillie GS. Short PDE4 Isoforms as Drug Targets in Disease. *Frontiers in Bioscience - Landmark*. 2023;28(7):133. doi:10.31083/J.FBL2807133/2768-6698-28-7-133/FIG2.JPG
202. Lavan BE, Lakey T, Houslay MD. Resolution of soluble cyclic nucleotide phosphodiesterase isoenzymes, from liver and hepatocytes, identifies a novel IBMX-insensitive form. *Biochem Pharmacol*. 1989;38(22):4123-4136. doi:10.1016/0006-2952(89)90694-1
203. Tulsian NK, Sin VJE, Koh HL, Anand GS. Development of Phosphodiesterase-Protein-Kinase Complexes as Novel Targets for Discovery of Inhibitors with Enhanced Specificity. *Int J Mol Sci*. 2021;22(10). doi:10.3390/IJMS22105242
204. Kotera J, Mochida H, Inoue H, et al. Avanafil, a potent and highly selective phosphodiesterase-5 inhibitor for erectile dysfunction. *J Urol*. 2012;188(2):668-674. doi:10.1016/J.JURO.2012.03.115
205. Pavlaki N, Nikolaev VO. Imaging of PDE2- and PDE3-Mediated cGMP-to-cAMP Cross-Talk in Cardiomyocytes. *J Cardiovasc Dev Dis*. 2018;5(1). doi:10.3390/JCDD5010004
206. Gao SY, Li CY, Shimokawa T, et al. Rho-family small GTPases are involved in forskolin-induced cell-cell contact formation of renal glomerular podocytes in vitro. *Cell Tissue Res*. 2007;328(2):391-400. doi:10.1007/S00441-006-0365-3/FIGURES/6
207. Endlich N, Endlich K. cAMP pathway in podocytes. *Microsc Res Tech*. 2002;57(4):228-231. doi:10.1002/JEMT.10079
208. Li X, Tao H, Xie K, et al. cAMP Signaling Prevents Podocyte Apoptosis via Activation of Protein Kinase A and Mitochondrial Fusion. *PLoS One*. 2014;9(3). doi:10.1371/JOURNAL.PONE.0092003
209. Lee HJ, Feliars D, Mariappan MM, et al. Tadalafil Integrates Nitric Oxide-Hydrogen Sulfide Signaling to Inhibit High Glucose-induced Matrix Protein Synthesis in Podocytes. *J Biol Chem*. 2015;290(19):12014-12026. doi:10.1074/JBC.M114.615377
210. Fang L, Radovits T, Szabó G, Mózes MM, Rosivall L, Kökény G. Selective phosphodiesterase-5 (PDE-5) inhibitor vardenafil ameliorates renal damage in type 1 diabetic rats by restoring cyclic 3',5' guanosine monophosphate (cGMP) level in podocytes. *Nephrol Dial Transplant*. 2013;28(7):1751-1761. doi:10.1093/NDT/GFS391

211. Tomita N, Hotta Y, Naiki-Ito A, et al. Protective effects of tadalafil on damaged podocytes in an adriamycin-induced nephrotic syndrome model. *J Pharmacol Sci.* 2022;149(2):53-59. doi:10.1016/J.JPHS.2022.03.003
212. Yan W, Wu F, Morser J, Wu Q. Corin, a transmembrane cardiac serine protease, acts as a pro-atrial natriuretic peptide-converting enzyme. *Proc Natl Acad Sci U S A.* 2000;97(15):8525-8529. doi:10.1073/PNAS.150149097
213. Sager G. Cyclic GMP transporters. *Neurochem Int.* 2004;45(6):865-873. doi:10.1016/j.neuint.2004.03.017
214. Ardaillou N, Lelongt B, Turner N, et al. Characterization of a simian virus 40-transformed human podocyte cell line producing type IV collagen and exhibiting polarized response to atrial natriuretic peptide. *J Cell Physiol.* 1992;152(3):599-616. doi:10.1002/JCP.1041520320
215. Evans JM, Day JP, Cabrero P, Dow JAT, Davies SA. A new role for a classical gene: White transports cyclic GMP. *Journal of Experimental Biology.* 2008;211(6):890-899. doi:10.1242/JEB.014837
216. Tchernychev B, Ge P, Kessler MM, et al. MRP4 Modulation of the Guanylate Cyclase-C/cGMP Pathway: Effects on Linacotide-Induced Electrolyte Secretion and cGMP Efflux. *J Pharmacol Exp Ther.* 2015;355(1):48-56. doi:10.1124/JPET.115.224329
217. Kashgari FK, Ravna A, Sager G, Lyså R, Enyedy I, Dietrichs ES. Identification and experimental confirmation of novel cGMP efflux inhibitors by virtual ligand screening of vardenafil-analogues. *Biomedicine & Pharmacotherapy.* 2020;126:110109. doi:10.1016/J.BIOPHA.2020.110109
218. Sasaki S, Siragy HM, Gildea JJ, Felder RA, Carey RM. Production and Role of Extracellular Guanosine Cyclic 3', 5' Monophosphate in Sodium Uptake in Human Proximal Tubule Cells. *Hypertension.* 2004;43(2 I):286-291. doi:10.1161/01.HYP.0000112421.18551.1e
219. Rocznik A, Burns KD. Nitric oxide stimulates guanylate cyclase and regulates sodium transport in rabbit proximal tubule. *Am J Physiol.* 1996;270(1 Pt 2). doi:10.1152/AJPRENAL.1996.270.1.F106

220. Bhargava P, Janda J, Schnellmann RG. Renal Mechanisms of Tissue Remodeling: Elucidation of cGMP-dependent induction of mitochondrial biogenesis through PKG and p38 MAPK in the kidney. *Am J Physiol Renal Physiol*. 2020;318(2):F322. doi:10.1152/AJPRENAL.00533.2019
221. Linas SL, Repine JE. Endothelial cells regulate proximal tubule epithelial cell sodium transport. *Kidney Int*. 1999;55(4):1251-1258. doi:10.1046/j.1523-1755.1999.00360.x
222. Jin XH, Siragy HM, Carey RM. Renal Interstitial cGMP Mediates Natriuresis by Direct Tubule Mechanism. *Hypertension*. 2001;38(3):309-316. doi:10.1161/01.HYP.38.3.309
223. Tu YC, Shu HP, Sun LL, et al. The Physiopathologic Roles of Calcium Signaling in Podocytes. *Frontiers in Bioscience - Landmark*. 2023;28(10):240. doi:10.31083/J.FBL2810240/2768-6698-28-10-240/FIG5.JPG
224. James LR, Griffiths CH, Garthwaite J, Bellamy TC. Inhibition of nitric oxide-activated guanylyl cyclase by calmodulin antagonists. *Br J Pharmacol*. 2009;158(6):1454. doi:10.1111/J.1476-5381.2009.00416.X
225. Marsden PA, Brock TA, Ballermann BJ. Glomerular endothelial cells respond to calcium-mobilizing agonists with release of EDRF. *American Journal of Physiology - Renal Fluid and Electrolyte Physiology*. 1990;258(5 27-5). doi:10.1152/AJPRENAL.1990.258.5.F1295
226. Liu R, Gutiérrez AM, Ring A, Persson AEG. Nitric oxide induces resensitization of P2Y nucleotide receptors in cultured rat mesangial cells. *J Am Soc Nephrol*. 2002;13(2):313-321. doi:10.1681/ASN.V132313
227. Saoud R, Jaffa MA, Habib A, et al. Modulation of proteomic and inflammatory signals by Bradykinin in podocytes. *J Adv Res*. 2020;24:409. doi:10.1016/J.JARE.2020.05.021
228. Ardaillou N, Blaise V, Costenbader K, Vassitch Y, Ardaillou R. Characterization of a B2-bradykinin receptor in human glomerular podocytes. *Am J Physiol*. 1996;271(3 Pt 2):F754-61. doi:10.1152/AJPRENAL.1996.271.3.F754
229. Pavenstädt H, Späth M, Fiedler C, et al. Effect of bradykinin on the cytosolic free calcium activity and phosphoinositol turnover in human glomerular epithelial cells. *Ren Physiol Biochem*. 1992;15(6):277-288. doi:10.1159/000173464



230. Mundel P, Reiser J, Borja AZM, et al. Rearrangements of the Cytoskeleton and Cell Contacts Induce Process Formation during Differentiation of Conditionally Immortalized Mouse Podocyte Cell Lines. *Exp Cell Res.* 1997;236(1):248-258. doi:10.1006/EXCR.1997.3739
231. Fischer KG, Saueressig U, Jacobshagen C, Wichelmann A, Pavenstädt H. Extracellular nucleotides regulate cellular functions of podocytes in culture. *Am J Physiol Renal Physiol.* 2001;281(6):50-6. doi:10.1152/AJPRENAL.2001.281.6.F1075/ASSET/IMAGES/LARGE/H21210510009.JPG
232. Roshanravan H, Dryer SE. ATP acting through P2Y receptors causes activation of podocyte TRPC6 channels: Role of podocin and reactive oxygen species. *Am J Physiol Renal Physiol.* 2014;306(9):1088-1097. doi:10.1152/AJPRENAL.00661.2013/ASSET/IMAGES/LARGE/ZH20081472560009.JPG
233. Ilatovskaya D V., Palygin O, Levchenko V, Staruschenko A. Pharmacological characterization of the P2 receptors profile in the podocytes of the freshly isolated rat glomeruli. *Am J Physiol Cell Physiol.* 2013;305(10). doi:10.1152/AJPCCELL.00138.2013
234. Gyarmati G, Toma I, Izuhara A, et al. The role of TRPC6 calcium channels and P2 purinergic receptors in podocyte mechanical and metabolic sensing. *Physiol Int.* 2021;109(1):31-45. doi:10.1556/2060.2021.00205
235. Tian D, Jacobo SMP, Billing D, et al. Antagonistic regulation of actin dynamics and cell motility by TRPC5 and TRPC6 channels. *Sci Signal.* 2010;3(145). doi:10.1126/SCISIGNAL.2001200
236. Schaldecker T, Kim S, Tarabanis C, et al. Inhibition of the TRPC5 ion channel protects the kidney filter. *J Clin Invest.* 2013;123(12):5298. doi:10.1172/JCI71165
237. Burford JL, Villanueva K, Lam L, et al. Intravital imaging of podocyte calcium in glomerular injury and disease. *J Clin Invest.* 2014;124(5):2050. doi:10.1172/JCI71702
238. Miyamoto T, Mochizuki T, Nakagomi H, et al. Functional Role for Piezo1 in Stretch-evoked Ca<sup>2+</sup> Influx and ATP Release in Urothelial Cell Cultures. *J Biol Chem.* 2014;289(23):16565. doi:10.1074/JBC.M113.528638

239. Santana Nunez D, Malik AB, Lee Q, et al. Piezo1 induces endothelial responses to shear stress via soluble adenylyl Cyclase-IP3R2 circuit. *iScience*. 2023;26(5):106661. doi:10.1016/J.ISCI.2023.106661
240. Bartoli F, Debant M, Chuntharpursat-Bon E, et al. Endothelial Piezo1 sustains muscle capillary density and contributes to physical activity. *J Clin Invest*. 2022;132(5). doi:10.1172/JCI141775
241. Ogino S, Yoshikawa K, Nagase T, Mikami K, Nagase M. Roles of the mechanosensitive ion channel Piezo1 in the renal podocyte injury of experimental hypertensive nephropathy. *Hypertension Research* 2023 47:3. 2023;47(3):747-759. doi:10.1038/s41440-023-01536-z
242. Dalghi MG, Clayton DR, Ruiz WG, et al. Expression and distribution of PIEZO1 in the mouse urinary tract. *Am J Physiol Renal Physiol*. 2019;317(2):F303. doi:10.1152/AJPRENAL.00214.2019
243. Greif DM, Sacks DB, Michel T. Calmodulin phosphorylation and modulation of endothelial nitric oxide synthase catalysis. *Proc Natl Acad Sci U S A*. 2004;101(5):1165. doi:10.1073/PNAS.0306377101
244. Dalal PJ, Muller WA, Sullivan DP. Endothelial Cell Calcium Signaling during Barrier Function and Inflammation. *Am J Pathol*. 2020;190(3):535. doi:10.1016/J.AJPATH.2019.11.004
245. Ballermann BJ. Glomerular endothelial cell differentiation. *Kidney Int*. 2005;67(5):1668-1671. doi:10.1111/J.1523-1755.2005.00260.X
246. Bachmann S, Bosse HM, Mundel P. Topography of nitric oxide synthesis by localizing constitutive NO synthases in mammalian kidney. *American Journal of Physiology - Renal Fluid and Electrolyte Physiology*. 1995;268(5 37-5). doi:10.1152/AJPRENAL.1995.268.5.F885
247. Kasai N, Sugimoto K, Horiba N, Suda T. Effect of D-glucose on nitric oxide release from glomerular endothelial cells. *Diabetes Metab Res Rev*. 2001;17(3):217-222. doi:10.1002/DMRR.195
248. Dolinina J, Sverrisson K, Rippe A, Öberg CM, Rippe B. Nitric oxide synthase inhibition causes acute increases in glomerular permeability in vivo, dependent upon reactive

- oxygen species. *Am J Physiol Renal Physiol.* 2016;311(5):F984-F990. doi:10.1152/AJPRENAL.00152.2016
249. Green DF, Duruibe VA, Blyden G, Laskey RE, Bourgoignie JJ. Uptake of atrial natriuretic peptide and production of cGMP in cultured human glomerular endothelial cells. *J Am Soc Nephrol.* 1994;5(4):1091-1098. doi:10.1681/ASN.V541091
250. Vollmar AM. The role of atrial natriuretic peptide in the immune system. *Peptides (NY).* 2005;26(6):1086-1094. doi:10.1016/J.PEPTIDES.2004.08.034
251. Oates JC, Russell DL, Van Beusecum JP. Endothelial cells: potential novel regulators of renal inflammation. *Am J Physiol Renal Physiol.* 2022;322(3):F309-F321. doi:10.1152/AJPRENAL.00371.2021
252. Kiemer AK, Weber NC, Fürst R, Bildner N, Kulhanek-Heinze S, Vollmar AM. Inhibition of p38 MAPK Activation via Induction of MKP-1. *Circ Res.* 2002;90(8):874-881. doi:10.1161/01.RES.0000017068.58856.F3
253. Van Den Akker F. Structural insights into the ligand binding domains of membrane bound guanylyl cyclases and natriuretic peptide receptors. *J Mol Biol.* 2001;311(5):923-937. doi:10.1006/JMBI.2001.4922
254. Robinson JW, Potter LR. Guanylyl Cyclases A and B Are Asymmetric Dimers That Are Allosterically Activated by ATP Binding to the Catalytic Domain. *Sci Signal.* 2012;5(240):ra65. doi:10.1126/SCISIGNAL.2003253
255. Sangaralingham SJ, Whig K, Peddibhotla S, et al. Discovery of small molecule guanylyl cyclase A receptor positive allosteric modulators. *Proc Natl Acad Sci U S A.* 2021;118(52):e2109386118. doi:10.1073/PNAS.2109386118/SUPPL\_FILE/PNAS.2109386118.SAPP.PDF
256. Gupta G, Azam M, Yang L, Danziger RS. The beta2 subunit inhibits stimulation of the alpha1/beta1 form of soluble guanylyl cyclase by nitric oxide. Potential relevance to regulation of blood pressure. *J Clin Invest.* 1997;100(6):1488-1492. doi:10.1172/JCI119670
257. Sadhu K, Hensley K, Florio VA, Wolda SL. Differential expression of the cyclic GMP-stimulated phosphodiesterase PDE2A in human venous and capillary endothelial cells. *J Histochem Cytochem.* 1999;47(7):895-905. doi:10.1177/002215549904700707

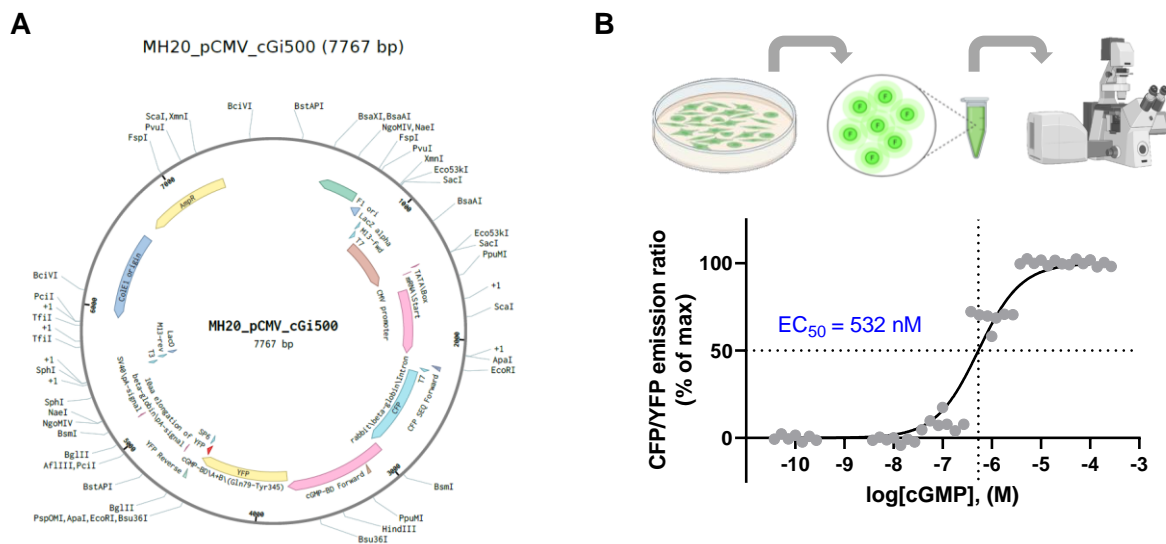
258. Surapisitchat J, Jeon KI, Yan C, Beavo JA. Differential regulation of endothelial cell permeability by cGMP via phosphodiesterases 2 and 3. *Circ Res*. 2007;101(8):811-818. doi:10.1161/CIRCRESAHA.107.154229
259. Surapisitchat J, Beavo JA. Regulation of Endothelial Barrier Function by Cyclic Nucleotides: The Role of Phosphodiesterases. *Handb Exp Pharmacol*. 2011;204(204):193. doi:10.1007/978-3-642-17969-3\_8
260. Netherton SJ, Maurice DH. Vascular endothelial cell cyclic nucleotide phosphodiesterases and regulated cell migration: implications in angiogenesis. *Mol Pharmacol*. 2005;67(1):263-272. doi:10.1124/MOL.104.004853
261. Keravis T, Komasa N, Lugnier C. Cyclic nucleotide hydrolysis in bovine aortic endothelial cells in culture: differential regulation in cobblestone and spindle phenotypes. *J Vasc Res*. 2000;37(4):235-249. doi:10.1159/000025738
262. Urbanczyk M, Zbinden A, Schenke-Layland K. Organ-specific endothelial cell heterogeneity and its impact on regenerative medicine and biomedical engineering applications. *Adv Drug Deliv Rev*. 2022;186:114323. doi:10.1016/J.ADDR.2022.114323
263. Dumas SJ, Meta E, Borri M, et al. Phenotypic diversity and metabolic specialization of renal endothelial cells. *Nat Rev Nephrol*. 2021;17(7):441. doi:10.1038/S41581-021-00411-9
264. Feng W, Chen L, Nguyen PK, Wu SM, Li G. Single Cell Analysis of Endothelial Cells Identified Organ-Specific Molecular Signatures and Heart-Specific Cell Populations and Molecular Features. *Front Cardiovasc Med*. 2019;6:483953. doi:10.3389/FCVM.2019.00165/BIBTEX
265. Nikolaev VO, Gambaryan S, Lohse MJ. Fluorescent sensors for rapid monitoring of intracellular cGMP. *Nat Methods*. 2006;3(1):23-25. doi:10.1038/NMETH816
266. Niino Y, Hotta K, Oka K. Blue Fluorescent cGMP Sensor for Multiparameter Fluorescence Imaging. *PLoS One*. 2010;5(2):e9164. doi:10.1371/JOURNAL.PONE.0009164
267. Grant DM, Zhang W, McGhee EJ, et al. Multiplexed FRET to image multiple signaling events in live cells. *Biophys J*. 2008;95(10):L69-L71. doi:10.1529/biophysj.108.139204

268. Paolillo M, Peters S, Schramm A, Schlossmann J, Feil R. Real-Time Imaging Reveals Augmentation of Glutamate-Induced Ca<sup>2+</sup> Transients by the NO-cGMP Pathway in Cerebellar Granule Neurons. *Int J Mol Sci.* 2018;19(8). doi:10.3390/IJMS19082185
269. Lam AJ, St-Pierre F, Gong Y, et al. Improving FRET dynamic range with bright green and red fluorescent proteins. *Nat Methods.* 2012;9(10):1005-1012. doi:10.1038/NMETH.2171
270. Rich TC, Britain AL, Stedman T, Leavesley SJ. Hyperspectral imaging of FRET-based cGMP probes. *Methods in Molecular Biology.* 2013;1020:73-88. doi:10.1007/978-1-62703-459-3\_5/FIGURES/00053
271. Zhang Y, Wang Y, Cao WW, et al. Spectral Characteristics of Autofluorescence in Renal Tissue and Methods for Reducing Fluorescence Background in Confocal Laser Scanning Microscopy. *J Fluoresc.* 2018;28(2):561-572. doi:10.1007/S10895-018-2217-4
272. Dixit R, Cyr R. Cell damage and reactive oxygen species production induced by fluorescence microscopy: effect on mitosis and guidelines for non-invasive fluorescence microscopy. *The Plant Journal.* 2003;36(2):280-290. doi:10.1046/J.1365-313X.2003.01868.X
273. Raarup MK, Fjorback AW, Jensen SMR, et al. Enhanced yellow fluorescent protein photoconversion to a cyan fluorescent protein-like species is sensitive to thermal and diffusion conditions. <https://doi.org/10.1117/1.3103338>. 2009;14(3):034039. doi:10.1117/1.3103338
274. Kindt F, Hammer E, Kemnitz S, et al. A novel assay to assess the effect of pharmaceutical compounds on the differentiation of podocytes. *Br J Pharmacol.* 2017;174(2):163. doi:10.1111/BPH.13667
275. Nitschke R, Henger A, Ricken S, et al. Angiotensin II increases the intracellular calcium activity in podocytes of the intact glomerulus. *Kidney Int.* 2000;57(1):41-49. doi:10.1046/J.1523-1755.2000.00810.X
276. Goldblatt ZE, Cirka HA, Billiar KL. Mechanical Regulation of Apoptosis in the Cardiovascular System. *Ann Biomed Eng.* 2021;49(1):75. doi:10.1007/S10439-020-02659-X

277. Lagadic-Gossmann D, Huc L, Lecureur V. Alterations of intracellular pH homeostasis in apoptosis: origins and roles. *Cell Death & Differentiation* 2004 11:9. 2004;11(9):953-961. doi:10.1038/sj.cdd.4401466
278. Betolngar DB, Erard M, Pasquier H, et al. pH sensitivity of FRET reporters based on cyan and yellow fluorescent proteins. *Anal Bioanal Chem*. 2015;407(14):4183-4193. doi:10.1007/S00216-015-8636-Z/FIGURES/7
279. Schor N, Ichikawa I, Brenner BM. Mechanisms of action of various hormones and vasoactive substances on glomerular ultrafiltration in the rat. *Kidney Int*. 1981;20(4):442-451. doi:10.1038/KI.1981.160

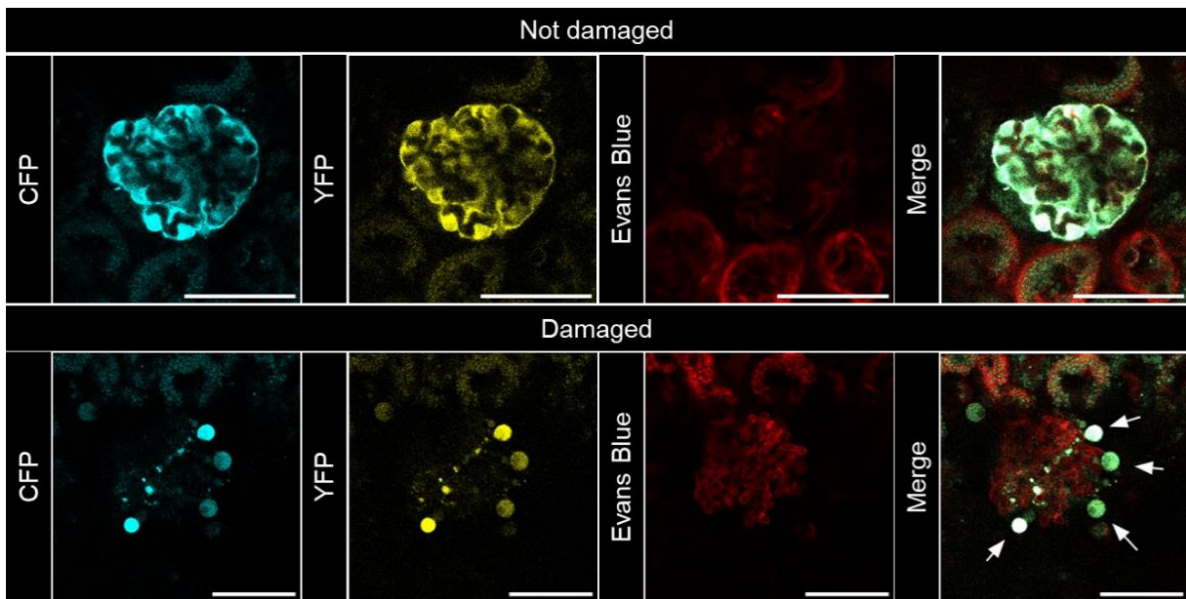
# Appendix

## Supporting information (SI 1)



### Supplemental Figure 1: *In vitro* characterization of cGi500

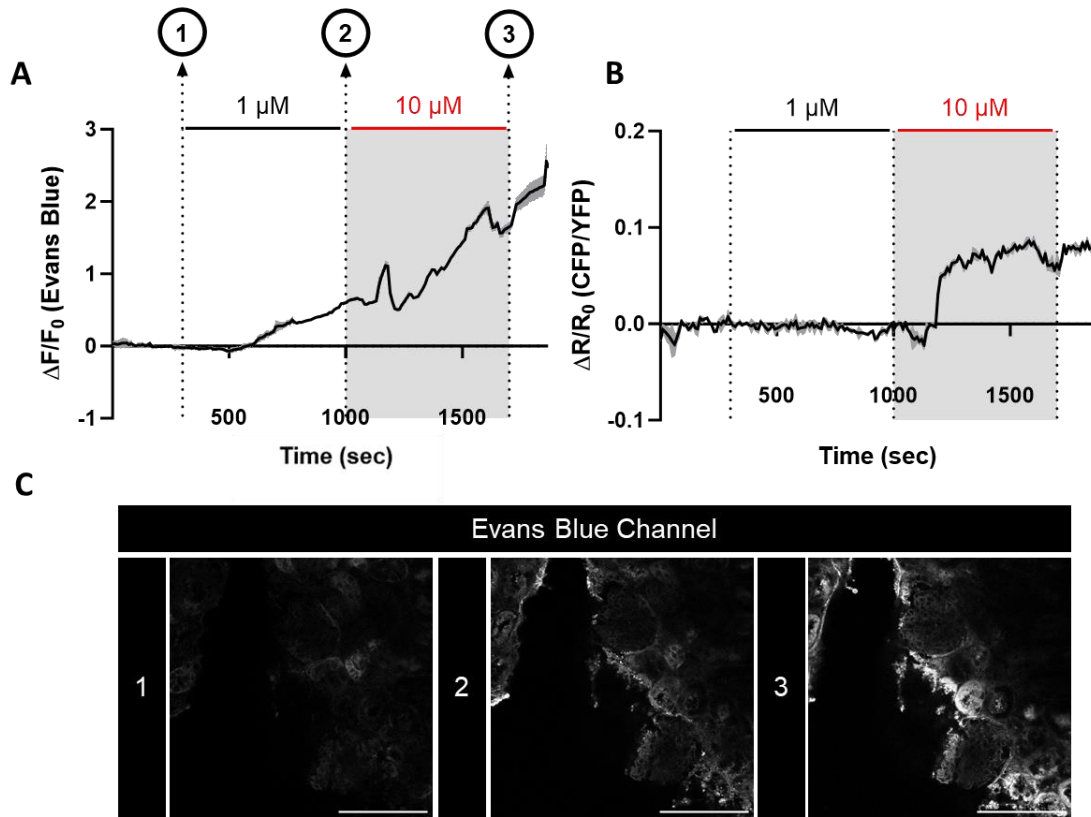
**(A)** Plasmid map of MH20\_pCMV\_cGi500 encoding the monomolecular FRET-based cGMP biosensor cGi500. **(B)** Concentration-response curve analysis of cGi500-transfected HEK 293T cell homogenates. Fluorescence measurements started with the highest cGMP concentration (100  $\mu\text{M}$  cGMP) and progressed to the lowest. Biosensor excitation was conducted with a diode laser at 405 nm together with a dichroic beam splitter (MBS-405) and simultaneous detection of CFP and YFP emission at  $480 \pm 25 \text{ nm}$  and  $535 \pm 20 \text{ nm}$ . The FRET (CFP/YFP) ratio changes were normalized to the first value (absence of cGMP) and the largest value (highest cGMP concentration) in the data set (Hill Slope = 1.0). Data are displayed for each replicate of seven independent experiments.



**Supplemental Figure 2: Visualization of the cutting process-related damage to glomeruli**

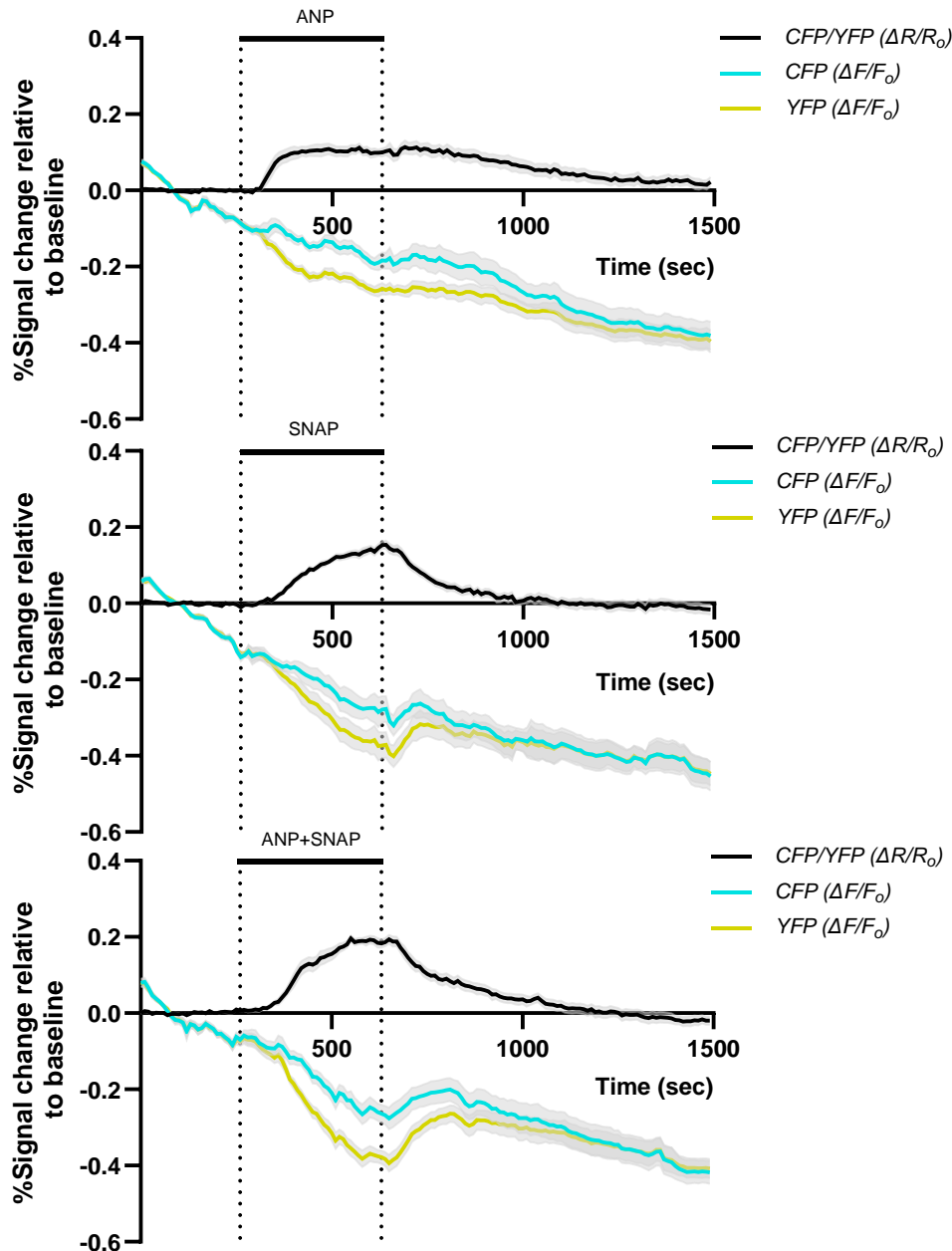
(**Top row**) Undamaged glomerulus shown in the CFP (cyan), YFP (yellow), Evans Blue (red) channel and the overlay of all channels (merge). The fluorescence in the Evans blue channel is due to expression of mTomato in all Cre-negative cells. (**Bottom row**) A glomerulus severely damaged by the cutting process with markedly deformed cells (white arrows). The uptake of Evans Blue into the glomerulus is visible in the red channel. Scale bar 50  $\mu$ M.





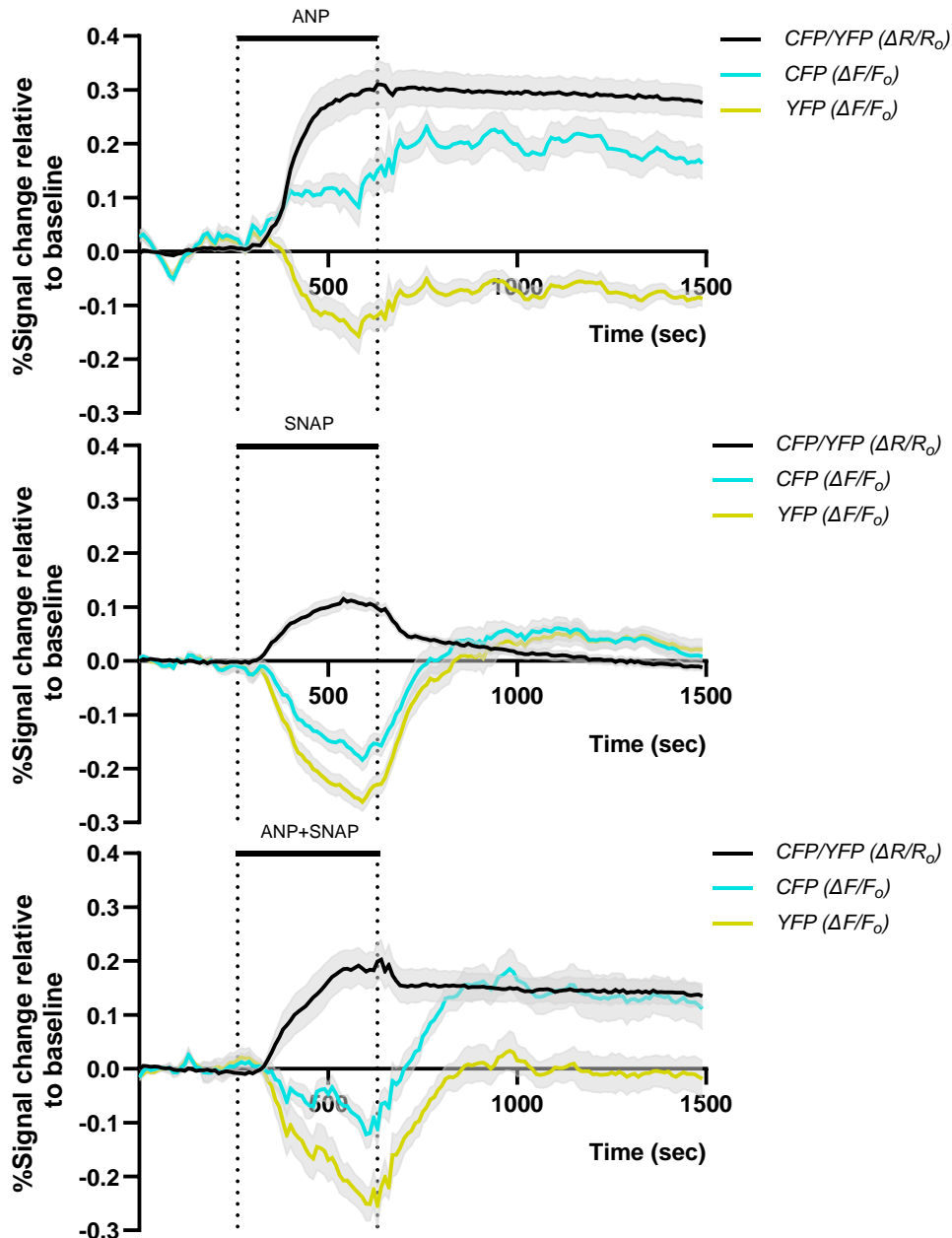
**Supplemental Figure 3: Evans Blue interferes at high concentrations with the FRET-based biosensor cGi500**

Acute kidney slice of a Pod:Cre/cGi500 mouse superfused with 1  $\mu\text{M}$  and 10  $\mu\text{M}$  Evans Blue solution (dotted lines) while recording time-lapse images. **(A)** While the fluorescence ( $\Delta F/F_0$ ) in the Evans Blue channel increases after superfusion with 1  $\mu\text{M}$  Evans Blue, a non-specific increase in the **(B)** FRET (CFP/YFP) ratio ( $\Delta R/R_0$ ) is only detectable after exposure to 10  $\mu\text{M}$  Evans Blue. **(C)** Images of the Evans blue channel at the time points 1 (300 sec), 2 (1000 sec) and 3 (1700 sec). All experiments shown in this manuscript were conducted with 1  $\mu\text{M}$  Evans Blue. Data represent mean  $\pm$  SEM. Scale bar 100  $\mu\text{M}$ .



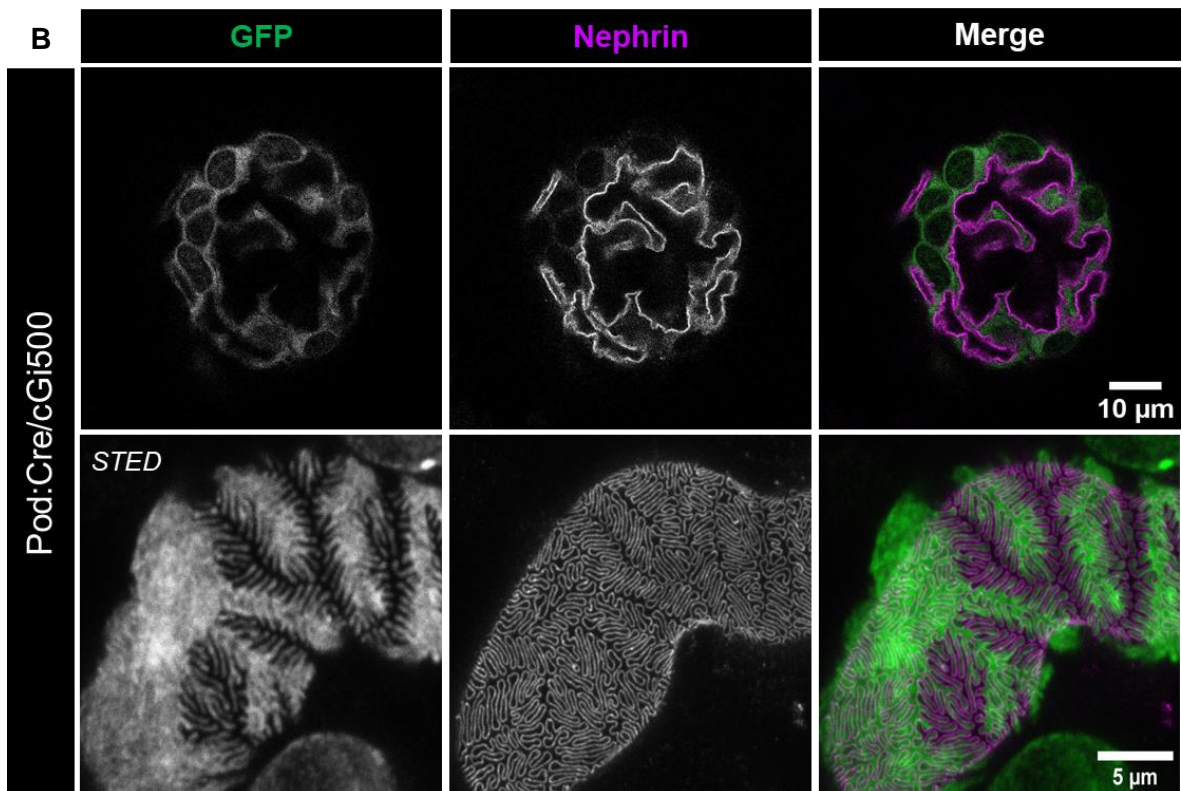
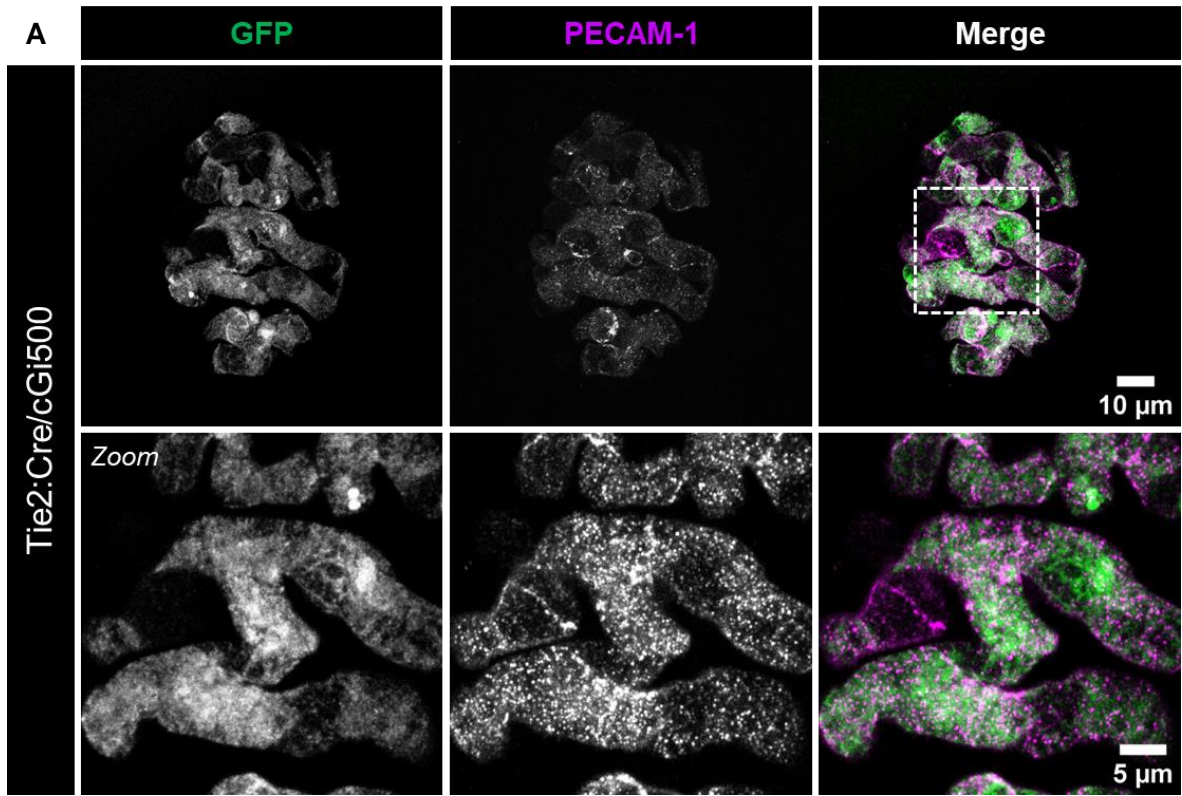
**Supplemental Figure 4: Calculated FRET (CFP/YFP) ratio from CFP and YFP fluorescence traces demonstrates cGMP generation after activation of the ANP/pGC or/and NO/sGC pathway in GECs**

Acute kidney slices from Tie2:Cre/cGi500 mice were subjected to stimulation with either 1  $\mu$ M ANP, 1 mM SNAP or a combination of both in the time period from 200 sec to 570 sec (dotted line). Displayed is the emission intensity change over a measurement period of 1500 sec with visualization of the individual CFP (cyan) and YFP (yellow) traces ( $\Delta F/F_0$ ) and the FRET (CFP/YFP) ratio (black,  $\Delta R/R_0$ ). Data represent mean  $\pm$  SEM of all analyzed glomeruli of six mice ( $n = 10$  for ANP,  $n = 9$  for SNAP,  $n = 10$  for ANP+SNAP).



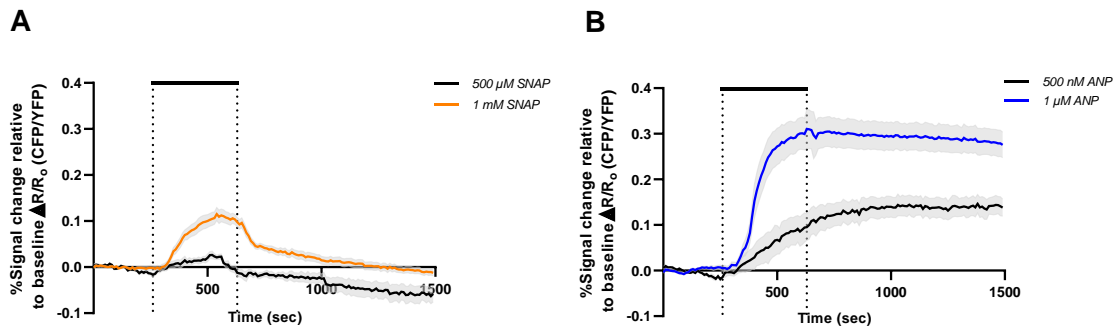
**Supplemental Figure 5: Calculated FRET (CFP/YFP) ratio from CFP and YFP fluorescence traces demonstrates cGMP generation after activation of the ANP/pGC or/and NO/sGC pathway in podocytes**

Acute kidney slices from Pod:Cre/cGi500 mice were subjected to stimulation with either 1  $\mu$ M ANP, 1 mM SNAP or a combination of both in the time period from 200 sec to 570 sec (dotted line). Displayed is the emission intensity change over a measurement period of 1500 sec with visualization of the individual CFP (cyan) and YFP (yellow) traces ( $\Delta F/F_0$ ) and the FRET (CFP/YFP) ratio (black,  $\Delta R/R_0$ ). Data represent mean  $\pm$  SEM of all analyzed glomeruli of five mice ( $n = 10$  for ANP,  $n = 11$  for SNAP,  $n = 10$  for ANP+SNAP).

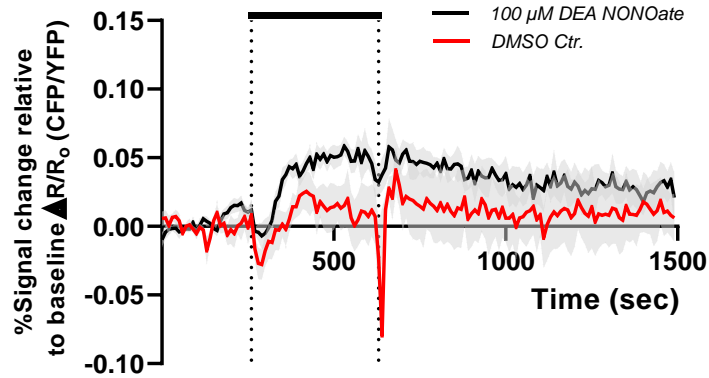


**Supplemental Figure 6: Cell-specific expression of the cGMP biosensor in optically cleared AKS**

(A) Tie2:Cre/cGi500: Confocal images show GFP staining (green) in GECs, thereby confirming cGi500 expression in this cell type. PECAM-1 staining (magenta) functions as a cell-specific marker for GECs and colocalizes with GFP-stained GECs. Bottom panels: High magnification of the area marked with a dashed rectangle in the right upper panel (Zoom). Both panels display a maximum intensity projection of a Z-stack. (B) Pod:Cre/cGi500: Confocal images demonstrate positive GFP staining (green) of podocytes, confirming the presence of biosensor cGi500 expression and overlapping nephrin staining (magenta), which labels the slit diaphragm. Higher magnification STED images (maximum intensity projection of Z-stacks) show a capillary area surrounded by podocytes (green) with characteristic slit diaphragm morphology (magenta).

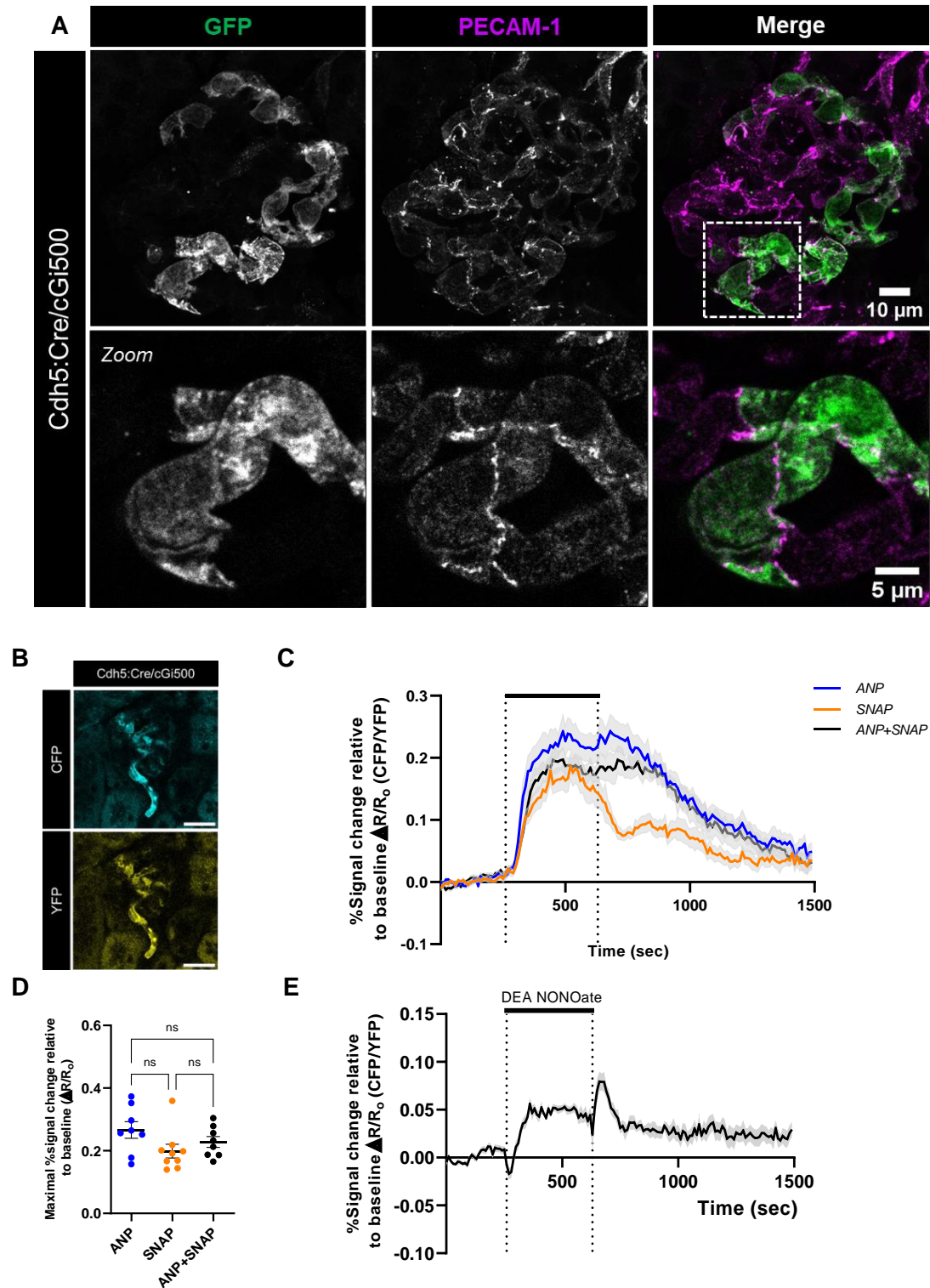
**Supplemental Figure 7: High doses of ANP and SNAP are required to elicit measurable cGi500-mediated cGMP signals**

Acute kidney slices from Pod:Cre/cGi500 mice were superfused (dotted lines) in the time period from 200 sec to 570 sec with (A) 1 mM SNAP (orange trace) and 500  $\mu$ M SNAP (black trace) or (B) 1  $\mu$ M ANP (blue trace) and 500 nM ANP (black trace). Stimulation was followed by pre-tempered 1X KHB (37°C), a time frame of 1500 sec was recorded. Graphs represent the mean of baseline-normalized FRET (CFP/YFP) ratios ( $\Delta R/R_0$ ) of all analyzed glomeruli. Data represent mean  $\pm$  SEM of all analyzed glomeruli of eight Pod:Cre/cGi500 mice ( $n = 6$  for 500 nM ANP,  $n = 10$  for 1  $\mu$ M ANP,  $n = 8$  for 500  $\mu$ M SNAP,  $n = 11$  for 1 mM SNAP).



### Supplemental Figure 8: DEA NONOate triggers cGMP synthesis in Tie2:Cre/cGi500 mice

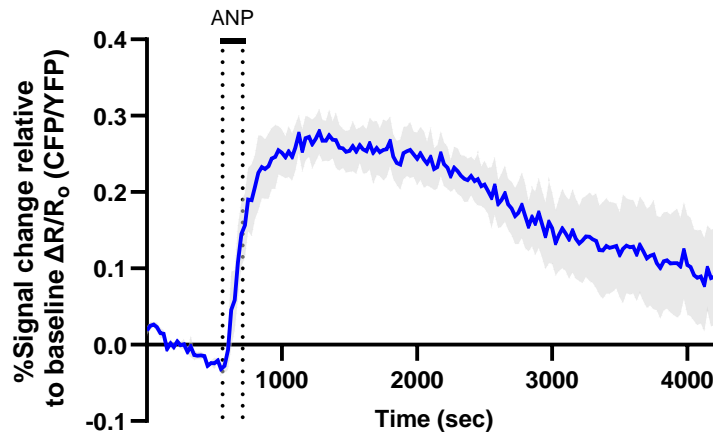
Acute kidney slices from Tie2:Cre/cGi500 mice were superfused (dotted lines) in the time period from 200 sec to 570 sec with 100 μM DEA NONOate (black trace) or DMSO (red trace). Stimulation was followed by pre-tempered 1X KHB (37°C), a total time frame of 1500 sec was recorded. Graph represent the mean of baseline-normalized FRET (CFP/YFP) ratios ( $\Delta R/R_0$ ) of all analyzed glomeruli. Data represent mean  $\pm$  SEM of all analyzed glomeruli of two Tie2:Cre/cGi500 mice ( $n = 7$  for DEA NONOate,  $n = 4$  for DMSO Ctr.).



**Supplemental Figure 9: GECs of *Cdh5:Cre/cGi500* mice respond similar to *Tie2:Cre/cGi500* mice**

(A) Immunostained kidney slice of a *Cdh5:Cre/cGi500* mouse. Confocal images show GFP staining (green) in GECs, thereby confirming cGi500 expression in this cell type. PECAM-1 staining (magenta) functions as a cell-specific marker for GECs and colocalizes with GFP-stained GECs. Bottom panels: High magnification of the area marked with a dashed rectangle in the right upper panel (Zoom). Acute kidney slices of *Cdh5:Cre/cGi500* mice (B, C) were superfused (dotted lines) in the time period from 200

sec to 570 sec with 1  $\mu$ M ANP (blue trace), 1 mM SNAP (orange trace), or the combination of both (black trace). Stimulation was followed by pre-tempered 1X KHB (37°C), a time frame of 1500 sec was recorded. Graphs represent the mean of baseline-normalized FRET (CFP/YFP) ratios ( $\Delta R/R_0$ ) of all analyzed glomeruli. (D) Scatter dot plot displays the maximal  $\Delta R/R_0$  response for each glomerulus derived from the indicated stimulation in (C) during the entire measurement period of 1500 sec. (E) Another NO donor (100  $\mu$ M DEA NONOate) was applied (dotted lines) in the time period from 200 sec to 570 sec, while a time series was recorded. Graph represents the mean of baseline-normalized FRET (CFP/YFP) ratios ( $\Delta R/R_0$ ) of all analyzed glomeruli. Data represent mean  $\pm$  SEM of all analyzed glomeruli of five Cdh5:Cre/cGi500 mice ( $n = 8$  for ANP,  $n = 9$  for SNAP,  $n = 8$  for ANP+SNAP,  $n = 7$  for DEA NONOate). One-way ANOVA, Tukey's post hoc test, \* $P < 0.05$ . Scale bar 25  $\mu$ M.

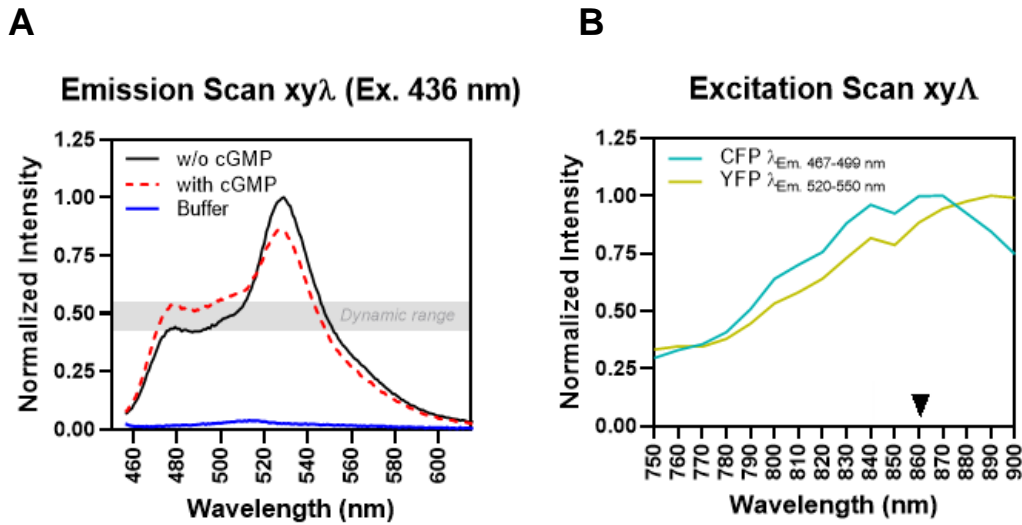


#### Supplemental Figure 10: Long-term measurement of the cGMP/FRET response in podocytes after ANP administration

Acute kidney slices from Pod:Cre/cGi500 mice were subjected to stimulation with 1  $\mu$ M ANP in the time period from 500-650 sec. Stimulation was followed by pre-tempered 1X KHB (37°C) for a total recording time of 4250 sec. The graph represents the mean of baseline-normalized FRET (CFP/YFP) ratios ( $\Delta R/R_0$ ) of 4 analyzed glomeruli.



## Supporting information (SI 2)



Supplemental Figure 11: Fluorescence spectra of cGi500

(A) Emission scan of cGi500 from transfected HEK 293T homogenates incubated without (black line) and with 100  $\mu$ M cGMP (red dashed line). Buffer A (without cGi500) served as control (blue line). The fluorescence was measured using the EnSpire® multimode plate reader. Data were normalized to maximum fluorescence in the absence of cGMP. (B) Excitation scan of cGi500 from transfected HEK 293T homogenates. Fluorescence in the CFP channel (cyan) and YFP channel (yellow) was measured using the multiphoton microscope TCS SP8 MP-OPO. Data were normalized to maximum fluorescence.